STRUCTURAL PERFORMANCE OF A PROPOSED UHP-FRC SHIELD IN HARSH ENVIRONMENT

by

©Mohamed Hamed, B.Sc.

A thesis submitted to the

School of Graduate Studies

in partial fulfillment of the requirement for the degree of

Master of Engineering

Faculty of Engineering & Applied Science

Memorial University of Newfoundland

May 2018

St. John’s Newfoundland Canada

Abstract

Offshore structures are used in harsh ice-infested environments. Shields for such structures are necessary to protect them from ice abrasion. An ice shield is proposed using ultra high performance fibre reinforced concrete (UHP-FRC). This type of concrete is attractive due to its high abrasion resistance that would be beneficial to protect the structure from ice-wear. In order to examine the interaction between the ice shield and the offshore structure, composite flexural and shear specimens were investigated in this thesis.

Ten flexural specimens were cast and tested. All specimens were made with two layers of concrete. The top layer was UHP-FRC and the bottom layer was high performance fibre reinforced concrete (HP-FRC). The parameters tested were the thickness of the top layer (50 mm and 75 mm), the spacing between the shear connectors (390 mm and 195 mm), and the type of shear connectors (shear keys and T-headed studs). The structural behaviour of the specimens was examined in terms of crack development, specimen deformation, strains in steel and concrete, horizontal shear slip and capacity, and ultimate capacity.

The results revealed that the thickness of the top layer did not have a significant effect on the serviceability behavior of the specimens. However, increasing the thickness led to an increase in the ultimate capacity. The specimens with 390 mm spacing between the shear keys were unable to develop a full composite action and had an interface failure. The specimens with T-headed studs and 195 mm developed fully composite action with high ductility.

Direct shear specimens were also cast and tested. The shear specimens duplicated the interface geometry of the flexural specimens and had the same parameters. The results of the direct shear tests were compared to the predictions of different code and some proposed equations in the literature. The results of the comparison revealed that most code and proposed equations can adequately predict the interface capacity of the composite specimens. In addition, the interface shear capacity of both the flexural and the direct shear tests were compared. It was concluded that the shear specimens yielded higher shear capacity than the flexural specimens for the specimens with shear keys that failed due interface failure.

Acknowledgment

I would first and foremost like to take this opportunity and gratefully thank my supervisors and research advisors Dr. Amgad Hussein, Head of Department of Civil Engineering at Memorial University of Newfoundland, and Dr. Heasham Marzouk Professor of Civil Engineering at Ryerson University. A sincere acknowledgment is needed for their great guidance, endless support, and long constructive discussions and comments. This project would not have happened without them. I would also like to thank them for providing me with this great opportunity, which had a significant effect on my growing at a professional and personal level.

Furthermore, I would like to thank both Mr. Shawn Organ and Mr. Jason Murphy the laboratory staff at Memorial University of Newfoundland for their help that made this work happen.

Moreover, I would have to thank all my colleges who helped me in the experimental phase of this investigation Mahmouad Essam Said, Mohamed Zorgani, Kareem Rageh, Sherif Mansour, Ahmed Soliman, Mohamed Essam Said, Moftah Elwehashy, and Fahd Elzahrany. A special thanks to the rest of the graduate students whom I worked with.

Finally, my deepest appreciation and gratitude goes to my parents and my family for their endless support and encouragement and believing in me at all times. I would like to thank my sisters and my brother in law for continuous motivation and support all through my life.

Table of Content

List of Figures

List of Tables

List of Notations:

ACI	=	American Concrete Institute
ASTM	=	American Society for Testing and Materials
a	=	shear span of the specimen
A	=	Area of the concrete around a steel bar
a_{cr}	=	Distance from the point to the surface of the nearest longitudinal bar
A_s	=	Area of the steel reinforcement in tension
A_k	=	Area of all the used shear keys
A_{sm}	=	Contact area between the two surfaces in the joint plane
A_{cv}	=	Area of concrete in which the interface shear stress is being transferred
A_v	=	Area of interface shear reinforcement crossing the shear plane within A_{cv}
BS	=	British Standard
b or b_v	=	Width of the specimen
CSA	=	Canadian Society Association
C	=	Concrete cover
c	=	Cohesion factor (ACI 318M-14), equal to 0.52 MPa for clean surface and not roughened, 1.9 MPa for roughened surface with 6 mm amplitude, and 2.8 MPa for concrete cast monolithically.
d_c	=	Thickness of the concrete cover from tension face to the center of the bar
d	=	Depth of the specimen
d_f	=	Diameter of the fibre
EC	=	European Code

E_c	=	Modulus of elasticity of the concrete
E_s	=	Modulus of elasticity of the reinforcement
f_c'	=	Concrete compressive strength
f_{ck}	=	Characteristic cylinder strength of concrete
f_{cm}	=	Mean value of compressive strength
f_s	=	Stress in the steel at the cracked stage
f_r	=	Modules of rupture
F_{ctm} *or* f_{ctm}	=	Mean of tensile strength concrete
f_y	=	Yield stress of transverse reinforcement
HP-FRC	=	High Performance Fiber Reinforced Concrete
h	=	Height of the specimen
I_u	=	Second moment area for the uncracked section
I	=	Moment of inertia where,
I_e	=	Effective moment of inertia
I_{cr}	=	Cracked moment of inertia
I_g	=	Gross moment of inertia
k_1	=	Bond coefficient, equal to, 0.8 for high bond reinforcement bars, and 1.2 for effective plain bars
k_2	=	Loading coefficient, equal to, 0.5 for a specimen subjected to bending load, and 1.0 for a specimen subjected to tension
K_t	=	Coefficient for the duration of the loading, equal to, 0.6 for short term loading, and 0.4 for long term loading
K_1	=	Cohesion of concrete related to concrete strength (AASHTO), equal to, 0.3 for a slab cast in place on a roughened girder surface, 0.25 for normal concrete cast monolithically, normal concrete and lightweight concrete cast on a roughened surface, and 0.2 for normal concrete cast on a non-roughened surface or cast on a studded steel girder

K_2	=	Maximum interface shear stress allowed on the specimen (AASHTO), equal to, 12.4 MPa for a deck made from normal concrete placed against a roughened girder surface, 10.3 MPa for normal concrete cast monolithically or on a roughened surface, 9.0 MPa for a concrete deck made from lightweight concrete placed against a girder surface, 6.9 MPa for lightweight concrete cast monolithically or cast on a roughened surface, and 5.5 MPa for any concrete cast on a studded steel girder
L	=	Length of the specimen
L_f	=	Length of the fibre
M_{cr}	=	Theoretical moment cracking
M_a	=	Moment at the service load
P_c	=	Permanent net compressive force normal to the shear plane
S_{rm}	=	Crack spacing
s	=	Spacing between interface shear reinforcement
UHP-FRC	=	Ultra High Performance Fiber Reinforced Concrete
v_u	=	Horizontal shear stress in the interface of the composite element
V	=	Shear stress on the composite element
V_{nh}	=	Nominal horizontal shear strength
V_u	=	Shear strength on the composite element
V_{ri}	=	Factored interface shear resistance (kip)
V_{ni}	=	Nominal interface shear resistance (kip)
V_{ui}	=	Factored interface shear force due to total load based on the applicable strength and extreme event load combination (kip)
W_1	=	Modules of the section
W_k	=	Theoretical crack width
x_u	=	Distance from the neutral axis to the area of extreme fibre
Y_t	=	Distance from the centroid to the extreme tension fibre

α_f = Angle between the shear plane and the shear reinforcement

β = Ratio from tension face to the neutral axis

β = Coefficient of the design of the value, equal to, 1.7 for a minimum dimeson of 800 mm, and 1.5 for a minimum dimension of 300 mm

β_1 = Coefficient to account the bond properties of the bar, equal to, 0.8 for high bond bar, and 1.2 for plain bars

β_2 = Coefficient for the duration of the load, equal to, 0.6 for short term loading, and 0.4 for long term loading

γ_f = Safety factor where equal to 2

ϕ_s = Resistance factor for reinforcement

ϕ_c = Resistance factor for concrete

δ_s = Maximum theoretical deflection at the service load

ε_m = Average strain at the level where the cracking is being considered

ε_{sm} = Mean strain in the tension reinforcement

ε_{cm} = Mean tensile strain

$\varnothing$ = Reinforcement bar diameter

σ = External stress acting along the interface from the external loading and tensioned shear reinforcement

λ = Concrete's density, equal to, 1.0 for normal weight concrete, 0.85 for sand light weight concrete, and 0.75 for all light weight concrete

μ = Friction factor, equal to, 1.0 for concrete placed against roughened surface with6 mm amplitude, 0.6 for concrete placed against non-roughened surface, and 1.4 for concrete cast monolithically.

ρ_v = Reinforcement ratio, $\rho_v = \frac{A_v}{A_{cv}}$

ρ_{eff}	=	Ratio of the area od reinforcement and the concrete effective area in tension
σ_{sr}	=	Stress in the tension longitudinal reinforcement under the first crack
σ_n	=	Compressive stress in the joints

Chapter One

Introduction

1.1 General

Some reinforced concrete bridges, lighthouses, marine, and offshore structures are constructed in harsh environments such as the North Atlantic. These structures are commonly subjected to harsh conditions. For example, ice abrasion, impact from keels of ice ridges and icebergs, and recurring freeze-thaw cycles. It is essential that such structures be designed to withstand such conditions. To ensure that the structures have adequate resistance to abrasion caused by ice, ice shields are used in some occasions. There have been a number of incidents such as Prince Edward Island Bridge and Sakhaline 2, where in both cases the steel ice shields underwent corrosion and separated from some piers. Some of the concrete used in lighthouses in the Baltic Sea were severely damaged due to ice abrasion (Convener & OtherAuthors, 2009).

The properties of UHP-FRC makes it promising to be used as an ice shield for marine and offshore applications in harsh environments. Standing as a great advancement in material applications in the field of structural engineering, UHP-FRC was first developed during the mid-1990's with a compressive strength of more than 160 MPa, (Nematollahi, R, Jaafar, & Voo, 2012). UHP-FRC has attractive properties, such as high durability, high tensile strength, flexibility, corrosion resistance, abrasion

resistance, toughness, aggressive environment resistance and self-consolidating (Wille et al., 2011). The steel fibres improve tension stiffening, confinement, shear resistance and ductility of the concrete mixture.

UHP-FRC have a modulus of elasticity from 45 to 55 GPa, direct tensile strength 8 to 15 MPa, Poisson's ratio 0.2, creep coefficient 0.2, thermal expansion of 100×10^{-6} and density between 2400 to 2550 kg/m^3(GU et al. 2015). UHP-FRC is usually composed of high quantity of cement, fine aggregate, low water to binder ratio, and steel fibers, and superplasticiser. In terms of cost, the price of the new material is becoming more affordable due to continuous development in the field of concrete materials, making it more sustainable, affordable, and easier to access to be used in aggressive and corrosive environments.

UHP-FRC has been used as a pre-cast material in bridges, building facades, stairs and panels. It was used in the construction of the Chillon Viaducts in Geneva Switzerland, Mud Creek bridge in Iowa United States of America, Nipoigon River bridge joint foundation in Ontario, Canada, and Mission Bridge in British Columbia Canada (Ductal, 2018).

A recent study revealed that UHP-FRC plates showed superior impact resistance properties, which was 7 to 18 times higher than the high-performance concrete. The used of the steel fibres in the UHP-FRC resulted in lower displacement and higher energy absorption capacity of concrete plates (Othman & Marzouk, 2016).

A composite structure is a structure member made of two or more materials that act together. Composite techniques are usually used in the rehabilitation and strengthening of old concrete structures, pre-cast concrete, and bridge decks.

The main concern for composite elements is the horizontal shear transfer between the two layers of concrete. The horizontal shear stress is usually transferred through the friction or interface reinforcement.

In order to utilize the properties of the UHP-FRC, composite specimens are investigated in this experimental program. Further research is needed to investigate the performance of the composite specimens. Two different thicknesses of the ice shield are used to examine the effect of the thickness on the flexural performance and capacity of the composite elements (50 mm and 75 mm were the two different thicknesses used in this investigation).

To avoid any slippage and to ensure that the two layers are acting monolithically, shear connectors are used. To examine the effect of the shear connectors on the interface shear strength, two different spacing's of 195 mm and 390 mm and two different types of shear connectors were used ,shear keys and T-headed studs, were investigated.

To evaluate the direct shear capacity of the specimens, smaller shear specimens are cast and tested. The shear specimens are designed to replicate the interface of the large composite flexural specimens.

UHP-FRC could be used as a thin plate in high load or impact zones or in areas subjected to ice-abrasion. Hence, this investigation will focus on developing an overlay

that could be utilized as an ice shield for offshore structures with improved shear connection between the two layers of concrete.

1.2 Project scope

The scope of this project is to develop a fully composite element that could be used as an ice shield for offshore structures made of UHP-FRC.

1.3 Project objective

- To study the interface shear between the two layers of the composite elements.
- To examine the shield thickness and its effect on the serviceability limit state of the composite specimens.
- To investigate the horizontal shear transfer between the two layers of the composite specimens along the interface with different types of shear connectors.
- To determine the effect of spacing between the shear connectors on the composite specimens.
- To study the direct shear capacity of the composite elements.

1.4 Thesis outline

Chapter 1 presents a short summary for UHP-FRC, and composite elements along with the scope, objectives and outline of the thesis.

Chapter 2 briefly explains the horizontal shear stress transfer mechanism and reviews previous work on the composite elements, code equations and expressions proposed by some researchers to calculate the interface horizontal shear stresses.

Chapter 3 illustrates the details of the experimental program in terms of material properties, casting of test specimens, instrumentations, test set-up, and test procedure for the flexural specimens.

Chapter 4 presents the results and analysis obtained from testing the flexural specimens.

Chapter 5 discusses the direct shear test and the results. The chapter also contains a comparison between the experimental results, the code and proposed equations available in the literature.

Chapter 6 summarizes the findings of the experimental investigation, and the main conclusions.

Chapter 2

Literature Review

2.1 Horizontal shear stress

Composite elements enable the structural engineers to take full advantage of both materials. For a composite element to properly function, the engineer should account for the horizontal shear stresses at the interface between the two layers of concrete. A sufficient connection capacity must be provided between the two layers to transfer the horizontal shear stresses and hence to develop the fully composite action, as shown in Figure 2.1.

The horizontal shear stress across the interface between the two layers of concrete is mainly transferred by three components: shear friction, cohesion between the concrete, and dowel action from the interface reinforcement. Each component has a different contribution, which is based on the stress level at the interface, as shown in Figure 2.2. The cohesion is the first mechanism to resist the shear stresses at the early stages. As the stress levels increases and the interface starts to crack, the cohesion between the two layers breaks and the shear friction and the dowel action begins to transfer the horizontal shear stresses across the interface together.

The shear friction concept was first introduced by Mast in 1964 and Birkeland and Birkeland in 1966. The Saw-tooth model is used to explain the shear friction

mechanism, as shown in Figure 2.3. At the interface, as the load is applied a horizontal displacement occurs followed by a vertical displacement due to the presence of the coarse aggregate. Some tension in the interface reinforcement occurs due to the vertical displacement. The tension in the interface reinforcement causes friction and clamping force along the interface. The dowel action is mobilized due to the resistance of the interface reinforcement between the two layers, as shown in Figure 2.4.

There are different types of tests used evaluate the capacity of composite specimens. The direct shear test is used to investigate the interface shear capacity of the composite specimens. As will be mentioned later, direct shear stresses could be done under different configurations. Figure 2.5 illustrates the typical interface shear stress versus slip for different cases. When the shear composite specimen does not have any interface reinforcement, as illustrated in Figure 2.5 (a), the shear strength is suddenly lost after the stresses reaches its peak. Figure 2.5 (b) explains the behavior of the shear specimens when the shear friction is resisting more load than the interface reinforcement. Figure 2.5 (c) describes the performance of the shear specimen when the contribution of the shear friction and the interface reinforcement are almost equal. Figure 2.5 (d) explains the shear specimen behavior when the interface reinforcement has a higher contribution than shear friction.

The second type of tests is conducted on flexural specimens. This test is used to evaluate the bending capacity of the composite specimens and examine its full flexural capacity is attained. Through the interface shear, the composite sections work like a monolithic element. For the composite element to attain its capacity, the interface bond between the layers should never be lost. Figure 2.6 (a) shows a composite element being

loaded. Figure 2.6 (b) shows the horizontal interface shear stress being completely transferred between the two layers and the element is functioning as a composite one. If the composite element has a weak bond at the interface between the two layers, slippage will occur due to the loss or failure of the interface, as shown in Figure 2.6 (c) and the horizontal shear stress is no longer transferred between the two layers ,then each layer will be working separately, as shown in Figure 2.6 (d).(Kovach, Naito, 2008)

The horizontal shear stress could be calculated using different equations at any point across the composite section. One of the most commonly used expressions is Equation 2.1 that is derived from elastic beam theory. This equation assumes linear elastic state and the element is uncracked. It was suggested that this equation could be used for the cracked section if the moment of inertia and the first area moment was calculated based on cracked section analysis (Loov & Patnaik, 1994). However, Equation 2.1 may not give accurate estimates at high loads.

$$v_n = \frac{VQ}{Ib} \tag{2.1}$$

Another expression that is also commonly used at ultimate loads, is derived from the equilibrium of forces. This equation is implied from ACI (318M-14). The code allows the calculation of the horizontal shear stress from the equilibrium of forces along the interface at the ultimate loads. The equilibrium of the compressive and tensile forces on the composite section, can be calculated using Equation 2.2.

$$v_n = \frac{C_f}{b_v l_v} \tag{2.2}$$

This equation could be applied at all loading stages, where the composite specimen is in a non-linear state and at ultimate load. The current ACI 318M-14 code requires at a sectional level that the horizontal shear strength should be equal to the stresses due to the vertical shear force. Hence, Equation 2.3 could be used to calculate the horizontal shear stress. In fact, the three equations are fairly similar. frequently, the composite elements have different types of concrete overlaying each other. The different types of concrete usually have a different compressive strength. In this investigation, the concrete of the top layer has a higher compressive strength than the concrete in the bottom layer.

$$v_n = \frac{V}{b_v d} \tag{2.3}$$

2.2 Previous research

2.2.1 Historical background

Previous research on interface shear was conducted firstly by Andreson (1960). Based on his experimental results, he proposed the following equation:

$$v_u = v_o + k\rho_v \tag{2.4}$$

Where v_o and k are both adjusted parameters based on the compressive strength of concrete (20.7 MPa or 51.7 MPa). Some empirical values where reported for these parameters.(Anderson, 1960)

Between 1960 and 1990, several investigations were conducted on interface shear strength and different expressions were proposed such as:

$$v_u = \frac{18.6}{(\frac{x}{d}+5)} + 121\rho$$ (Mattock & Kaar, 1961) (2.6)

$$v_u = \rho f_y \tan\phi = \rho f_y \mu$$ (Birkeland & Birkeland, 1966) (2.7)

$$v_u = \rho_v f_y \mu$$ (Mast, 1968) (2.8)

$$v_u = 1.38 + 0.8(\rho f_y + \sigma_n)$$ (Mattock & Hawkins, 1972) (2.9)

$$v_u = 1.38 + 0.8\rho f_y$$ (Mattock, Li, & Wang, 1976) (2.10)

$$v_u = C_s 3.11\sqrt{\rho f_y}$$ (Raths, 1977) (2.11)

$$\frac{v_u}{f_c'} = k\sqrt{\frac{\rho f_y + \sigma_n}{f_c'}}$$ (Loov, 1978) (2.12)

$$v_u = C_1(\rho f_y)^{C_2}$$ (Walraven, Frenay, & Pruijssers, 1987) (2.13)

Where, $C_1 = 0.822 f_c^{0.406}$ and $C_2 = 0.159 f_c^{0.303}$ (2.15)

$$\frac{v_u}{f_c'} = k(\frac{\rho f_y}{f_c'})^{\alpha}$$ (Mau & Hsu, 1988) (2.14)

In this chapter, only research that were published after 1990 will be reviewed and presented.

2.2.2 Shear keys

2.2.2.1 Buyukozturk, Bakhoum, and Beattie

Buyukozturk, et al. (1990) studied the capacity of the joints of segmental bridges under both shear and normal forces. The joints had different types of preparations: flat joints, joints with shear keys, and joints with or without epoxy and different epoxy thickness. Some of the specimens had single and others had multiple shear keys along

the interface. The conventional push-off test was chosen and 17 specimens were cast. A monolithic specimen was cast as a reference specimen.

The specimens with flat joints experienced an increase in the capacity when epoxy was added; the specimens experienced a decrease in stiffness as the thickness of the epoxy increased. The specimens with shear keys acted differently as the confining pressure was increased. Although the strength of the shear keys increased when the epoxy was added, the specimens experienced a brittle failure. The change in the epoxy thickness did not have a significant effect on the strength of the specimens. The shear keys specimens had a higher strength than the monolithic specimen, unlike the flat and without epoxy specimens which had the same strength of the monolithic specimen. The researchers developed an equation to estimate the bond strength of the composite specimens. The equation is as follows:

$$V_u = A_k \sqrt{(6.792 \times 10^{-3}) f_{cm}} (12 + 2.466\sigma_n) + \mu A_{sm} \sigma_n \quad (2.16)$$

2.2.2.2 Rombach

Rombach (2002) studied the design and construction of precast segmental bridge decks and developed a design equation. The precast segmental bridge is a more functional and a faster way to construct a bridge. The bridge segments usually come in parts, each part is usually about 45 m long. But one of the disadvantages is combining the parts makes a weak bond between the segments. hence shear keys could be used to join the segments together and allow a better transfer of shear stresses at the joints. A numerical investigation was conducted to evaluate the forces on the segmental bridge and the different types of joints. It was noticed that the plain joints failed at earlier stages and only transferred compression forces, while the joints with shear keys had a better

transfer of both compression and torsion loads. The author the developed an equation to predicate the shear capacity of the shear keys to combine both the friction and the shear key follows:

$$V_u = \frac{1}{\gamma_f}(0.14 f_{ck} A_k + \mu A_{sm} \sigma_n) \tag{2.17}$$

2.2.2.3 Turmo, Ramos, and Aparicio

Turmo et al. (2006) studied the behavior of joints in segmental bridges and evaluated the different existing design equations. Eight panels were cast. Four panels were cast with reinforced concrete and four panels were cast with SFRC. Some of the panels were cast without any shear keys to test the friction strength and other were cast with a different number of shear keys along the interface to test the friction and the shear strength of the shear keys.

It was noted that the SFRC did not contribute to an increase in the shear capacity of the panels. The specimens with shear keys long the interface were able to sustain the load after the friction was lost. When the number of the shear keys increased in the panels, the shear capacity of the panels was increased. The authors noted that the European codes do not have an equation to predict the shear strength of specimens with shear keys and developed an equation as follows:

$$V_u = A_k \sqrt{f_{cm}}(0.9064 + 0.1863\sigma_n) + \mu A_{sm} \sigma_n \tag{2.18}$$

2.2.3 Direct shear (push-off) test

2.2.3.1 Kahn and Mitchell

Kahn and Mitchell (2002) examined the use of the ACI 318M-99 equation for horizontal shear friction, when applied to composite elements constructed with high strength concrete. Fifty push-off specimens were cast and tested. The specimens had different interface treatment, concrete strength, and transverse reinforcement ratios. The interface treatments are un-cracked, cracked, and cold joint. The compressive strength of the concrete varied from 46 to 123 MPa. The transverse reinforcement ratio varied from 0.37 % to 1.47%.

The experimental investigation showed that the ACI equation for the horizontal shear stress gave a conservative estimate for high strength concrete. They suggested the following equation to better estimate the horizontal shear friction for the composite elements. (Kahn & Mitchell, 2002)

$$v_n = 0.05 f_c^{'} + 1.4 \frac{A_v f_y}{b_v s} \leq 0.2 f_c^{'} \quad \text{(psi)} \tag{2.19}$$

2.2.3.2 Momayez, Ehsani, Ramezanianpour, and Rajaie

Momayez et al. (2005) used different types of tests to evaluate the shear strength at the interface between two layers of concrete, as shown in Figure 2.7. Four tests were conducted and compared to examine the best way to evaluate the shear strength. The four tests were pull-off test, splitting prism test, bi-surface shear test, and slant shear test. The bi-surface shear test was a recent method that the researchers developed to better investigate the shear strength. The specimens dimension and test types are shown

in Figure 2.7. The researcher cast 164 specimens for the entire investigation. The specimens had two different surface roughnesses: a low and a high roughness.

The authors observed that the interface shear strength depended on the type of test used. The slant shear test gave a high value when compared with other experimental results. This could be caused by the compressive force that the specimen was subjected to during the test. The pull-off and splitting prism test were close in their values and gave conservative estimates. The bi-surface shear test was the most consistent and was a fair estimate, around 80%, of the shear bond strength. An advantage of the bi-surface shear test is that it is simple in casting and the testing of the specimens.

2.2.4 Composite beam

2.2.4.1 Saiidi, Vrontinos and Douglas

Saiidi et al. (1990) studied the effect of different thickness, reinforcement, and concrete strength of the overlay in composite elements when placing the overlay in both tension and compression. Before the researchers started their investigation, some assumptions were made to simplify their modeling. The assumptions were: the beams could have an overlay made of plain concrete or reinforced concrete, the assumption of a perfect bond between the two layers of concrete, shrinkage and the temperature effects on the concrete was ignored, the beam remains plane, the curvature of the beam and the overlay is the same, the composite would have yielded if reinforcement of either the beam or the overlay yields, and a bilinear relation between the stress-strain was assumed. They cast 14 beams and divided them into six categories. Each category had different overlay thickness, reinforcement, and concrete strength. The thickness of the overlays

were 2 inches (51 mm) and 4 inches (102 mm). The reinforcement ratios used in this investigation was 1.26% and 2.5%. The concrete compressive strength varied from 3000 psi (20.6 MPa) to 6000 psi (41.4 MPa). All the composite elements were compared to a non-composite element. The data that the researchers considered was the ratio for the ultimate moment of the composite elements over the ultimate moment of the non-composite elements, the ratio of the maximum shear at the interface to the shear flow at the breaking point, and the ductility of the beams.

For the ultimate moment ratio and ductility, there was a linear relation with the compressive strength of concrete. As the strength of the concrete increased the ratio of the ultimate moment and ductility increased. The shear flow ratio gave a relatively different trend: the ratio increased greatly when the thickness and the reinforcement of the overlay increased. The loss of the interface strength between the two layers could lead to premature failure of the composite element. The researchers reported that the compressive strength of the overlay is drastically higher than that for the bottom beam as this might generate high shear flow at the interface. The high intensity of the shear forces flowing at the interface is harmful to the composite beam as it leads to interface failure. The authors also recommended that the use of thick overlay with a low percentage of reinforcement is better than using a thin overlay with a high percentage of reinforcement (Saiidi, Vrontinos, & Douglas, 1990).

2.2.4.2 Loov and Patnaik

Loov and Patnaik (1994) examined the use of the equation ACI 318M-90 design equation to calculate the horizontal shear stress in composite beams. They cast and tested 16 composites beam. The objective of the reach was to simplify the code equation. Two

main parameters were investigated the concrete strength and the clamping stress. First, the concrete strength remained constant at 5000 psi (34.5 MPa), while the clamping stress had a range that varied from 58 psi (0.4 MPa) to 1120 psi (7.7 MPa). Second, the clamping stress remained constant at 120 psi (0.8 MPa), while the concrete strength had a range that varied from 6400 psi (44.2 MPa) to 70000 psi (48.3 MPa). The clamping stress is the interface reinforcement ratio multiplied by the yielding strength. All the beams were T-beams. The samples were divided into two groups: the first group was beams with their top layer covering the entire beam top, while the second group had a smaller layer that did not cover the whole beam. The beams had a length of 10 feet and 6 inches (3231 mm). The small top layer on the beams with a small overlay had a length of 6 feet and 22 inches (1900 mm). The top layer had a width of 400 mm and a height of 120 mm and the bottom layer had a width of 150 mm and a height of 230 mm. Most of the samples had a rough surface. The amount of reinforcement used in each beam depended on the amount of clamping stress needed in the beams. The beams were used to simulate a pre-stressed deck and slab on top.

Three-point bending load was used. The supports were located at 3 inches from the face of the beam on each side. The full top layer beams experienced flexural cracking before any cracking in the interface. Unlike the beams with a small top layer, the cracks reached the interface or the horizontal shear stress zone. The failure of all the beams was divided into two groups: the first group failed because of horizontal shear stresses while others failed in flexure. Loov and Patnaik suggested the following equation to calculate the horizontal shear capacity of composite elements: (Loov & Patnaik, 1994)

$$v_n = k\lambda\sqrt{(15+\rho_v f_y) f_c^{'}} \le 0.25 f_c^{'} \quad \text{(psi)} \tag{2.20}$$

2.2.4.3 Ali and White

Ali and White (1999) developed a simple way to estimate the shear friction for both normal and high strength concrete. The researchers took into consideration the surface roughness, the concrete strength, and the reinforcement across the interface. The constant density model was used to develop the model. The fracture energy was used to combine both the surface roughness and the concrete strength. The method was validated for concrete with a compressive strength up to 100 MPa. The authors developed an equation to estimate the ultimate shear capacity along the interface; the method was then compared to the Canadian code, Mau and Hsu's equation, and ACI code. The proposed method gave acceptable results. The proposed equation is as follows: (Ali & White, 2000).

$$\frac{\tau}{f_c'} = 1.47a\sqrt{\frac{\rho f_y + P}{f_c'}} \le 1.2b \tag{2.21}$$

2.2.4.4 Kahn and Slapkus

Kahn and Slapkus (2004) studied the ACI and AASHTO equations for horizontal shear friction in beams made from high performance concrete. Six beams were cast and tested. The beams were constructed from a precast web with a concrete strength of 83 MPa and a flange with a concrete strength that varied from 50 MPa to 77 MPa. The transverse reinforcement ratio that crossed the cold joint in the interface between the web and the flange varied from 0.19 % to 0.37 %.

The experimental investigation showed that the ACI and AASHTO equations for horizontal shear stress could only be used for composite elements with concrete that has

a compressive strength up to 76 MPa. The results also showed that the Loov and Patnaik's (1994) equation gave the most accurate estimation of the interface shear strength (Kahn & Slapkus, 2004).

2.2.4.5 Grepstad and Overli

Grepstad and Overli (2008) studied the structural behavior of the hybrid beams under a four-point bending load. They divided the investigation into three groups: small scale testing, large-scale testing, and finite element modeling. The small-scale testing consisted of six small hybrid beams which were used to obtain the parameter of the design for the large-scale testing. The large-scale testing consisted of four large hybrid beams. For the small-scale testing, normal fibre reinforced concrete was used for the bottom layer with a thickness of 50 mm. The top layer was lightweight concrete with a thickness of 100 mm, making the height 150 mm in total. The small hybrid beams were 600 mm long and 150 mm wide. For the large-scale testing, half of the hybrid beams had normal fibre reinforced concrete and the other half had a normal synthetic fibre reinforced concrete, for which a thickness of 50 mm was used for the bottom layer, with a compressive strength of 60 MPa. The top layer was lightweight concrete with a thickness of 200 mm with a compressive strength of 38 MPa, making a total height of 250 mm. The large hybrid beams were 3000 mm long and 150 mm wide. The bottom layer had a reinforcement of 2 bars with a diameter of 8 mm. After testing all the small and the large beams, a finite element model was developed for all the samples and the numerical results were compared to the experimental ones.

The beams failed in shear as they were designed. The beams did not experience any failure in the interface and did not influence the crack pattern. The capacity of the

beams did not increase with the use of fibres in the beams. The numerical verification gave similar results to the results obtained from the experimental investigation (Nes & Øverli, 2015).

2.2.4.6 Crane

Crane (2010) studied the shear capacity along the interface between UHP-FRC and high performance concrete. Thirty-eight push-off tests were cast and tested. Twelve specimens were cast monolithically using UHP-FRC with a compressive strength of 200 MPa. Twenty-six specimens were cast from UHP-FRC overlay with a compressive strength of 200 MPa and high-performance concrete with a compressive strength of 84 MPa. The interface had a dimension of 174 mm by 288 mm. The surface of UHP-FRC were prepared before casting of the high-performance concrete. Three types were used: roughened with an amplitude of 6 mm, mild rough surface using the burlap, and a smooth surface which is the cold joint. The interface also had reinforcement to transfer the horizontal shear stresses. Four categories of reinforcements were used: 0, 1, 2, or 3 in the form of two-legged stirrups.

The authors found that the specimens that were cast monolithically. had initial cracks that started between 20 to 65% of the ultimate load. The specimens without shear reinforcement recorded an ultimate load lower than the specimens with 2 two-legged stirrups by 33%. When comparing the composite specimens with shear reinforcement to the composite specimens without shear reinforcement, the first yielded a more ductile failure. This could be attributed to the fact that the reinforcement caused a gradual transfer of the shear stress across the interface. The specimens with rough surface showed a higher stiffness than the other specimens until failure. Even when compared

to highly reinforced smooth surface specimens, the specimens with rough surface showed higher stiffness. The ACI 318M-08 and AASHTO LRFD equations, for horizontal shear stress, showed a conservative estimate when compared to the experimental results. It was also noticed that the specimens with a cold joint had a weaker stiffness than the un-cracked specimens. This could be explained that the specimens initiate a micro-slipping along the interface at low loads. The fibres also had a contribution in the transfer of the shear stress as it was noticed in the specimens with a smooth surface. The interface shear reinforcement yielded a more ductile failure than the specimens without reinforcement. The specimens recorded an increase in the load up to 170% more than the unreinforced equivalent. The effect of the surface preparation and reinforcement across the interface for the specimens with UHP-FRC and high-performance concrete, the surface preparation increased the shear capacity by 127% over the smooth surface. The reinforcement was linearly proportional to reinforcement, that the shear reinforcement increased the shear capacity of the specimen increase (Crane, 2012).

2.2.4.7 Tsioulou and Dritsos

Tsioulou and Dritsos (2011) developed a model to predict the interface slip and proposed an analytical procedure to calculate and evaluate the slip distribution for a concrete composite element subjected to bending. The authors considered three types of interface shear transfer components. The three mechanisms were concrete to concrete adhesion, concrete to concrete friction, and reinforced interface by steel bar connection. The adhesion connection is usually used for small interface slip, while the friction and the dowel action are usually used in cases of a high interface slip. They made some

assumptions to simplify the model. They explained the detailed procedure of the calculation.

The model was verified by using a beam from Loov and Patnaik's (1994). Both results from the model and experimental study were fairly close. Another composite beam was used to verify the model. The researchers first developed and analyzed a composite beam model with finite element. The analytical method gave close results to the finite element model prediction (Tsioulou & Dritsos, 2010).

2.2.4.8 Crane and Kahn

Crane and Kahn (2012) studied the utilization of the UHP-FRC in the precast industry; UHP-FRC to be used as a bridge deck and high-performance concrete for the girder of the bridge. Five composite beams were cast and tested. The beams had dimensions as follows: length of pre-cast web was 3.05 m (with a distance of 2.9 m between the supports), length of cast in place deck was 2.2 m, the pre-cast web was 152 mm wide and 254 mm high, and the cast in place deck had a width of 419 mm and a height of 140 mm. The main differences between the beams were the surface preparation (smooth and rough) and the amount of the shear reinforcement across the interface (the number of the two-legged stirrups was 0,4, or 7). The top layer had a smaller length from the bottom layer as to initiate an interface failure.

The authors noticed the main reason for failure was the cracking and the slip across the interface between the two layers of concrete. A comparison of the shear capacity from the experimental results to the predictions of the ACI code and other proposed equations, it was noted that the ACI equation gave the best estimate for the shear capacity of the composite beams. The shear capacity increased, as the interface

reinforcement was increased. The shear capacity of the composite beams also increased when the surface preparations were changed from smooth to rough (Crane & Kahn, 2012).

2.2.4.9 Baran

Baran (2015) studied the flexural behavior of a composite hollow core element under flexural loading and calculated the horizontal shear strength using different code equations. Five samples were cast, which were divided into two groups with a width of 1200 mm and 550 mm, respectively. All the samples were 4600 mm long with a thickness of 150 mm for the hollow core element and 50 mm for the concrete overlay. Each group had three specimens, one was without an overlay and two were with an overlay. Only one composite specimen from the first group had restricted ends to act as fixed supports.

The rest of the samples were tested on simple supports. The researcher found an increase in the ultimate moment capacity and stiffness of the composite hollow core element when compared to the non-composite ones. When the slippage at the interface occurred, it was accompanied by a sudden drop in the moment capacity of the composite element, confirming that the element was no longer acting as fully composite element. On the other hand, the sample with restricted supports showed no interface slippage until the failure of the sample (Baran, 2015).

2.3 Other research

Most of the relevant work previously discussed was for the utilization of the overlay in compression. Other researchers also tested specimens with overlay on the tension side.

2.3.1 École Polytechnique Fédérale de Lausanne (EPFL)

In a key note paper, Brühwiler (2016) summarized the utilization of the UHP-FRC in composite structures based on the research conducted at EPFL as will be mentioned in this section. The main application was used in rehabilitation, strengthening of an existing structure or in new constructions. The preparations of the concrete surface were carried out by high pressure water jetting or by sand blasting.

The author first explained the fresh properties of the UHP-FRC and the tensile strength increase when adding reinforcement to the concrete. UHP-FRC also have high compressive strength, better stiffness, high durability, low permeability, high abrasion resistance, and high fire resistance. The paper is then divided into the rehabilitation and strengthening of existing structures and the construction of new structures based on the research conducted at EPFL since 2006.

The rehabilitation and the strengthening apply to structures that have been damaged by severe weather and environmental conditions or to structures that endured high loads. The process is to go the damaged areas and use the UHP-FRC on top of the reinforced concrete structure after preparing the surface and laying the steel reinforcement. When the UHP-FRC was placed on the top of the reinforced concrete structure, they act as a composite structure. If the overlay was used for flexural composite structures, the composite structure experiences an increase in the stiffness and in the ultimate resistance.

Noshiravani and Brühwiler (2013) studied the behavior of a reinforced concrete element with a UHP-FRC as an overlay in tension, as shown in Figure 2.8. The bond between the two layers of the composite structure was achieved by preparing the surface

by water jetting and sand-blasting and there was shear connectors along the interface. The composite elements were subjected to both shear and bending stresses. When the forces are combined on the composite structure a different type of failure occurs, as shown in Figure 2.8 (Noshiravani & Brühwiler, 2013). Makita (2014) studied the fatigue behavior of composite Reinforced Ultra High Performance Fibre Reinforced Concrete (R-UHP-FRC) – reinforced concrete members, to simulate a bridge deck strengthened with R-UHP-FRC layer (Makita, 2014). Bastien Masse (2015) studied the bending and punching shear behavior of composite two-way slabs strengthened with UHP-FRC layer on the tension side.

Several structures had been strengthened or rehabilitated by the UHPFRC. The first project to use UHP-FRC as a strengthening material in Switzerland was in and 2004 from that point more than 50 projects have been constructed.

The construction of a new structure in a composite manner enables the structure to reduce its own dead load and be more cost-effective. Recently, Martinet pedestrian bridge, in Lausanne Switzerland, used an overlay of UHP-FRC during its construction. The bridge was designed in accordance with the Swiss standers of the UHP-FRC (Masse, 2015).

2.3.2 Hussein and Amleh

Hussein and Amleh (2015) studied the flexural behavior of composite beams from UHP-FRC and high performance concrete (HPC) or normal strength concrete (NSC). The UHP-FRC layer was used at the tension side of the beam. Sixteen beams were cast for this investigation. The beams were divided into two groups. The first group and second group had non-composite beams and composite beams, respectively. The

beams were 1284 mm long, 300 mm high, and 150 mm wide. The beams were subjected to a four-point bending load. In order to test the interface strength between the two layers of concrete, 150 mm cubes were cast. The cubes were tested in the same manner of the splitting tensile strength cylinder test.

The experimental investigation revealed that the shear capacity of the beams has increased significantly when compared to the non-composite beams. The crack patterns for all the composite beams were the same and the researchers reported a significant increase in the ductility. The bond strength between the UHP-FRC and HSC/NSC was higher than the composite sample of HSC and NSC. The dowel shear studs did not increase the shear capacity of the composite samples. (Hussein & Amleh, 2015)

2.4 Code equations for horizontal shear strength

2.4.1 ACI 318M-14/318RM-14

The ACI design is based on the concept

$$\phi V_{nh} \geq V_u \tag{2.22}$$

where the reduction factor ϕ is taken as 0.75 for shear.

Calculating the nominal horizontal shear strength (V_{nh}) is based on the shear stress (V_u) acting on the section that is being designed. The first step is to check if V_n is

$$V_u > \phi(3.5 b_v d) \tag{2.23}$$

In this case, V_{nh} will be taken as V_u.

$$V_{nh} = A_{vf} f_y \mu \leq \min\left[(0.2 f_c' A_c, (3.3 + 0.08 f_c') A_c, 11 A_c)\right] \tag{2.24}$$

If $V_u \le \phi(3.5 b_v d)$, the horizontal shear strength will be calculated according to the following paragraphs.

There are three conditions to determine which design equation to use. The shear transfer reinforcement and the contact surface preparation should be taken into consideration. If shear transfer reinforcement is used, $A_{v\,min}$ should be calculated using:

$$A_{v,\min} \text{ the greater of } \quad 0.062\sqrt{f_c'}\,\frac{b_w s}{f_y} \text{ or } 0.35\,\frac{b_w s}{f_y} \tag{2.25}$$

The first condition is that if A_v is greater than $A_{v\,min}$ and the concrete contact surface is intentionally roughened, the lesser of the following equations should be used:

$$V_{nh} = \lambda\left[1.8 + 0.6\,\frac{A_v f_y}{b_v s}\right] b_v d \tag{2.26}$$

$$V_{nh} = 3.5 b_v d \tag{2.27}$$

The second condition is that if A_v is greater than $A_{v\,min,}$ and the concrete contact surface is not intentionally roughened, the following equation should be used:

$$V_{nh} = 0.55 b_v d \tag{2.28}$$

The third condition is that if other cases for shear transfer reinforcement and the concrete contact surface are intentionally roughened the following equation should be used:

$$V_{nh} = 0.55 b_v d \tag{2.29}$$

2.4.2 AASHTO LRFD Bridge Design Specification

The AASHTO (2012) basic equation for the interface shear resistance should be taken as:

$$V_{ri} = \phi V_{ni} \tag{2.30}$$

and this design should satisfy the following equation:

$$V_{ri} \geq V_{ui} \tag{2.31}$$

Where the nominal horizontal shear resistance at the interface of the plane should be calculated as:

$$V_{ni} = cA_{cv} + \mu(A_{vf}\, f_y + P_c) \leq \text{ Smaller of } K_1 f_c' A_{cv} \text{ or } K_2 A_{cv} \tag{2.32}$$

$$\text{For } A_{cv} = b_{vi} L_{vi} \tag{2.33}$$

It is important to note that AASHTO assumes that the horizontal shear stress transfer across the interface should be at a location in which a crack could happen or have already happened, or at the interface between two different types of concrete, or at the interface of concrete cast at different times, or at the interface of different materials constructed on top of each other. (AASHTO LRFD Bridge design Specifications, 2012)

2.4.3 CAN/CSA A.23.3-14

The Canadian code assumes that the crack should occur along the shear plane and the relative displacement should be restrained by friction and cohesion. The horizontal shear stress along the interface should be calculated with:

$$v_n = \lambda \phi_c (c + \mu\sigma) + \phi_s \rho_v f_y \cos\alpha_f \tag{2.34}$$

where the limit of this equation is that the term $\lambda\phi_c(c+\mu\sigma)$ should not exceed $0.25\phi_c f_c^{'}$

The code suggests some values for the cohesion and friction factors according to certain criteria. If concrete is laid on top of hardened concrete with a clean surface and not intentionally roughened, the factors should be taken as c = 0.25 MPa and μ = 0.60. If the concrete is laid on top of hardened concrete with a clean surface and intentionally roughened with an amplitude of at least 5 mm, the factors should be taken as c = 0.5 MPa and μ = 1. If the concrete is cast monolithically, the factors should be taken as c = 1 MPa and μ = 1.40. If the concrete is anchored to a steel structure with reinforced bars or with headed studs, the factors should be taken as c = 0 MPa and μ = 0.60.

The code provides an alternative method to calculate the horizontal shear stress along the interface. This method could be used, when the concrete is cast monolithically or the concrete is laid on hardened concrete with a clean or intentionally roughened surface with an amplitude of at least 5 mm. The equation is:

$$v_n = \lambda\phi_c k\sqrt{\sigma f_c^{'}} + \phi_s\rho_v f_y \cos\alpha_f \qquad (2.35)$$

The limit of this equation that the term $\lambda\phi_c k\sqrt{\sigma f_c^{'}}$ should not exceed $0.25\phi_c f_c^{'}$ (Standards, 2014).

2.5 Flexural capacity of UHP-FRC

The flexural capacity of UHP-FRC beams is not available in any design codes. Bae, Choi, and Choi (2015) summarized different models to calculate the flexural strength of UHP-FRC concrete sections with fibres. An experimental program was conducted the different models when applied to UHP-FRC. The authors presented nine different models of stress block, as shown in Figure 2.9. The test results were compared

with the model predictions. A triangle stress distribution gave the best results. This could be attributed to the fact that the UHP-FRC exhibits almost linear behavior in compression till failure. The authors concluded that the validation of the existing models is a hectic process, but the linear model could be used with a 10% error.

2.6 Summary

This chapter reviewed several research programs that had been conducted on composite elements over many years. It also presented different code and proposed equations to predict the interface shear strength of the composite elements.

There exists a lot of research on composite elements using conventional normal and high strength concrete overlays. Based on the literature review presented in this chapter, there is a lack of research on using UHP-FRC overlays that are placed in the compression zone of a composite element. In the literature, there is only one study on UHP-FRC overlays, in the compression zone, that was conducted by Crane and Kahn (2012) on UHP-FRC bridge decks on top of girders. The researchers tested five composite beams and three composite girders in flexure. The researchers used an overlay that did not cover the entire girder in order to induce interface failure.

Hence, there is a lack of research on the use UHP-FRC overlays in the compression zone that develop a full composite action. The current investigation is mainly focused on the interface shear behavior of UHP-FRC overlays on top of HP-FRC element. The study covered the behaviour in flexure and direct shear.

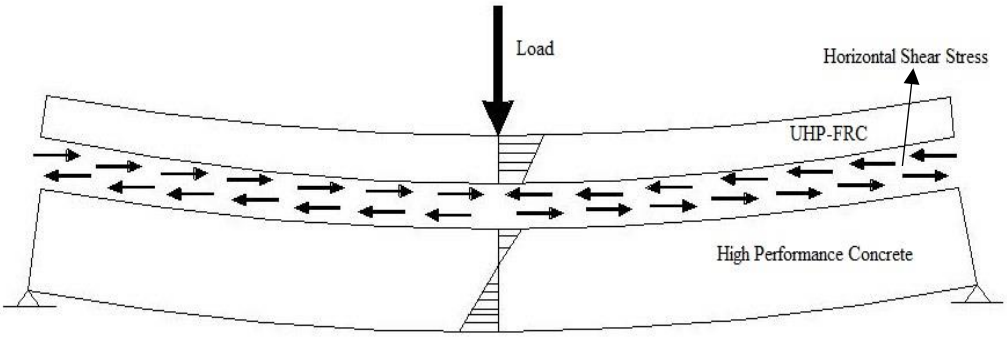

Figure 2.1: Horizontal shear stress transfer along the interface.

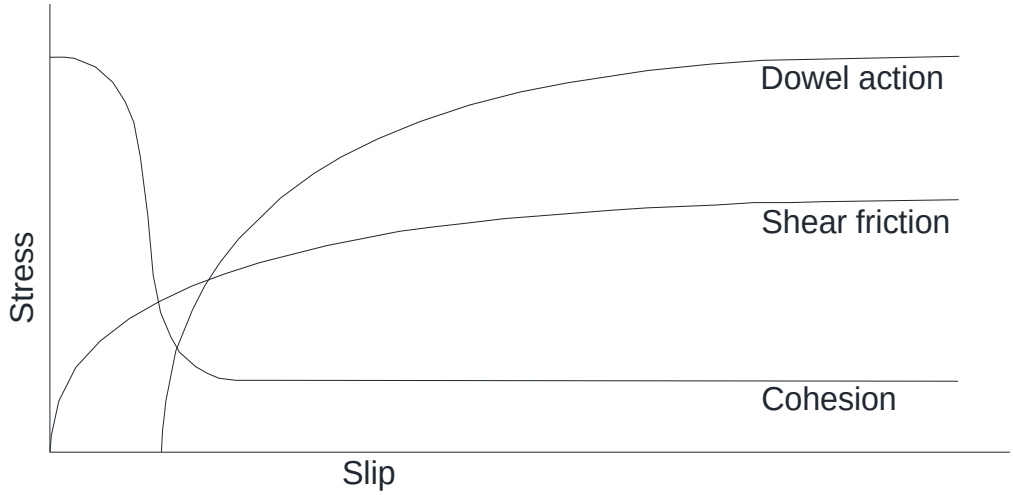

Figure 2.2: Stress mechanisms, (Santos & Júlio, 2014).

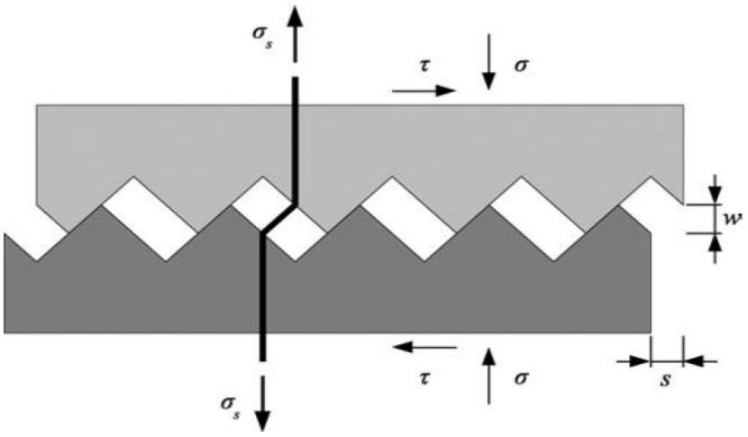

Figure 2.3: Saw-tooth model, (Santos & Júlio, 2014).

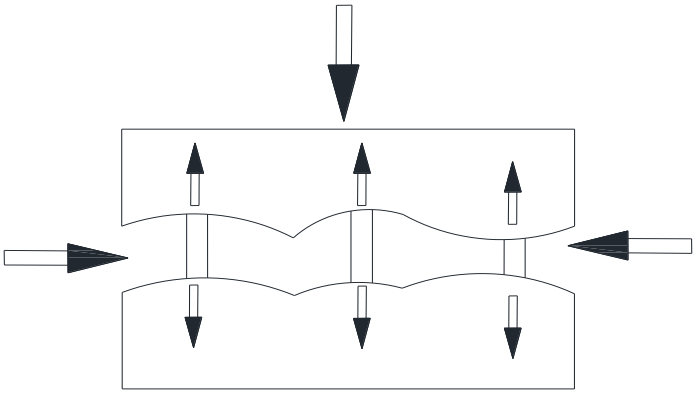

Figure 2.4: Reinforced steel after cohesion is lost.

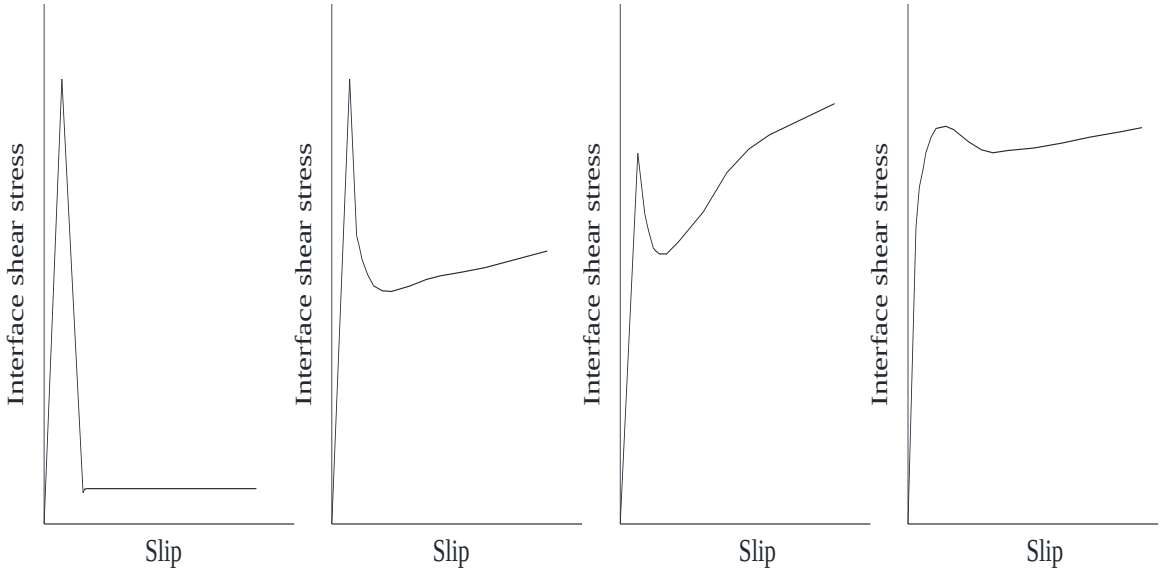

(a) No reinforcement (b) $Af_y < cA_{cv}$ (c) $Af_y \approx cA_{cv}$ (d) $Af_y > cAcv$

Figure 2.5: Stress versus slip behaviour. ($A_s f_y$ is the resistance due to reinforcement and cA_{cv} is the resistance due to shear friction)

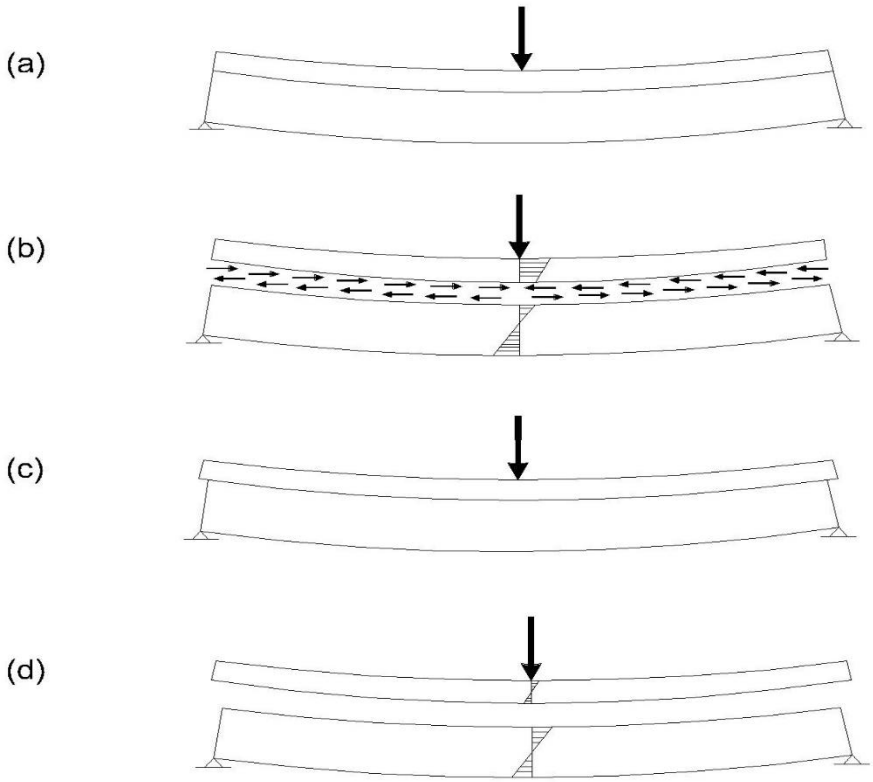

Figure 2.6: Simply Supported Beam (a) Composite Beam, (b) Fully composite Beam, (c) Horizontal shear slip, (d) non-composite beam, .

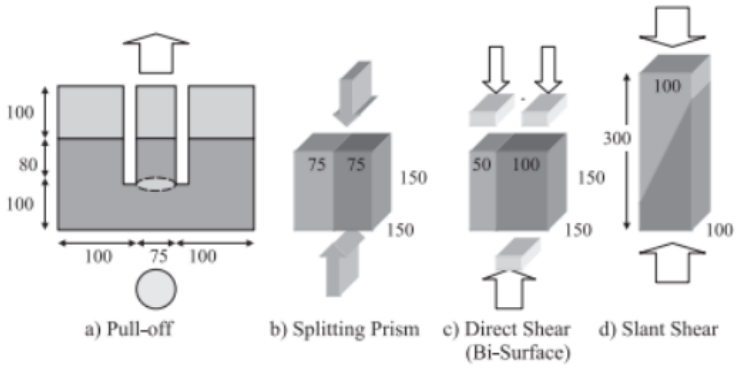

Figure 2.7: Different test types and dimensions (Momayez, Ehsani, Ramezanianpour, & Rajaie, 2005).

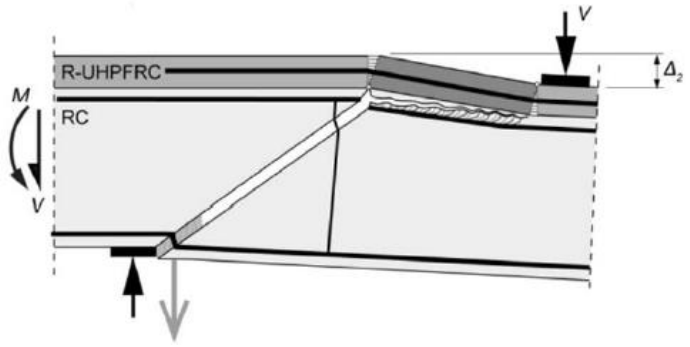

Figure 2.8: Failure of composite section subjected to both shear and bending stresses (Brühwiler, 2016).

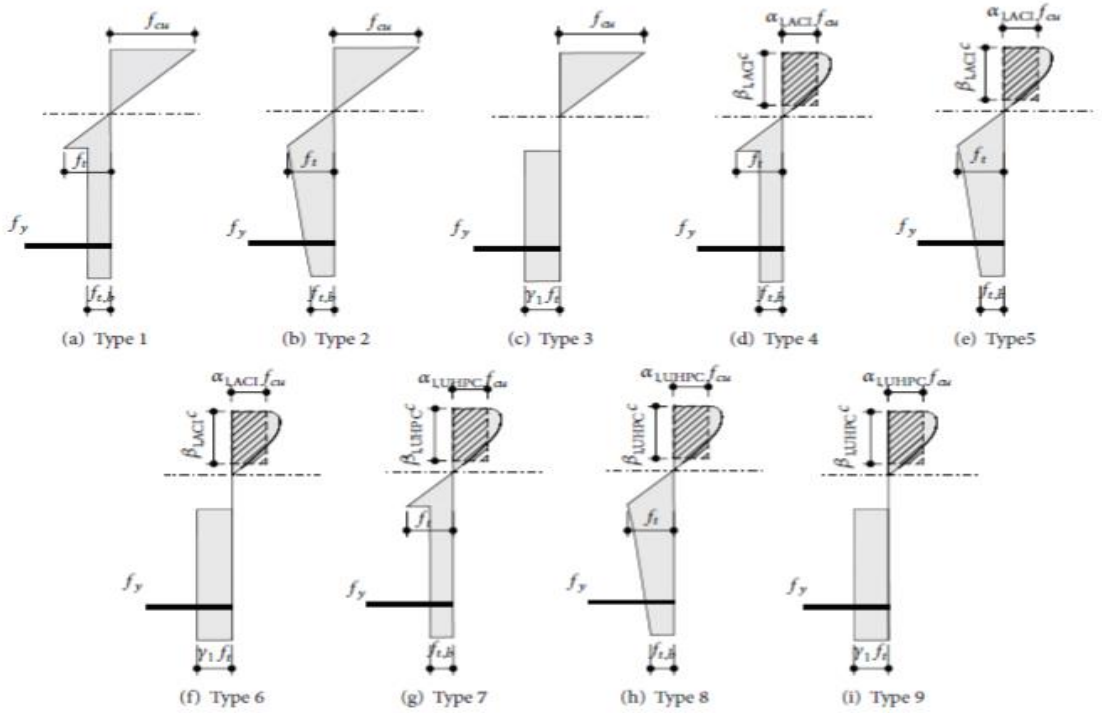

Figure 2.9:Different models of stress blocks for UHP-FRC sections (Bae, Choi, & Choi, 2016).

Chapter 3

Experimental Details and Test set-up

The main objective of the current experimental work is to investigate the flexural behavior and test the interface shear capacity for the composite specimens. The composite specimens could be used as an ice shield for gravity based structures. The composite specimens were made of two layers of concrete on top of each other. This chapter covers a detailed description of the specimens, materials, test set-up, and instrumentation used in the experimental investigation.

3.1 Material

Two types of concrete were used to construct the composite specimens. The top layer was cast with UHP-FRC and the bottom layer was cast with high-performance fibre reinforced concrete (HP-FRC). All cylinders and prisms, for each type of concrete, were cast on the same day of pouring each type of concrete to test their mechanical properties.

3.1.1 Ultra-High Performance Fibre Reinforced Concrete

UHP-FRC was used to manufacture the top layer of the composite specimens, with a targeted compressive strength of 170 MPa, after 28 days. All the samples were poured at Ryerson University. Short straight steel fibres were used in the mixture, and the fibre volume content was of 2%. The properties of the fibre as per the manufactures specification are: an aspect ratio of 65, a minimum tensile strength of 2600 MPa, a diameter of 0.2 mm, a length of 13 mm, and Young's modulus of 205 GPa. A certain mixing procedure was followed since the concrete had more fine particles than the normal types of concrete. Table 3.1 shows the mix properties of the UHP-FRC.

The following procedure was used to cast the UHP-FRC:

1- All the desired quantities were weighed.
2- The pre-mix bags were added to the mixer and mixed for one minute before adding the steel fibres, half of the water, high range water reducer, and superplasticizer.
3- Half the measured amount of water and super-plasticizer were added to the mixer, the water was added and the super-plasticizer followed.
4- The short fibres were gradually added to the mixture for five minutes, to ensure that the fibres are mixed well with the rest of the mixture content.
5- The reaming amount of water and superplasticizer were added in the same manner as before.
6- The concrete was left to continue mixing for 5 minutes.
7- The specimens were poured

3.1.2 High-Performance Fibre Reinforced Concrete

The bottom layer was made of conventional High-Performance Fibre Reinforced concrete (HP-FRC) with a targeted compressive strength of 85 MPa, after 28 days. The fibre volume content was 0.75% of cold drawn steel wire fibres with hooked ends. The manufacturer specifications for the fibres are: an aspect ratio of 65, a minimum tensile strength of 1345 MPa, a diameter of 0.55 mm, a length of 35 mm, and Young's modulus of 210 GPa. This concrete was poured at Memorial University of Newfoundland.

A general use Portland cement (GU) was used, with a specific gravity of 3.15. Silica Fume, superplasticizer, and water reducing agent were used in the mixture. The Silica Fume is a by-product of the production of the Ferrosilicon and silicon metal. Adding the silica fume reduces the permeability and absorption of the concrete mixture. The silica fume has a specific gravity of 2.2. The coarse aggregate used in the mixture was mostly crushed granite, with a maximum aggregate size of 10 mm, with a specific gravity of 2.7, and water absorption of 1%. The fine aggregate used in the mixture had the same composition of the coarse aggregate. Table 3.1 shows the mix properties of the HP-FRC.

3.1.3 Compressive strength and modulus of elasticity

The compressive strength of both types of concrete was tested according to the ASTM C39-15 standards. For each batch, three (100 mm × 200 mm) cylinders were made. The cylinders were poured on the day of the casting of the top layer, then the cylinders were cured and stored in the same place as the UHP-FRC specimens four flexural and direct shear tests. After 28 days, the cylinders were ground and then tested

in the MTS 815 testing machine at Ryerson University shown in Figure 3.1. Table 3.2 shows all the compressive strength of the UHP-FRC.

The cylinders of HP-FRC were poured and tested on the day of casting and testing of the bottom layer. The cylinders were capped with high strength sulphur compound and tested in AutoMax5 testing machine shown in Figure 3.2. Table 3.3 contains all the compressive strength of the High-Performance concrete. The modulus of elasticity was tested on the same machine and had a value of 41 GPa, as shown in Figure 3.3.

3.1.4 Flexural tensile strength

A flexural tensile strength test was performed with a quasi-static loading for UHP-FRC. A three-point bending test was performed using a MTS 793 machine at Ryerson University according to ASTM C1609 / C1609M – 12. Three prisms were cast on the same day of casting for each mixture and cured in the same way as the flexural and direct shear tests. The prisms dimensions were 100 mm × 400 mm ×100 mm. The prisms were tested under clear span of 300 mm using three point loading, as shown in Figure 3.4. Table 3.4 shows of the flexural tensile strength for the UHP-FRC specimens.

For HP-FRC, the modulus of rupture was tested for each mixture according to ASTM C78. Four 100 mm × 400 mm ×100 mm prisms were cast on the same day of casting the bottom layer and cured in the same manner for flexural and direct shear samples. Four-point bending test was carried out with a Tinus Olsun Machine at Memorial University. The test had a stress rate of 0.015 MPa/second and a clear span of 300 mm between the supports, as shown in Figure 3.5. the test results showed an average value of 9.5 MPa for the modulus of rupture of the HP-FRC.

3.1.5 Splitting tensile strength test

The splitting tensile test was conducted for the two-materials used to cast the composite specimens. The test was performed according to ASTM C496 standards of testing. The cylinders tested were 100 mm × 200 mm. The samples were loaded on a diametrical plane. For the UHP-FRC, the test was conducted using MTS 815 testing machine at Ryerson University shown in Figure 3.6. The machine has a capacity of 46000 kN in compression and 2300 kN in tension. Table 3.5 shows the splitting tensile strength of all specimens.

For the HP-FRC, the test was conducted using the AutoMax 5 testing machine at Memorial University, as shown in Figure 3.7. the test results showed an average value of 7.4 MPa for the splitting tensile strength of the HP-FRC, as shown in Table 3.6.

3.2 Flexural specimen details

Ten composite specimens were cast to test the flexural behavior and capacity of the specimen. The top UHP-FRC layer had two different thickness; 50 mm and 75 mm. The layer was reinforced with 10M mesh at the middle of the layer. The bottom layer was 180 mm thick HP-FRC. The specimens were 300 mm wide, 1950 mm long, and had variable thicknesses. In order to transfer the horizontal shear between the two layers of concrete, two types of shear connectors were used. Half of the composite specimens had concrete filling the shear connectors, which were called shear keys, and the other half had T-headed shear studs placed in the shear connectors to improve the shear transfer between the two layers of concrete.

The specimens were divided into three groups. The first group was the reference specimens and it consisted of two non-composite specimens. These specimens were cast

using HP-FRC. They each had a different thicknesses one 230 mm and the other was 255 mm, as shown in Figures 3.8 (a) and (f) respectively.

The second and third group consists of composite specimens (two layers of concrete on top of each other). The bottom layer of all the composite specimens in both groups had the same reinforcement and dimensions. The bottom layer was made of HP-FRC with a thickness of 180 mm. The flexural reinforcement consisted of four 15M bars. The top reinforcement was two 10M bars. Shear reinforcement was used to enhance the shear capacity and to ensure that the shear failure would not occur. The shear reinforcement was two-legged 10M stirrups every 200 mm, as shown in Figure 3.8.

The second group consisted of four specimens. The top UHP-FRC layer had a thickness of 50 mm. The two layers were connected together using shear connectors; with spacing of 195 mm and 390 mm. The shear connectors, which were located in the top layer, had a width of 75 mm, a length of 75 mm, and a height of 25 mm. Both layers were 1950 mm long and 300 mm wide. Figures 3.8 (b) to (e) shows the details of the specimens.

The third group consisted of four specimens. The specimens were similar to the corresponding ones in group two. The top UHP-FRC layer had a thickness of 75 mm. the only difference between the group two and three specimens were the thickness of the top layer for group three specimens had a thickness of 75 mm. Figures 3.8 (g) to (j) shows the details of the specimens in group three. All the specimens had a cover of 20 mm. The reinforcement used was grade 400 MPa deformed steel bars.. Table 3.7 shows a summary of the test specimens that were tested.

3.3 Casting

All the composite specimens were cast in two stages. The first stage was the casting of the top UHP-FRC layer at the structural lab of Ryerson University. Before casting, white foam blocks were placed in the location of the shear connectors and the concrete was poured on top, as shown in Figures 3.9 and 3.8. Then the specimens were shipped to Memorial University of Newfoundland.

The flexural specimens were poured in an upside-down position. The bottom layer was later cast at the concrete laboratory of Memorial University. The casting of the bottom layer took several steps before casting. The areas of the shear connectors were already filled with white foam blocks. The white foam blocks were removed and cleaned to be able to fill the shear connectors with concrete or T-headed studs. The T-headed studs were placed in the void and epoxy was used to fill the cavities. The two-component high strength epoxy was used to eliminate any weak connections that could develop between the concrete and the T-Headed studs. The T-headed studs used shown in Figure 3.11.

Then the formwork was placed around the UHP-FRC top layer and the bottom layer was poured. That is, the composite specimens were cast upside-down. To ensure that the concrete had properly been placed in the shear connectors. Small quantities of concrete were poured first and compacted into the shear key connectors at the beginning of the casting procedure. The rest of the specimen was conventionally cast, as shown in Figure 3.10.

3.4 Curing

All the specimens were cured for the first seven days after casting. Water curing was used for both types of concrete. The water curing is an effective way to reduce the shrinkage of the concrete and to avoid any early concrete cracks. For UHP-FRC, the exposed surface was sprayed with water daily and then covered by a plastic cover for the first seven days, as shown in Figure 3.12. For the bottom layer, a sheet of moist burlap was placed on the exposed surface and sprayed with water daily, as shown in Figure 3.13.

3.5 Test set-up

After 28 days of casting the bottom layer, the specimens were prepared to be tested. All the specimens were tested in the structures lab of Memorial University. Figure 3.14 shows the set-up used for flexural tests. The loading frame applied the load on the specimen. All the specimens were simply supported.

The specimens were placed on the supports with the top layer the UHP-FRC in the compression zone and the bottom layer of HP-FRC in the tension zone. All the strain gauges, LVDTs, and the crack gauges were placed on the specimen. Four-point loading was used. The load was applied through the MTS hydraulic actuator to a thick plate with 38 mm horizontal rods to apply two-point loads on the specimen. The horizontal spacing between the two vertical loads was 130 mm between the loads. The supports were 75 mm away from the face of the specimen from both sides and the span between the supports were 1800 mm, as shown in the Figure 3.14.

3.6 Instrumentation and measurements

Several transducers were used to measure the deflection, the applied load, the concrete strains, the steel strains and the interface slippage and the cracking between the two layers of concrete.

3.6.1 Load

A hydraulic actuator was used to apply the load on all the specimens. The actuator had a maximum capacity of 670 kN, and full stroke of 150 mm. All the tests were conducted in displacement control.

3.6.2 Deflection

Linear variable differential transducers (LVDTs) were used to measure the deflection of all the specimens. The deflection was measured and recorded at three different locations. One LVDT was used to record the deflection in the middle of the specimen and the other two at a distance of (L/4) mm from the left and the right of the specimen, as shown in Figure 3.13. LVDTs had a stroke of 100 mm and linearity of 0.3% at 10 volts.

3.6.3 Steel strain

Electric strain gauges were used to measure the strain in the steel reinforcement. The strain gauges were located at several places on the tension reinforcement of the bottom layer of the concrete in the composite specimen. The strain gauges had a resistance factor of 120 Ω and gauge factor of 2.04 with ± 5%. The length of the strain gauge was 10 mm. Six strain gauges were placed on the two middle bars. Two of the stain gauges were located at the middle of the bars with one on the left and one on the right at a distance of 555 mm and 470 mm, respectively, as shown in Figure 3.15. The

surface of the bar was first grinded lightly to avoid any loss in the diameter of the bar and cleaned using alkaline and acidic chemicals. The gauges were then attached with a glue and left to dry. After 24 hours the wires were connected to the strain gauge. A layer of protective coating was added and an electric tape was wrapped around the gauges to preserve and protect from any damages that could occur from the water or concrete while casting.

3.6.4 Concrete strains

Electric strain gauges were also used to measure the concrete strain in the compression zone of the composite specimens which means on the top of the UHP-FRC. Two strain gauges were placed at the middle of the specimen with a distance of 100 mm between them. The surface was lightly grinded and a thin layer of epoxy was added. The strain gauges were then glued and the wires were attached to the gauges and to the data acquisition system, as shown in Figures 3.16.

3.6.5 Crack detection

The crack formation and propagation was monitored by the naked eye. The crack width was measured using a microscope. The microscope had a magnification capacity of 10x and minimum reading of 0.025 mm.

3.6.6 Slippage detection

In order to detect and measure the slippage along the interface between the two layers of the composite specimens, three Crack Displacement Transducers were attached to the specimens at the interface zone. An L-shaped metal plates were manufactured and glued to bottom layer and a small metal plates were glued to the top layer. The Crack Displacement Transducers were attached to the specimens, as shown

in Figure 3.17. Three gauges were used in some of the test to measure the vertical separation between the two layers. The gauges did not record any significant values,

The Crack Displacement Transducers had capability of ± 5 mm, a rated output of 2 mv/v, and a 1% nonlinearity.

3.7 Testing procedure

The specimen was first placed on the supports. The specimens were then loaded by the hydraulic actuator. The specimen was first pre-loaded with 13.4 kN (3 kips) and then unloaded to eliminate any settlement during testing and to ensure that all the gauges were working properly. The test then began by loading the specimen, with increments of 8.8 kN (2 kips) until the first crack occurred. After the first crack, the load increment of 8.8 kN (2 kips) continued to be used and the load was paused at the end of each step. The specimen was carefully checked for new cracks, the crack propagation was marked. Also, the crack width was measured before proceeding to the next load step. This procedure continues until the failure of the specimen, as shown in Figure 3.18.

All the data generated from the Crack Displacement Transducers, LVDTs and stain gauges were recorded with a high-speed data acquisition system using Lab-View software. The data were recorded at time increment of 3 seconds.

Table 3.1: Mix design for UHP-FRC and HP-FRC.

Concrete mix	HP-FRC	UHP-FRC
Cement (kg/m^3)	460	712
Silica fume (kg/m^3)	40	231
Fine sand (kg/m^3)	690	1020
Ground quartz	-	211
C/F Ratio	1.5	-
Coarse aggregate (kg/m^3)	1035	-
Maximum nominal size (mm)	10	-
Water (L/m^3)	165	109
Super-plasticizer (L/m^3)	3.4	30.7
Accelerator (L/m^3)	-	30
Retarder (L/m^3)	0.625	-
Volume of fibre content	0.75%	2%
Steel fibers (kg/m^3)	58.9	156

Table 3.2: UHP-FRC compressive strength.

Specimen	Compressive strength MPa
A	170.5
B	166.2
C	165.4
Average	167.4

Table 3.3: HP-FRC compressive strength.

Specimen	Compressive strength MPa
HSC-00-50	86.7
SK-390-50	86.1
SK-195-50	82.5
THS-390-50	89
THS-195-50	87.6
HSC-00-75	83.9
SK-390-75	83.2
SK-195-75	86
THS-390-75	87.5
THS-195-75	89.6
Average	86.2

Table 3.4: Flexural strength of the UHP-FRC.

Specimen	Maximum load kN	Flexural strength MPa
A	48.7	21.9
B	42.9	19.3
C	33.5	15.1
Average	41.7	18.8

Table 3.5: Splitting tensile strength for UHP-FRC.

Specimen	Maximum load kN	Tensile strength MPa
A	468.1	14.9
B	439.8	14
C	458.7	14.6
Average	455.5	14.5

Table 3.6: Splitting tensile strength for HP-FRC.

Specimen	Displacement Rate MPa/Second	Maximum Load kN	Tensile Strength MPa
A	0.25	226.2	7.2
B		232.5	7.4
C		234.2	7.5
Average		231.0	7.4

Table 3.7: Test specimens details.

Specimen	UHP-FRC Thickness mm	HP-FRC Thickness mm	Total thickness mm	Shear connections mm	Spacing mm
HSC-00-50	0	230	230	N/A	N/A
SK-390-50	50	180	230	Shear Key	390
SK-195-50	50	180	230	Shear Key	195
THS-390-50	50	180	230	T-Headed Studs	390
THS-195-50	50	180	230	T-Headed Studs	195
HSC-00-75	0	255	255	N/A	N/A
SK-390-75	75	180	255	Shear Key	390
SK-195-75	75	180	255	Shear Key	195
THS-390-75	75	180	255	T-Headed Studs	390
THS-195-75	75	180	255	T-Headed Studs	195

Figure 3.1: MTS testing machine (Ryerson University).

Figure 3.2: AutoMax5 testing machine (MUN).

Figure 3.3: Modulus of elasticity testing (MUN).

Figure 3.4: MTS 793 testing machine (Ryerson University).

Figure 3. 5: Tinius Olsen UTM machine (MUN).

Figure 3.6: MTS 815 machine for splitting tensile strength of UHP-FRC (Ryerson University).

Figure 3.7: AutoMax 5 for testing the splitting tensile strength (MUN).

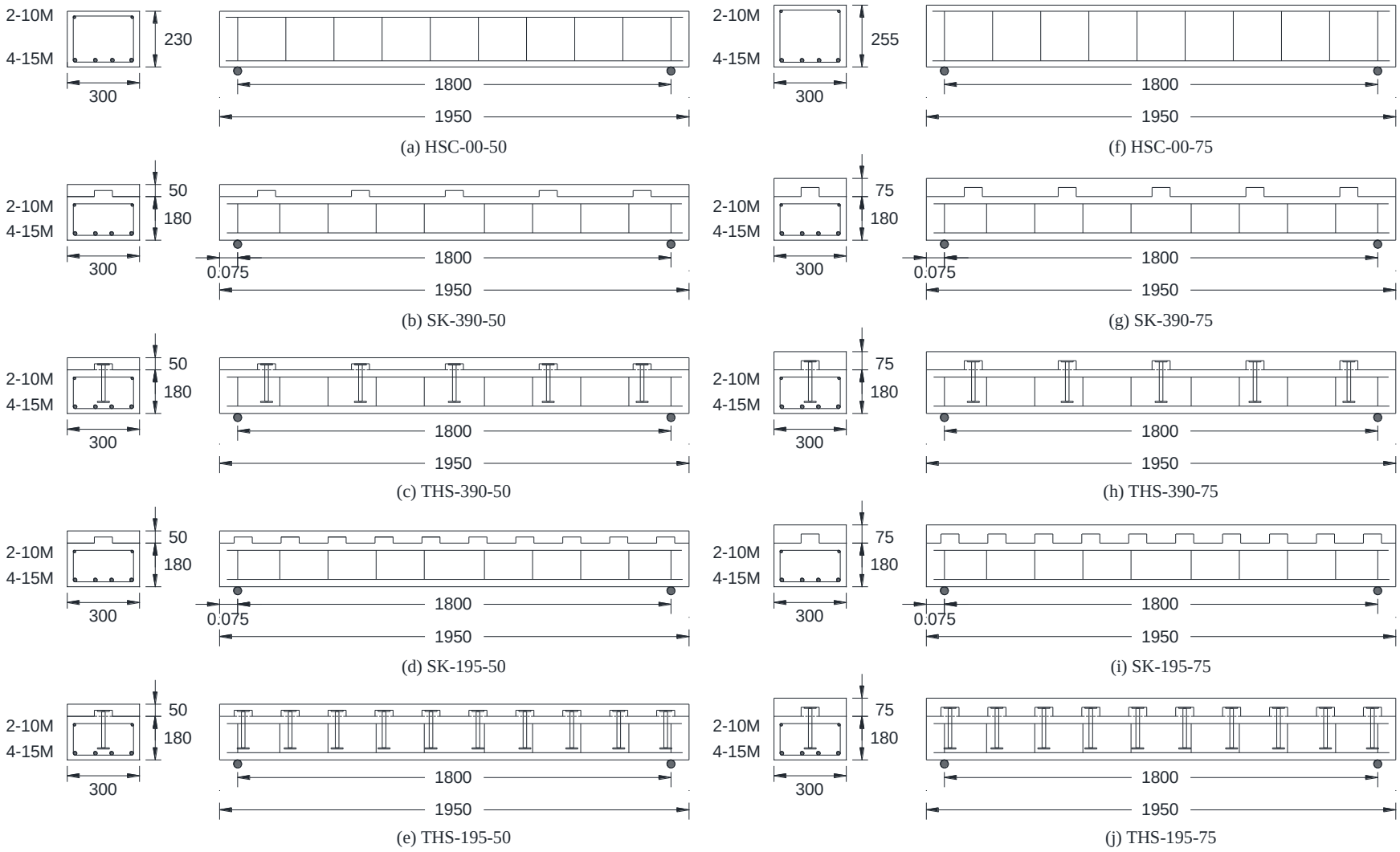

Figure 3.8: Details of flexural test specimens.

Figure 3.9: UHP-FRC (the top layer) casting at Ryerson University (the white foam to create voids for of the shear connectors).

Figure 3.10: The casting procedure of the bottom layer HP-FRC, the middle figure shows the manual pouring of the concrete in the shear keys (MUN).

Figure 3.11: A typical T-headed stud.

Figure 3.12: UHP-FRC (the top layer) curing procedure (Ryerson University).

Figure 3.13: HP-FRC (the bottom layer) after casting and during curing (MUN).

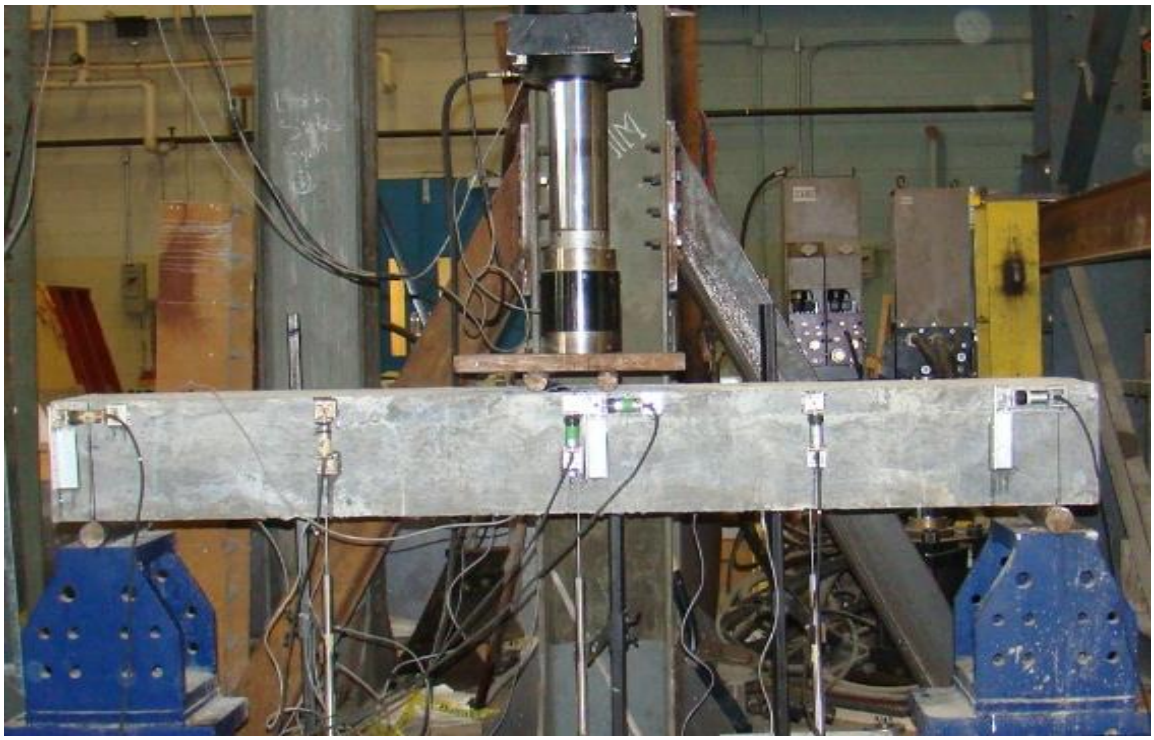

Figure 3.14: Four-Point load test set-up for flexural specimens (MUN).

Figure 3.15: Steel strain gauges location.

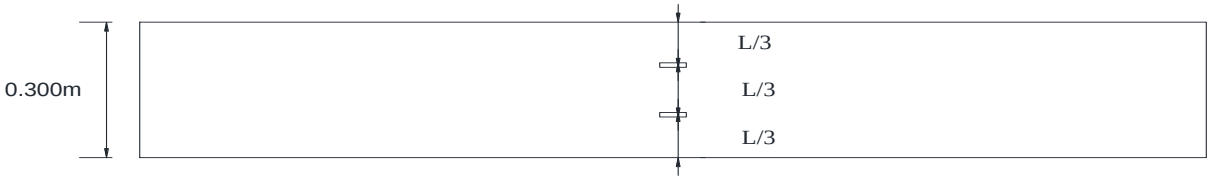

Figure 3.16: Typical Concrete Strain gauge placement.

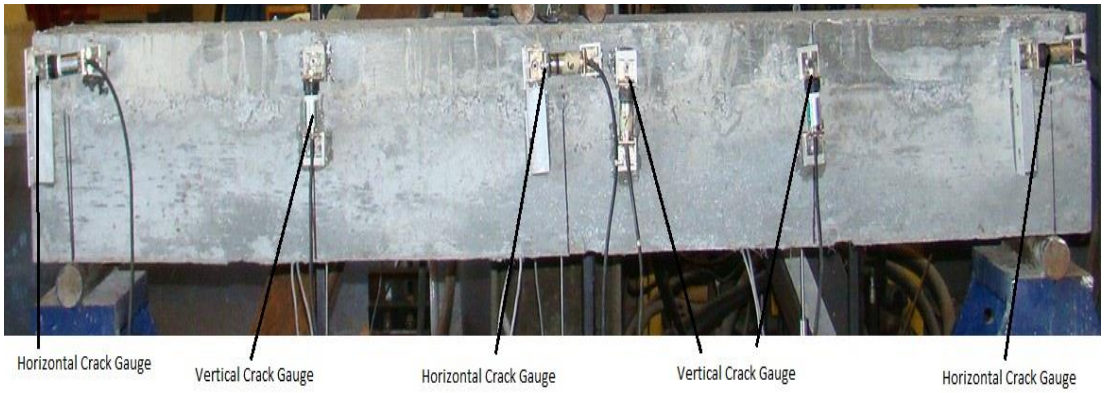

Figure 3.17: Crack displacement transducers used to measure and detect the crack and slippage in the interface between the two layers of concrete.

Figure 3.18: Test procedure (MUN).

Chapter 4

Results and Analysis

4.1 Introduction

The experimental results from the flexural tests are discussed in this chapter. As was previously stated, a total of ten flexural specimens were cast. Eight of the specimens were composite and two were reference non-composite specimens. The parameters were the thickness of the UHP-FRC (top layer), the type of shear connectors, and the spacing between the shear connectors. Details of the flexural specimens are given in Section 3.2 of the thesis.

The experimental data are presented in terms of the crack patterns, load versus deflection, horizontal shear stress versus slip at the interface between the UHP-FRC top layer and the HP-FRC bottom layer, stiffness, ductility, energy absorption and capacity of the specimens. The experimental data was analyzed to investigate the effects of the parameters on the behaviour and capacity of the specimens.

4.2 Crack pattern

During a typical test, each specimen was inspected for the formation of cracks. The load was paused at each load step, which was 2 kips (8.8 kN), and the specimen was inspected for the development of cracks by the naked eye. The crack widths were

measured with a microscope (Section 3.6.5). Figure 4.1 shows the crack propagation for a typical test specimen. The thick lines in the figures show the cracks at failure. Small horizontal lines (dashes) were used to mark the end of the crack propagation, at each load step. The number to the left of the forward-slash at the bottom of the specimen represents the order of appearance of the crack. For example, 32/10 means that the crack appeared at an actuator load of 32 kips and it was the tenth crack to appear.

The first crack usually appeared at the mid-span of the bottom layer almost within the constant moment zone, as expected. The flexural cracks started at the bottom of the specimen and propagated vertically upward. As the load was further increased more vertical cracks started to appear. Few cracks propagated in an inclined manner towards the loading point. The inclined cracks resulted from the increase in the shear stresses. These cracks are called flexural-shear cracks. In most specimens, the cracks occurred in the HP-FRC bottom layer and did not extend into the UHP-FRC top layer. However, in few specimens, the vertical flexural cracks at the mid-span of the HP-FRC layer propagated into the UHP-FRC layer at higher load levels, when the specimen was close to failure. The photographs of all test specimens at failure are shown in Appendix A. Figures 4.2 and 4.3 shows the crack patterns for all the specimens at the service load. Figures 4.4 and 4.5 shows the crack patterns for all the specimens at failure loads.

The cracking patterns at the service load were observed for all specimens. The service load is defined as 40 % of the peak load (Fathifazl et al., 2009). For specimens with 50 mm top layer, the service load was denoted by 40% of the peak load of the reference specimen HSC-00-50. While for specimens with 75 mm top layer, the service load was denoted by 40% of the reference specimen HSC-00-75. All the specimens did

not develop any critical crack or interface crack at this load. Figures 4.2 and 4.3 shows the cracks patterns for the all specimens at the service load.

The cracks in the reference specimens HSC-00-50 and HSC-00-75 developed and propagated in the same manner as the composite specimens. These specimens failed with a major flexural crack forming in the middle of the specimen, as shown in Figures 4.4(a) and 4.5(a).

In general, the similar specimens with top layer thicknesses of 50 mm and 75 mm had approximately the same number and patterns of cracks indicating that the thickness of the top layer had no significant effect on the cracks that developed in the specimens, as shown in the corresponding specimens in Figures 4.4 and 4.5.

Specimens SK-390-50 and SK-390-75 had similar failure modes. These specimens failed prematurely at the interface. The major crack at the interface in those specimens is shown in Figures 4.4(b) and 4.5(b). These specimens did not develop their full flexural capacity due to the interface failure. Consequently, these specimens developed lesser number of cracks and the cracks were shallower.

Specimens SK-195-50 and SK-195-75 experienced similar cracking behavior, as shown in Figures 4.4(c) and 4.5(c). These specimens failed after they developed their full flexural capacity. The specimens also developed similar number of cracks.

Specimens THS-390-50 and THS-390-75 developed a similar cracking patterns. These specimens developed similar number of cracks and reached their full flexural capacity. These specimens also experienced a minor increase in the cracking density from the specimens with shear keys, as shown in Figures 4.4(d) and 4.5(d).

Specimens THS-195-50 and THS-195-75 experienced similar cracking behavior, as shown in Figures 4.4(e) and 4.5(e). The vertical cracks at mid-span in specimens THS-195-50 and THS-195-75 propagated and reached the top layer. These specimens developed a higher number of cracks, when compared to the reference specimens, SK-195-50, SK-195-75, THS-390-50, and THS-390-75. This could be attributed to the fact that the use of T-headed studs and decreasing the spacing between the shear connectors yielded higher deformability and ductility performance.

The specimens with shear keys at 390 mm spacing experienced complete separation between the two layers along the interface. The crack started at the middle then extended throughout the interface to the left or right of the specimens, as shown in Figures 4.4(b) and 4.5(b). The separation crack was accompanied by a sudden drop in the load. Specimens SK-195-50, SK-195-75, THS-390-50, and THS-30-75 experienced a hair line crack along the interface. The specimens with T-headed studs THS-195-50 and THS-195-75 did not develop any significant cracking at the interface. Only small and choppy hair line cracks were developed.

4.3 Load versus deflection

Three Linear variable differential transducers (LVDTs) were used to measure the deflections as mentioned in Section 3.6.1. One of the LVDTs was at the mid-span and the other two were placed, at each side, at quarter span. Figure 4.6 shows a typical load versus deflection for the three LVDTs. The support reactions were equal to half of the actuator load. The applied loads that appear in all the graphs are one half the actuator load and referred to as the applied loads. The deflection values were higher at the mid-span compared to those at a distance of L/4. The two LVDTs at L/4 had a similar

deflection values which is an indication that the specimens were symmetrically loaded. In this section, only the data of the LVDT at the mid-span is discussed. Appendix B shows the full load versus deflection for all test specimens.

Figure 4.7 shows three idealizations for the load versus deflection curve based on experimental observations. Figure 4.7 (a) shows the specimens that failed prematurely at the interface. The load increases gradually until multiple flexural hair line cracks develop and the slope of load deflection curve starts to change. As the load is further increased, the interface peak shear resistance is reached and a sudden drop in the load occurs. The specimen experiences an interface failure and do not develop any ductility. Figure 4.7 (b) shows typical load versus deflection for specimens that developed its full flexural capacity and composite action but with inadequate ductility. The specimen behaves at the beginning in a similar manner. As load is increased, the steel reinforcement starts to yield and the specimen behaves in a plastic manner. The load is further increased until a peak load is reached and the specimen is unable to sustain the load with increased deformation. The specimens fails without developing adequate ductility. Figure 4.7 (c) shows typical stages of a load versus deflection behaviour of a flexural that has developed its full flexural capacity and full composite action with adequate ductility. The specimen behaves in the same manner as specimens (b). However, after the peak load is reached, the specimen continues to sustain the load and it undergoes plastic deformation with gradual decrease in the load. Until the complete failure of the specimens at point (4). Figures 4.8 and 4.9 shows all the load versus deflections curves for all the specimens.

Figures 4.8 and 4.9 shows the load versus mid-span deflection for all specimens. Failure of the interface was accompanied with sudden drop in the load and a sudden change in the slip between the two layers.

4.3.1 Reference specimens

Specimen HSC-00-50 and HSC-00-75 were the reference specimens for those with a top layer thickness of 50 mm and 75 mm, respectively. The reference specimens were reached an peak load of 101 kN and 129 kN, respectively. Then, the load gradually decreased until they failed at load of 92 kN and 105 kN, respectively. The specimens experienced flexural failure similar to Figure 4.7 (c).

4.3.2 Flexural specimens with shear keys

Specimens SK-390-50 and SK-390-75 behaved a similar manner. The specimens reached a load of 70 and 90 kN respectively. At this load, the specimens experienced a sudden drop in the load and a loud noise was heard. That was due to the loss of the shear friction and the failure of one or more shear keys, while the rest of the shear keys were still transferring the horizontal shear stresses. The interface stresses were re-distributed among the other shear keys and the load started to increase again. were loaded until the load reached peak loads of 86 and 92 kN for SK-390-50 and SK-390-75respectively, as shown in Figures 4.8 and 4.9. The specimens maintained their peak load then the load started to decrease gradually until failure. Hence, the remaining shear keys were still transferring the horizontal shear stress along the interface between the two layers of concrete after one or more shear keys failed. The combination of shear keys and spacing of 390 mm yielded a brittle failure of the specimens. These specimens failed due to interface failure as illustrated in 4.7(a).

The peak load for specimen SK-195-50 was 110 kN. The load then started to decrease gradually until a sudden drop in the load occurred in the plastic region at a load of 104 kN, as shown in Figure 4.8.

SK-195-75 achieved a peak load of 130 kN. The load gradually decreased until reached a failure load of 128 kN, as shown in Figure 4.11. The specimen could not sustain the load for a long period and the specimen after developing its full flexural and composite action. The specimens did not develop an adequate ductility as illustrated in 4.7(b).

4.3.3 Flexural specimens with T-headed studs

THS-390-50 attained a peak load of 101 kN. The load gradually decreased until the load reached a failure load of 75 kN, as shown in Figure 4.10. The specimen failed after developing its full flexural capacity with adequate ductility and full composite action. This drop in the load could be attributed to the specimen enduring an excessive deflection. This specimen failed due to flexural failure after developing its full flexural capacity as illustrated in 4.7(c). Small relative slippage was observed in the interface during failure. Although, THS-390-50 had T-headed studs to transfer the horizontal shear stress, five T-headed studs in the specimen were not sufficient to transfer all the horizontal shear stress without relative slippage occurring along the interface between the two layers.

THS-390-75 achieved a peak load of 140 kN. The load gradually decreased until the load reached at a failure of 131 kN, as shown in Figure 4.9. The specimen developed its full flexural capacity and composite action with adequate ductility. The failure was due to flexural failure as illustrated in 4.7(c).

THS-195-50 with T-headed studs, had the highest peak load of 122 kN, of all the specimens with 50 mm top layer, and it failed at a load of 97 kN, as shown in Figure 4.8. The specimen did not experience any slippage at the interface between the two layers. Only choppy hairline crack at the interface was observed. The specimen acted as a true fully composite section and the studs were able to transfer the interface shear stress. The specimen failed after developing its full flexural capacity and adequate ductility as illustrated in 4.7(c). When comparing THS-195-50 to THS-390-50, the increase of the steel reinforcement of the interface, increased the flexural capacity of the specimen and reduces the slippage along the interface.

Specimen THS-195-75 reached a peak load of 150 kN, recorded the highest peak load when compared to all specimens with 75 mm top layer. The specimen reached a failure load of 136 kN after the load had been gradually decreasing, as shown in Figure 4.9. The specimen did not experience any slippage at the interface between the two layers. Only scattered hairline cracks at the interface was observed. The specimen acted as a true composite section and the T-headed studs transferred horizontal shear stresses along the interface shear until failure. This specimen was able to develop its full flexural capacity and composite action with adequate ductility as illustrated in 4.7(c). When comparing THS-195-75 to THS-390-75, the increase of the reinforcement at the interface, resulted in an increase in the flexural capacity of the specimen and reduced the slippage along the interface. THS-195-75 had a similar interface behavior but failed at a higher load than THS-195-50. That could be a result of an increase in the top layer thickness that contributed to the increase of the flexural capacity of the composite specimens, as shown in Figure 4.11.

4.3.4 Effect of other test parameters

There was a significant difference in the behavior of the specimens with T-headed and shear keys. The flexural capacity increased and the relative slippage at the interface between decreased when the shear keys were replaced with T-headed studs. The flexural capacity was further increased when the number of T-headed studs increased. When comparing THS-390-50 to SK-390-50, the first specimens developed a fully composite section, while the later specimen experienced failure at the interface. That resulted in specimen SK-390-50 not able develop the composite action between the two layers of concrete from the shear keys. Even when comparing SK-195-50 to THS-195-50, SK-195-50 was able to develop the full composite action but with insufficient ductility. On the other hand, the later specimen also developed a fully composite action with sufficient ductility, a higher load, and no relative slippage along the interface than SK-390-50. The same conclusion could be drawn for the other specimens when compared to each other. This indicted that the specimens with T-headed studs were able to perform and transfer the horizontal shear stress across the interface better than the specimens with shear keys.

The spacing between the shear keys and T-headed studs had an effect on the flexural capacity, and the horizontal shear transfer, when the spacing between the shear connectors was decreased from 390 to 195 mm. This also resulted in a decreased in the relative slippage along the interface. In some cases, the specimens developed a minimal relative slippage across the interface between the two layers of concrete, confirming that the T-headed studs have a better ability of transferring the horizontal shear stresses along the interface. A slippage of 0.25 mm is the minimum slippage that defines a relative

slippage failure, (Crane ,2012). SK-390-75 developed a slippage of more than 0.25 mm, which is defined as relative slippage failure.

The thickness of the top layer UHP-FRC also had an important impact on the flexural capacity and relative slippage at the interface. The thickness of the top layer was 50 and 75 mm. The specimens with 75 mm gave a higher flexural strength than the specimens with 50 mm top layer thickness. Even the relative slippage decreased, when the thickness of the top layer increased from 50 to 75 mm, as shown in Figures 4.10 and 4.11. All the specimens with a top layer of 75 mm endured a higher load and a decrease in the relative slippage. For example, the specimen SK-390-50 failed at 70 kN from a relative slippage along the interface, while specimen THS-390-75 failed at a higher load of 140 kN after it has developed its full composite abilities. Table 4.1 Summarizes all the peak loads and corresponding deflections for all specimens.

4.4 Ductility and energy absorption

Ductility could be defined as the deformation capability of the structural member without losing its strength during plastic deformation. For flexural specimens, deflection is usually used to estimate the ductility of the member. Therefore, ductility could be determined by the ratio of the mid-span deflection at the peak load (Δ_p) to the mid-span deflection at the yield load (Δ_y), as shown in Figure 4.12. Alternative definition of ductility that also was used the ratio of the mid-span deflection at the failure load (Δ_f) to the mid-span deflection for the yield load (Δ_y), as shown in Figure 4.12. Table 4.2 shows the ductility of all specimens. The composite specimens gave higher values than the reference ones, indicating that the top layer increased the ductility of the specimen. The composite specimens with a 75 mm top led a higher ductility index values than the

specimens with a 50 mm top layer. Specimens SK-390-50 and SK-390-75 failed prematurely and hence they showed poor ductility. The specimens with T-headed studs had better ductility than the specimens with shear keys. This could be due to the better ability of the T-headed studs in transferring the shear across the interface, which results in a better ductility. Using the second definition yielded a higher value of ductility

Table 4.2 shows the energy absorption for all specimens. The energy absorption was calculated as the area under the load versus mid-span deflection curve. The results are divided into two groups: first group are the energy absorption calculated for the specimen until the first load drop and the second group are the energy absorption calculated for the specimen for all the load drops until the specimen completely failed. The composite specimens showed a higher energy absorption values than the reference ones. The increase in the thickness of the top layer led to an increase in the energy absorption capacity. The energy absorption increased when the spacing between the shear connectors decreased and the type of the shear connector changed. THS-195-50 and THS-195-75 had the highest values for energy absorption than all the other composite and non-composite specimens.

4.5 Stiffness

Stiffness could be calculated from the slope of the load versus deflection curve. There is a loss in the stiffness of the member, when the member develops several cracks and goes from the first to the second stage. The stiffness of the member at the second stage is used in determining the deflections at the serviceability limit state. Table 4.3 lists the cracked stiffness for all the specimens. The top layer increased the stiffness after

cracking, when comparing the composite specimens to the reference ones, as shown in Table 4.3.

There was a small enhancement in the stiffness between the composite specimens with a top layer thickness of 75 mm and composite specimens with top layer thickness of 50 mm, as shown in Table 4.3. this could be as a result that the difference between the top two layers was only 25 mm.

4.6 Load-strain behavior

To measure the strain in the concrete and the reinforcement, a total of eight strain gauges were used. Six strain gauges were used to measure the strain in the reinforcement and two strain gauges were used to measure the strain the in the concrete. Figure 4.13 shows a typical load versus strain graph. For the reinforcement strain, the strain gauges experienced a linear behaviour for the pre-cracking stage. The reinforcement strain increased, after cracking, because the concrete started to lose its ability to resist the loads in tension, as shown in Figure 4.13. Some of the strain gauges were damaged during casting. The steel strain gauges stopped working after the reinforcement yielded. Appendix C shows of the entire load versus steel strain graphs for all specimens. Appendix D shows all the load versus concrete strain for all specimens.

All the steel strains experienced the same trend; each middle steel bar had three strain gauges one on the left, one on the right, and on the middle as mentioned before in section 3.6.3. However, the mid-span strains exhibited a sudden increase, after cracking. On the other hand, the strains on the left and right experienced a gradual increase, after cracking. This may be due to the sudden increase of the width of the crack close to the strain gauges, as shown in Figure 4.13. The strain continued to increase gradually, after

the sudden increase. All The concrete strains followed the same trend. The strains gradually increased, until the load peaked and the strain exhibited a sudden increase, as shown in Figure 4.13.

4.7 Crack width

The crack width is an important aspect to consider in the serviceability limit state. As previously stated the crack width was monitored and measured throughout the test. Figures 4.14 and 4.15 depicted the moment versus crack width for all the specimens. The crack width measurements were recorded for all the specimens until the specimen reached 70% of the moment capacity for safety purposes. Most of the crack width measurements revealed similar trends and values with the same group. This could be attributed to the fact that the bottom layer of all the composite specimens had the same concrete mixture, the same reinforcement ratio, and the same fibre ratio.

The specimens with 75 mm top layer recorded a smaller crack width than the specimens with 50 mm top layer. This was due to the larger thickness for the specimens with 75 mm top layer. The crack width for specimens SK-390-50 and SK-390-75 were not recorded.

4.8 Cracking moment

The experimental cracking moment is the moment that corresponds to the load at which the first crack that appeared in the test specimen. The crack was detected by the naked eye during the test. The first crack typically appeared in the area of constant moment. The theoretical moment cracking was also calculated based on the following codes: the ACI 318M-14, CSA A23.3-14, Eurocode 2-04, and the CEB-FIB. The code equations for calculating the crack width (Equation 4.1 to 4.4) are shown at the end of

the section. Table 4.4 shows a comparison between the code predictions and the experimental cracking moments and the deflection at the first crack. The results showed that the experimental cracking moment was slightly higher than the code values, as the ACI and CSA equations gave a conservative estimate. The Eurocode and CEB-FIB overestimated the cracking moment for most of the specimens. Most of the experimental results were similar to each other as the HP-FRC layer was the same for all specimens. Although, HP-FRC contains fibres, this did not affect the moment cracking. This could be explained as the fibres only start to work when the crack is formed and the modulus of rupture does not necessarily contribute to the first crack. The ratio for theoretical to experimental cracking moments varied from 0.68 to 1.19 for the ACI, from 0.66 to 1.15 for the CSA, from 0.69 to 1.5 a for the EC, and from 0.96 to 1.63 for the CEB-FIB. The could be resulting from the fact that ACI and CSA does not consider the effect of the longitudinal bars in the equation. EC2 and CEB-FIB considers the second moment of area for the cracked section which predicts a higher value of the moment cracking. None of the code equations included the effect of the fibres.

Code	Equation		Note	
ACI 318M-14	$M_{cr} = f_r \frac{I_g}{y_t}$	Where,	$f_r = 0.6\lambda\sqrt{f_c'}$	(4.1)
CSA A.23.3-14	$M_{cr} = f_r \frac{I_g}{y_t}$	Where,	$f_r = 0.62\lambda\sqrt{f_c'}$	(4.2)
EC 2-04	$M_{cr} = f_{ctm} \frac{I_u}{(h - x_u)}$	Where,	$f_{ctm} = 0.3 f_{ck}^{0.67}$	(4.3)

CEB-FIB $M_{cr} = W_1 f_{ctm}$ Where, $W_1 = \frac{bh^2}{6}$ (4.4)

4.9 Serviceability

The behaviour at the service load was investigated for all specimens. Two definitions were used to define the service loads for each specimen. For both definitions, the service load was denoted by 40 % of the peak moment as used by (Fathifazl et al., 2009) . The first definition is the design service load and is denoted as follows: for each group 50 mm and 75 mm top layer denoted by 40% of the peak load of the reference specimen. The second definition is the experimental service load, which is denoted by the 40 % of the peak moment of each specimens. The observations at the service loads were represented by the crack width and the deflection at this load. To calculate the theoretical deflection at the service load, the elastic beam theory (Equation 4.5) was used. The moment of inertia is calculated using the ACI code (Equation 4.6). Table 4.5 shows a list of all the design service load and experimental and theoretical deflection for each tested specimen. The theoretical deflections from the elastic beam theory (Equation 4.5), as shown in Table 4.5. The predicted deflections were conservative for the specimens with 50 mm top layer. On the other hand, the theoretical deflections were slightly unconservative. Table 4.6 shows the reference service load corresponding to 40 % of the peak load. The data showed that most of the specimens followed the same trend for the design service loads. The ACI 318-14 and CSA A23.3-14 loads recommend that the deflection should not exceed L/240, which is 8.1 mm. When comparing the experimental results to the code limits, none of the specimens exceeded this limit, as shown in Table 4.5. The ratio, of the experimental service load over the theoretical service load for the specimens with a 50 mm top layer thickness, ranged from 0.89 to

1.16 and for specimens with a 75 mm top layer thickness ranged from 0.93 to 1.3. The ratio was not calculated for specimens SK-390-50 and SK-390-75 as the two specimens failed pre-maturely from an interface failure. The deflection of the composite specimens did not have a significant difference from the non-composite specimens. The top layer did not contribute to the deflection at the serviceability level. This could be as a result that the deflection at the service load depended more on the modulus of elasticity. The modulus of elasticity of HP-FRC did not differ greatly from the UHP-FRC, with values of 40 GPa and 50 GPa, respectively.

$$\delta_{s,cal} = \frac{M_a}{24E_cI_e}(3L^2 - 4a^2) \tag{4.5}$$

$$I_e = I_{cr} + (I_g - I_{cr})(\frac{M_{cr}}{M_a}) \leq I_g \tag{4.6}$$

The crack width is an important aspect to check at the serviceability limit state. The same two definitions for service load were also used for comparing the experimental and code crack widths. Table 4.6 lists the comparison of the crack width for all the specimens at the design service load, to the code predictions. Table 4.7 shows the experimental crack width at the service load corresponding to 40 % of the peak moment of each specimen. The predictions of four code equations were used and compared to the experimental values. The codes were CSA A.23.3-14, Euro code 2-04 (CEN (Comité Européen de Normalisation), 2004), Rilem TDF (RILEM TC 162-TDF members, 2003), and Britch Standard (British Standard Institution, 2002). The code equations for predicting crack width are shown at the end of this section. The ACI 318M-14 equation does not provide explicit calculations for crack width. The Rilem equation is the only equation that takes into account the fibre contribution in the calculation of the crack

width. The British code equation is based on the factors: how close is the section to the reinforcement and concrete cover, how far is the concrete surface from the neutral axis, and the average strain at the section.

The crack widths of all specimens at the service load were almost the same, which means that the top layer did not make any affect for the crack width at the service load, as shown in Tables 4.7 and 4.8. This was due to the fact that all the cracks happened in the bottom at the tension reinforcement, at the bottom layer for the composite specimens, and all the specimens had at the same concrete mixture and reinforcement ratio. Most of the experimental crack width was below the allowed code limits. The two definitions yielded lower experimental values than the theoretical values, as shown in Tables 4.7 and 4.8. Most of the code equations over estimated the crack width. The crack width was not calculated for specimens SK-390-50 and SK-390-75as they experienced pre-maturely interface failure. For the design service load, the Rilem TDF was the most consistent, as it is the only code that takes the fibres into consideration, while calculating the crack width. While the CSA A.23.3-14 gave the highest estimates and hence it is overly conservative. The British Standard and the Eurocode gave similar predictions. The ratio of the experimental over the theoretical crack width for the British Standards varied from 0.29 to 1.00, for CSA ranged from 0.18 to 0.67, Eurocode varied from 0.31 to 1.09, and Rilem ranged from 0.47 to 1.71, as shown in Table 4.7. The British Standard equation was the most consistent with the experimental crack width, for the two definitions that were used. Based on a serviceability load of 40% of the experimental peak load, the ratio of the experimental over the theoretical crack width for the British

Standards varied from 0.31 to 0.78, for CSA ranged from 0.19 to 0.44, Eurocode varied from 0.31 to 0.71, and Rilem ranged from 0.50 to 1.75, as shown in Table 4.8.

CSA A.23.3-14

$$W_k = 0.011\beta\sigma_s \sqrt[3]{d_c A} * 10^{-3} \tag{4.7}$$

EC2 2-04

$$W_k = S_{rm}(\varepsilon_{sm} - \varepsilon_{cm}) \tag{4.8}$$

$$S_{rm} = 3.4c + 0.425k_1 k_2 \frac{\phi}{\rho_{eff}} \tag{4.9}$$

$$\varepsilon_{sm} - \varepsilon_{cm} = \frac{\sigma_s}{E_s} - \frac{k_t f_{ctm}(1 + n\rho_{eff})}{E_s \rho_{eff}} \tag{4.10}$$

BS 110-97

$$W_k = \frac{3a_{cr}\varepsilon_m}{1 + 2\frac{(a_{cr} - c_{\min})}{h - x}} \tag{4.11}$$

$$\varepsilon_m = \frac{h - x}{d - x}\varepsilon_s - \frac{b(h - x)^2}{3E_s A_s (d - x)} \tag{4.12}$$

Rilem TDF

$$W_k = \beta S_{rm} \varepsilon_{sm} \tag{4.13}$$

$$S_{rm} = (50 + 0.25k_1 k_2 \frac{\phi}{\rho_{eff}}) \frac{50}{L_f / d_f} \tag{4.14}$$

$$\varepsilon_{sm} = \frac{\sigma_s}{E_s}(1 - \beta_1 \beta_2 (\frac{\sigma_{sr}}{\sigma_s})^2) \tag{4.15}$$

β is the coefficient of the design of the value, where 1.7 for a minimum dimeson of 800 mm and 1.5 for a minimum dimension of 300 mm.

4.10 Moment capacity

Table 4.1 shows a summary of all the test results. The data showed that the adding of the top layer of UHP-FRC had increased the capacity of the specimens. The capacity has further increased with a better transfer of the horizontal shear stress across the interface. SK-390-50 and Sk-390-75 experienced a different behaviour than the other specimens. These specimens did not achieve their full flexural capacity when compared with the reference specimens. Table 4.9 consists of a comparison of the calculated nominal moment and the experimental testing moment.

Specimens SK-195-50 specimen had a slight increase in its flexural capacity by 9 % from the reference specimen (HSC-00-50), and 22 % increase from SK-390-50. SK-195-50 had a total of ten shear keys, as the increase in number of shear keys reduced the initial slippage in the specimen and increase the flexural capacity of the composite element. When comparing SK-195-75 to SK-195-50, specimen SK-195-75 had a higher flexural capacity by 20 % than SK-195-50. This is due to the increase in the top layer thickness which led to an increase in the flexural capacity of the composite specimen, as shown in Figure 4.11. SK-195-75 gave higher flexural capacity by 1 % from HSC-00-75.

For flexural specimens with T-headed studs, THS-390-50 gave the same peak load as HSC-00-50, as the bond slippage may have affected the flexural capacity of the composite specimen, as shown in Figure 4.8. When specimen THS-390-75 was compared with the reference specimen HSC-00-75, it resulted in an increase in the peak load by 5 %.. THS-195-50 had a 21% in flexural capacity over the reference specimen

(HSC-00-50), as shown in Figure 4.8. THS-195-50 also had an increase in its flexural capacity of 11 % from SK-195-50 because the T-Headed studs had a better performance in transferring the horizontal shear stress along the interface, as shown in Figure 4.11. THS-195-50 performed better than SK-390-50, which confirms that the T-headed studs are better than the shear keys in transferring the horizontal shear stress along the interface. THS-195-75 had an 11% in flexural capacity over the non-composite reference specimen (HSC-00-75), as shown in Figure 4.9. THS-195-75 also had an increase in its flexural capacity of 9 % from SK-195-75 and specimen THS-195-75 was also better than SK-390-75. THS-195-75 also had a significant increase in the flexural capacity by 23 % from specimen THS-195-50, due to the increase in the thickness of the top layer.

The nominal moment was calculated with different equations and compared to the experimental nominal moment for all of the composite and the non-composite specimens. Two code equations: CSA A23.3-14, and ACI 318M-14, ACI comitte 544 recommendations and the equation proposed by Imam et. Al (Imam, Vandewalle, & Mortelmans, 1995) were used. ACI 318M-14 and CSA A23.3-14 equations do not take the fibre contribution into account in calculating the nominal moment. On the other hand, ACI 544 and Imam's equation consider the fibre contribution. The main difference between ACI 544 and Imam's equation, is that the Imam takes the fibre contribution 2.6 times the value used by ACI 544. Table 4.9 lists the experimental nominal moment for all the tested specimens and the theoretical nominal moment calculated using the code and the proposed equations.

All the codes and the proposed equations were conservative in predicting the nominal moment. Higher flexural capacity for most specimens was observed when comparing the estimated nominal moment. This could be attributed to the high compressive strength of the top layer (which was made of UHP-FRC and a compressive strength of 170 MPa), which enhanced the ultimate capacity of the composite specimens. Specimens SK-390-50 and SK-390-75 had a lower nominal moment than expected as these specimens failed at the interface. When the shear connectors spacing was reduced and the T-headed Studs replaced the shear keys, a higher nominal moment than all the theoretical nominal moment was observed.

4.11 Horizontal shear transfer

To test the horizontal shear transfer along the interface between the two layers of concrete, slip gauges were place on the specimens at three different locations to measure the slippage. The slip gauges were Crack Displacement Transduces (CDT). The slip gauges were place in the middle and at the two ends on top of the supports of the specimen, as mentioned in Section 3.6.5. All specimens were loaded monotonically until failure. Failure of the interface was defined by a sudden drop in the load carting capacity. In addiction to specimen to have failed by relative slippage, the specimen should have a relative slippage more than 0.25 mm. All the data generated from the slip gauges were recorded on by high speed data acquisition system.

The interface shear stress versus slip graphs were plotted from the data for all specimens except for two, as shown in Figure 4.16. Most of the samples experienced similar mode of failure. As the load was increased and the interface started to crack and some slippage occurred, until the bond fails at the interface between the two layers of

concrete. THS-195-50 and THS-195-75 didn't record any relative slippage along the interface between the two layers of concrete. The failure in the interface was assumed to occur if the specimen had a slip of more than 0.25 mm. These specimens did not reach this value; hence there was no relative slippage at the interface along the two layers. The other composite specimens surpassed this number. The slip gauges were removed after the specimen experienced excessive deflection, in order to avoid any damage to the sensors.

SK-390-50 and Sk-390-75 experienced similar trend as both specimens failed when one of the shear keys started to fail, as shown in Figure 4.16. However, the specimens still sustained load as not all the shear keys have failed. Some of the shear keys were still functioning and after re-distribution transferred horizontal shear stress along the interface. The interface failure started with a crack in the middle of the specimens then extended to the left or the right side of the specimen. As the load increased the slippage tended to increase at only one side.

For specimen SK-195-50, there was an error in the data collected from the slip gauges. From all the other data collected for this sample, slippage occurred that was indicated by a sudden drop in the load.

The number of shear keys increased in specimen SK-195-75. The specimen endured a higher load and a smother failure of the bond, as shown in Figure 4.6. The failure trend of the specimen was similar to a typical trend. This was due the shear keys capability of transferring the horizontal shear stress along the interface between the two layers of concrete. The specimen also had a lower slip value than SK-390-75 and SK-390-50 and less than 0.25 mm. SK-195-75 did not fail from interface failure. This

resulted from decreasing the spacing between the shear connectors which lead to a better transfer of the horizontal shear stresses across the interface. The second reason of the decrease of the slip could be have due to the increase of the thickness of the top layer.

THS-390-50 and THS-390-75 experienced similar trend but with different loads. The specimens only developed hairline crack and minimal elastic slippage along the interface as the T-headed studs were still transferring the shear loads, as shown in Figure 4.1. These two specimens gave slip values lower than 0.25 mm, proving that the T-headed studs were more efficient in transferring the horizontal shear stresses along the interface.

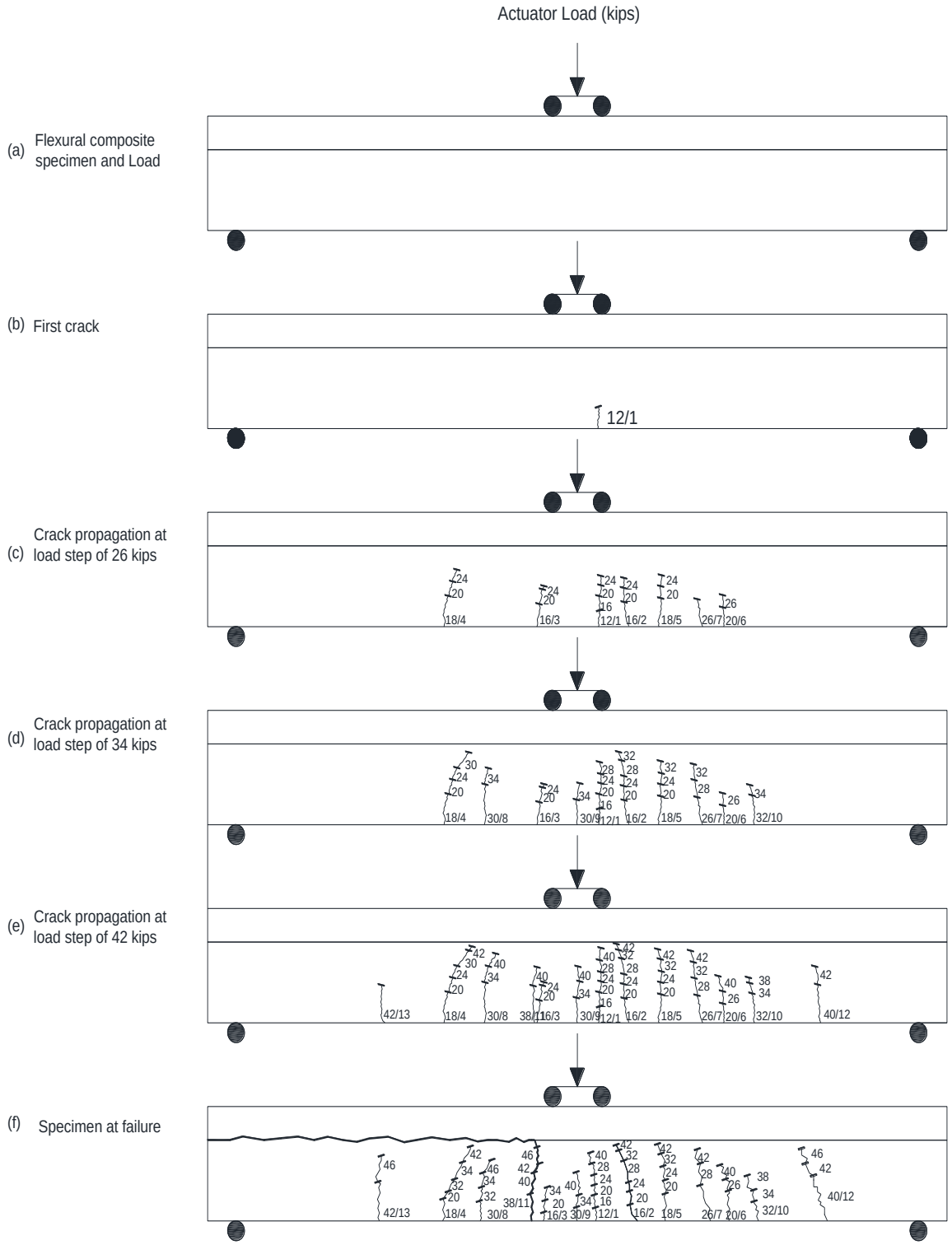

Figure 4.1: Typical crack formation and the corresponding actuator loads (SK-195-75).

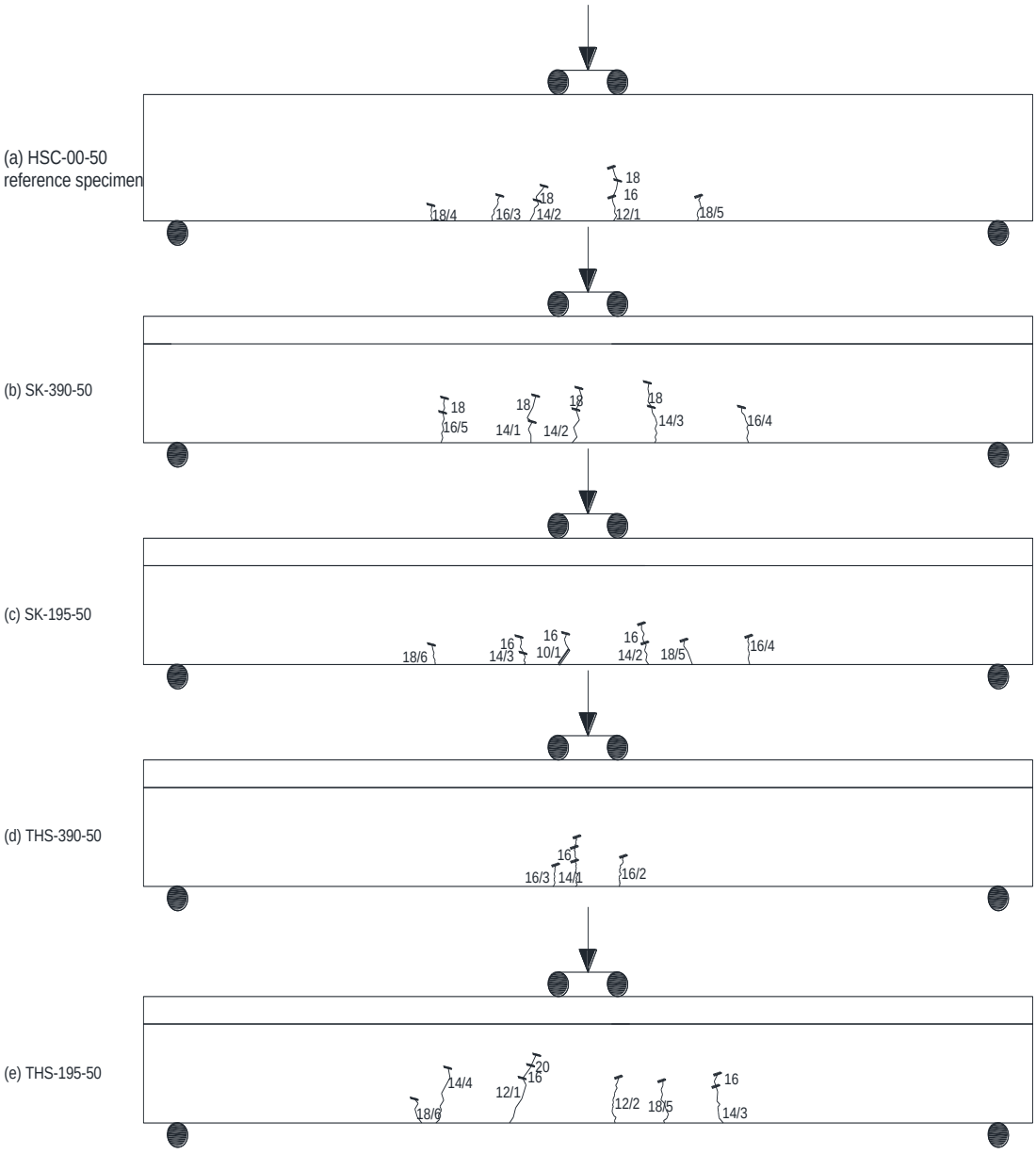

Figure 4.2: Crack patterns at service load (18 kips) for the specimens with a 50 mm top layer.

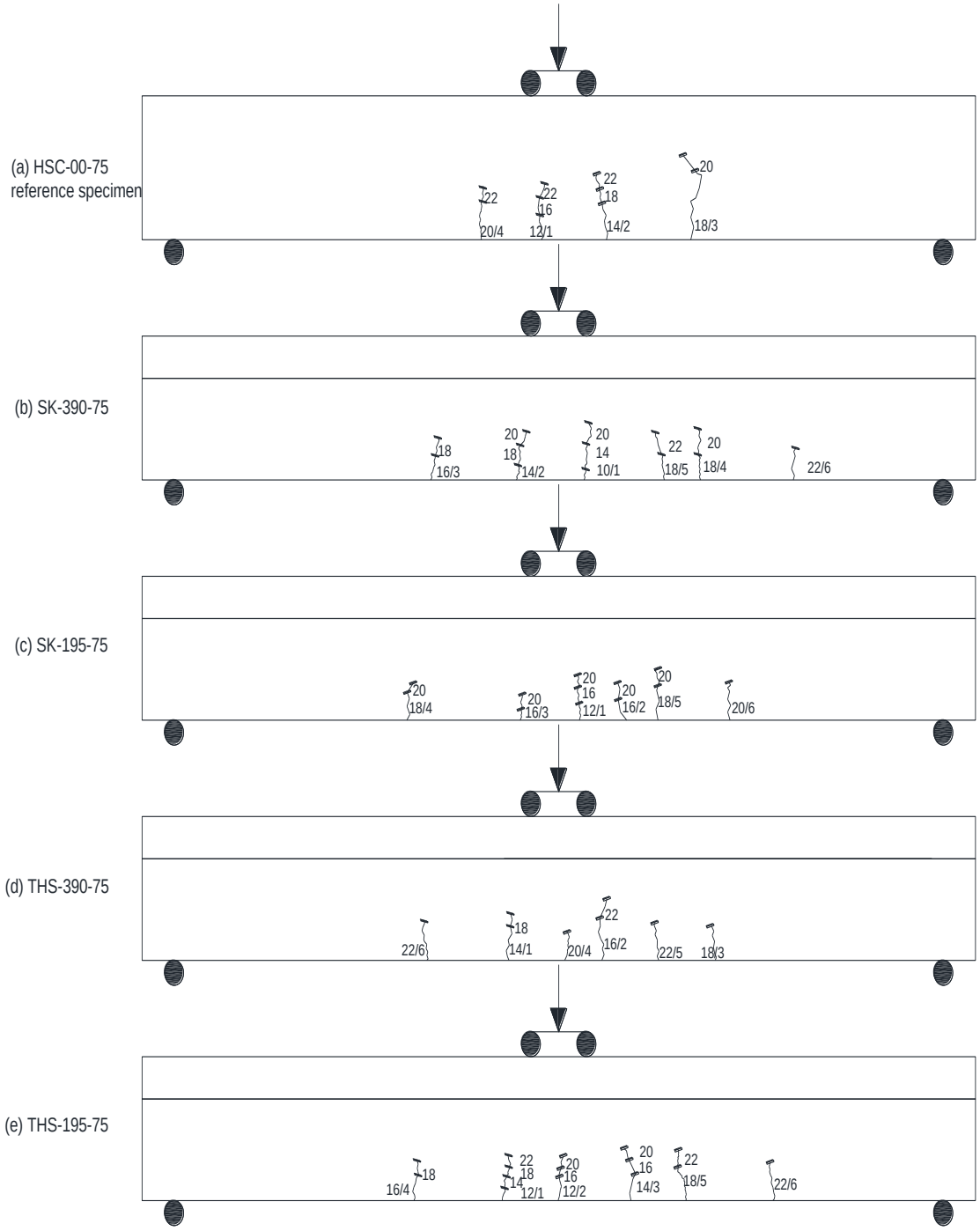

Figure 4.3: Crack patterns at service load (22 kips) for the specimens with a 75 mm top layer.

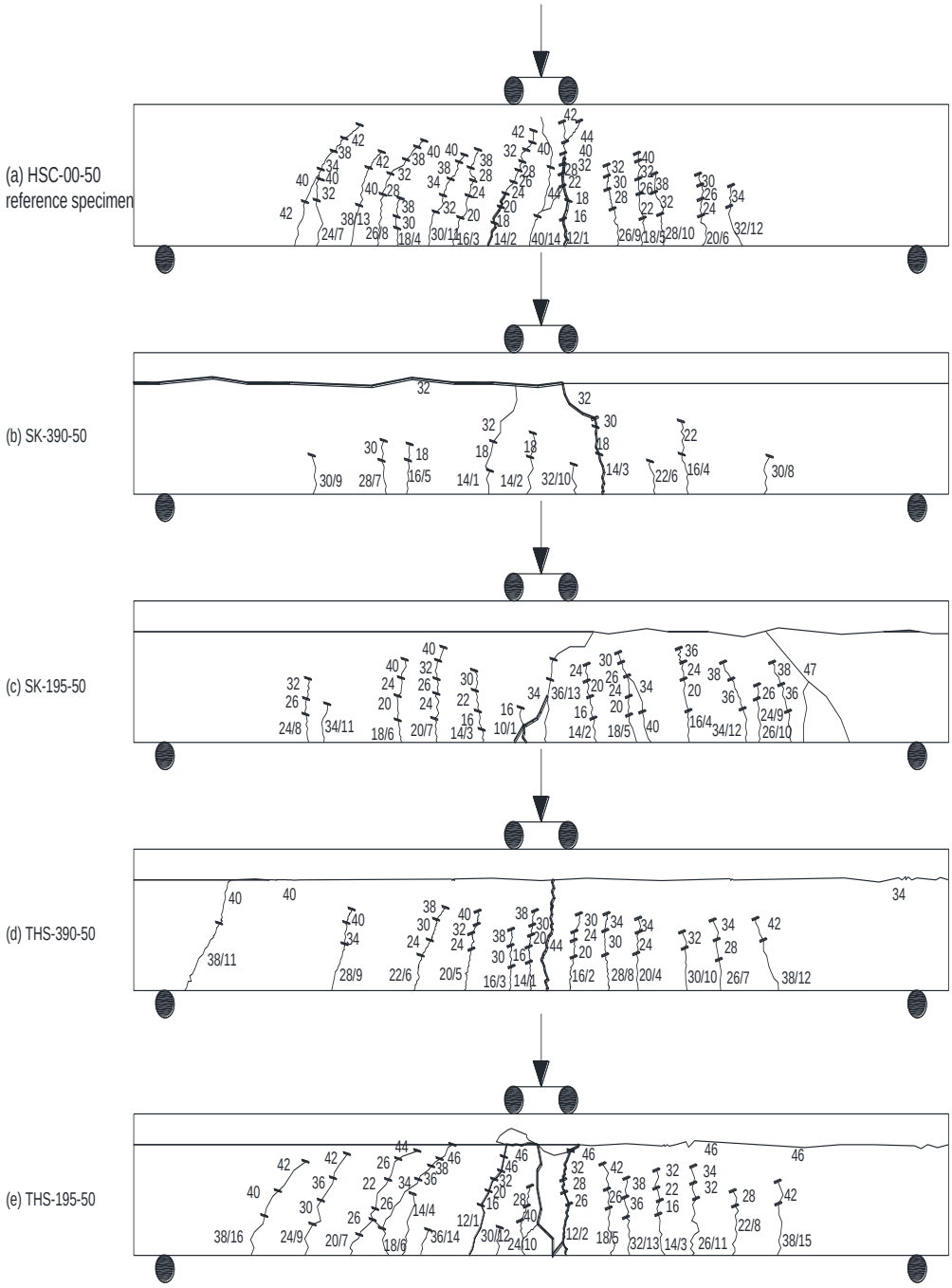

Figure 4.4: Crack patterns at failure for the specimens with a 50 mm top layer.

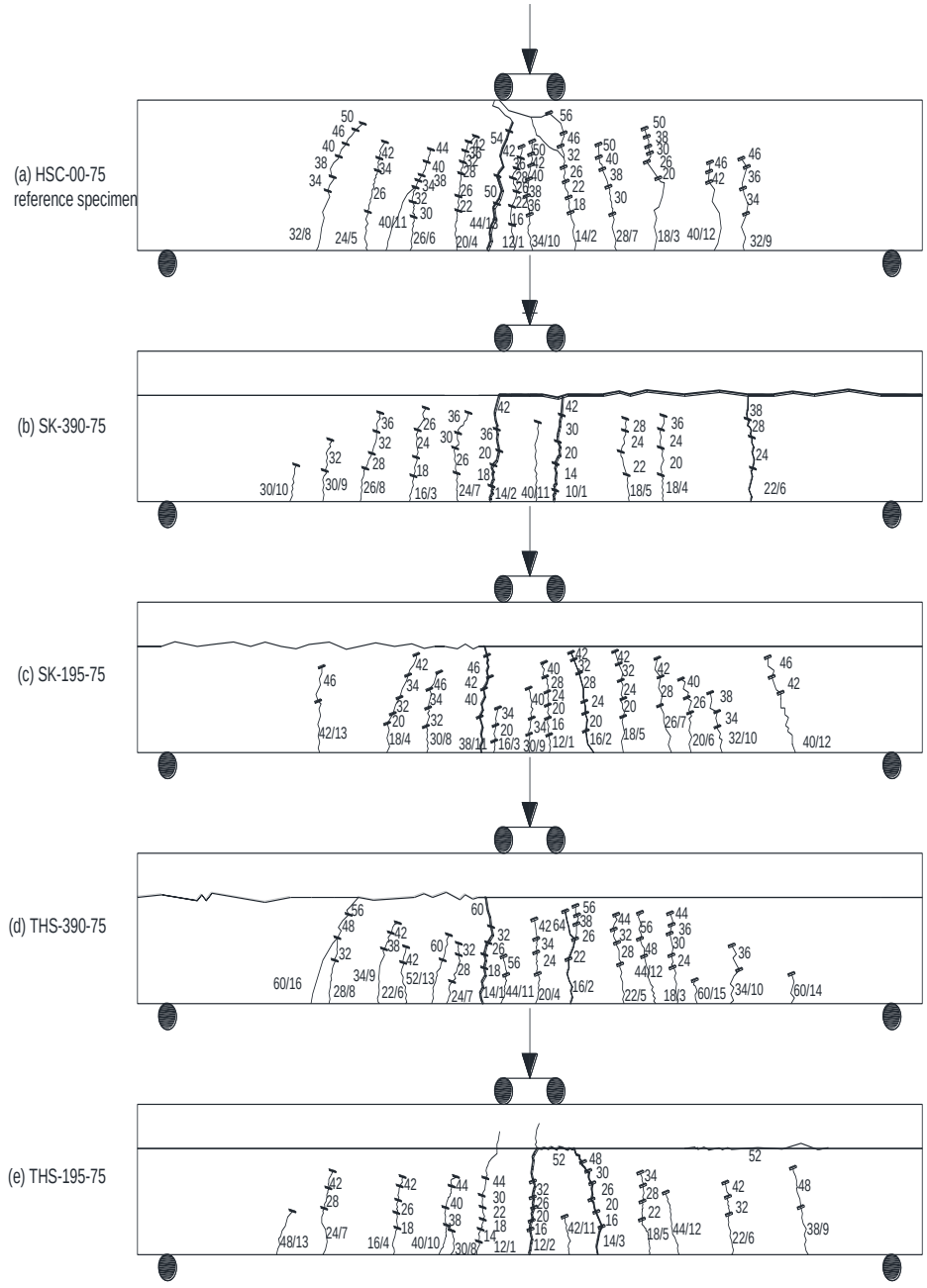

Figure 4.5: Crack patterns at failure for the specimens with a 75 mm top layer.

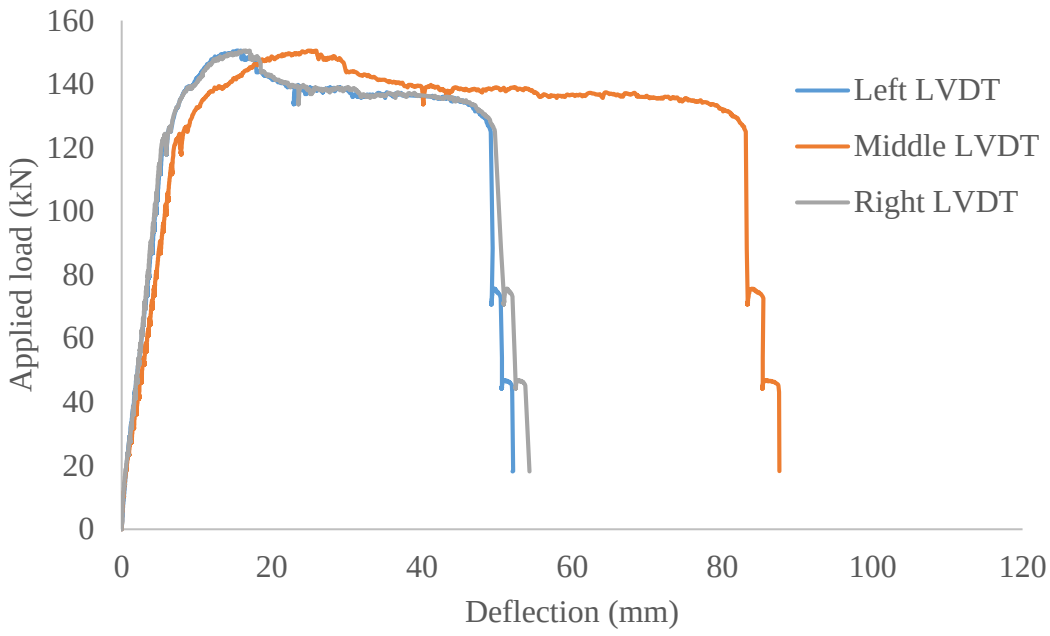

Figure 4.6: Typical load versus deflection curves.

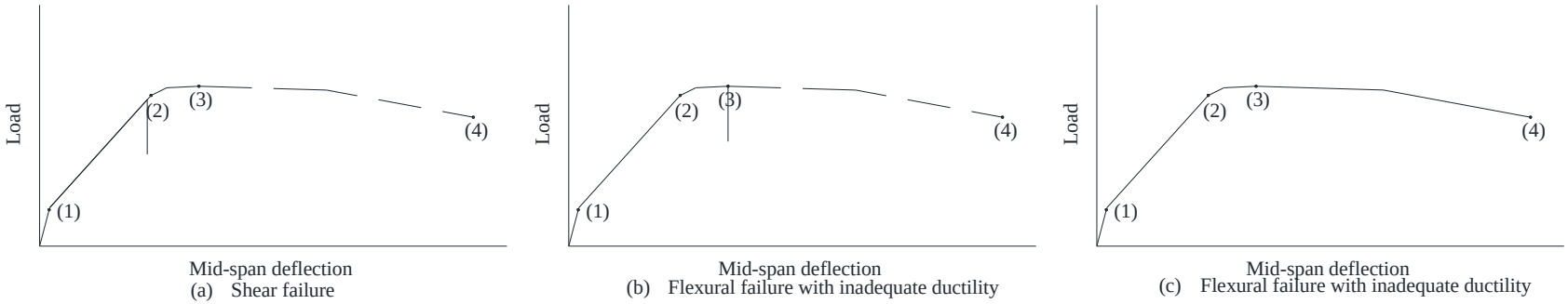

Figure 4.7: Typical idealization of load versus deflection of a flexural specimen; (1) multiple hairline cracks, (2) yielding of steel, (3) peak load, and (4) specimen failure.

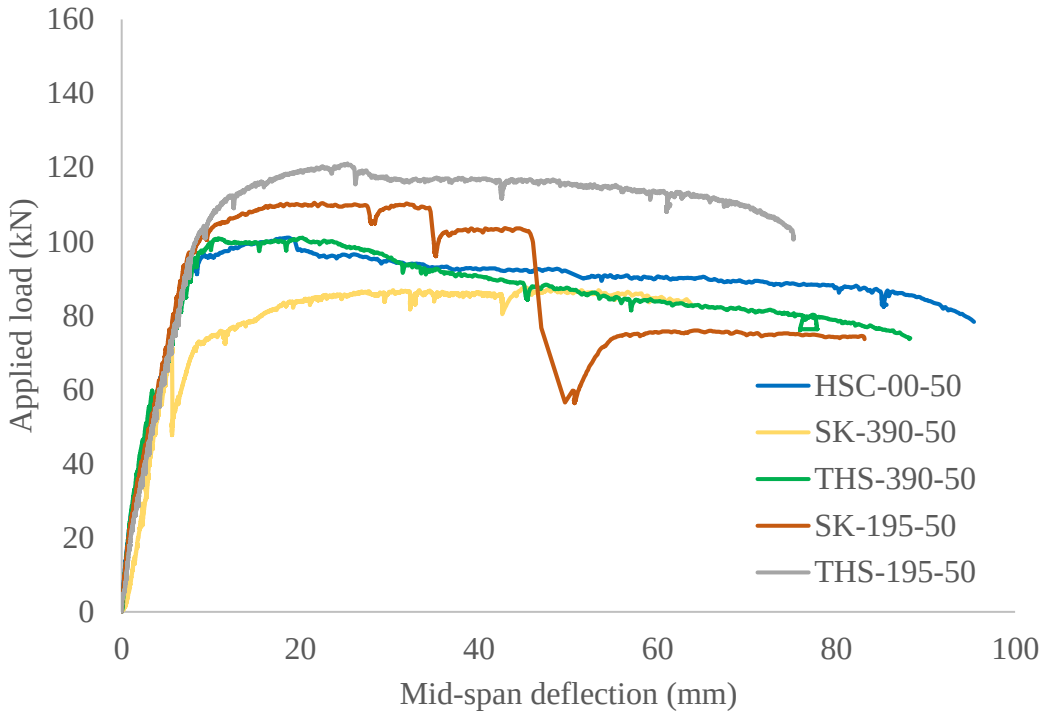

Figure 4.8: Load versus mid-span deflection for specimens with a 50 mm top layer.

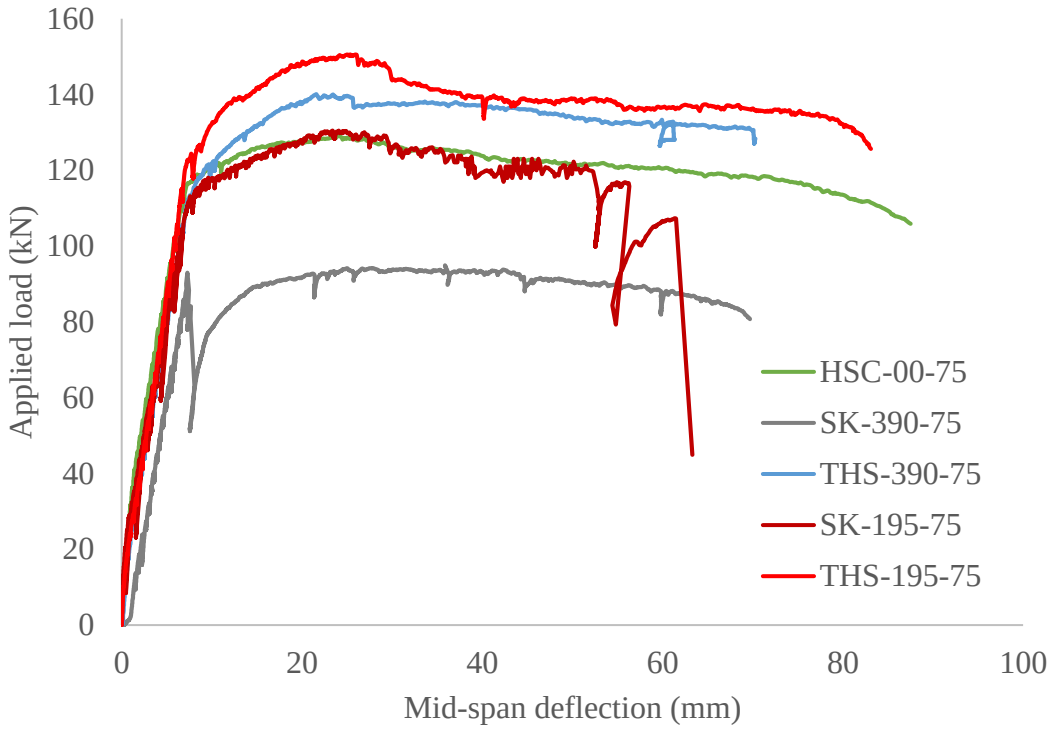

Figure 4.9: Load versus mid-span deflection for specimens with a 75 mm top layer.

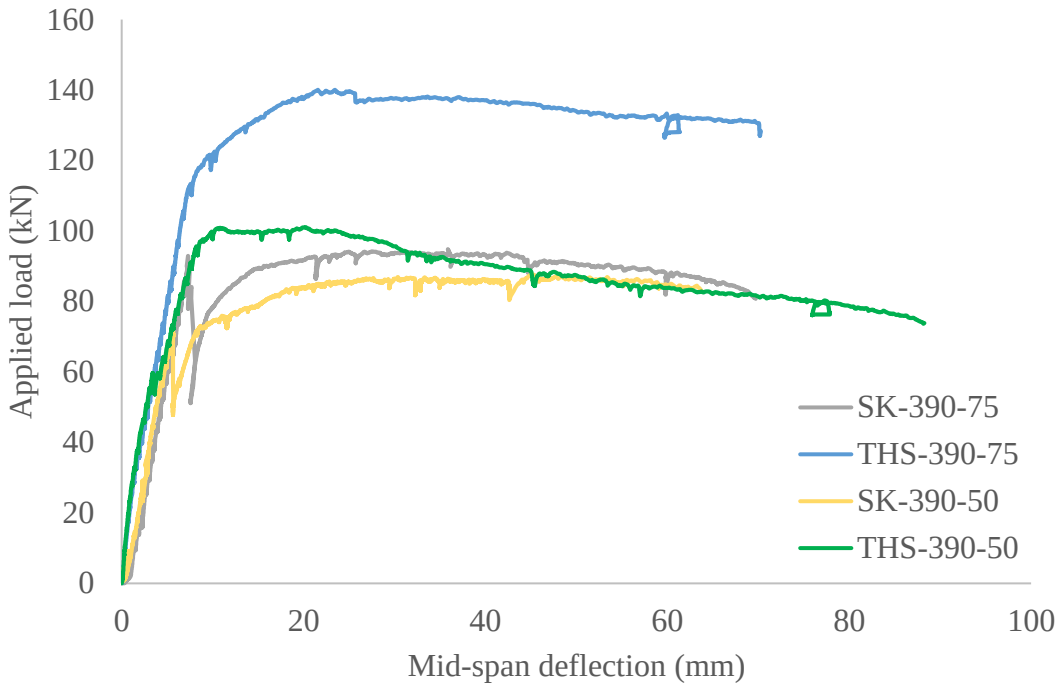

Figure 4.10: Load versus mid-span deflection for composite specimens with shear connector spacing of 390 mm.

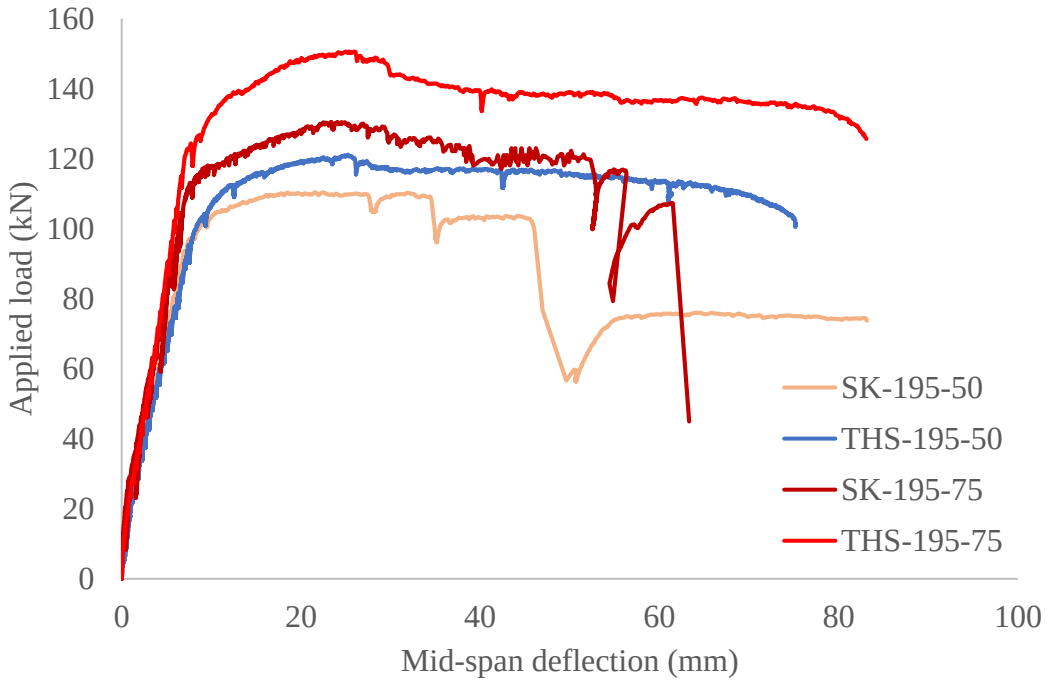

Figure 4.11: Load versus mid-span deflection for composite specimens with shear connector spacing of 195 mm.

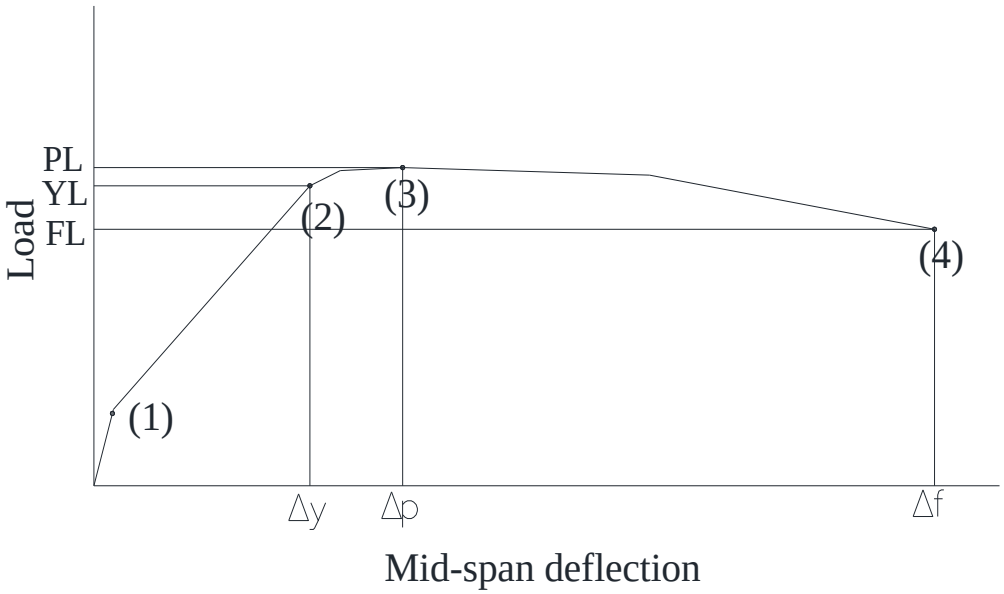

Figure 4.12: Notations used for ductility definitions.

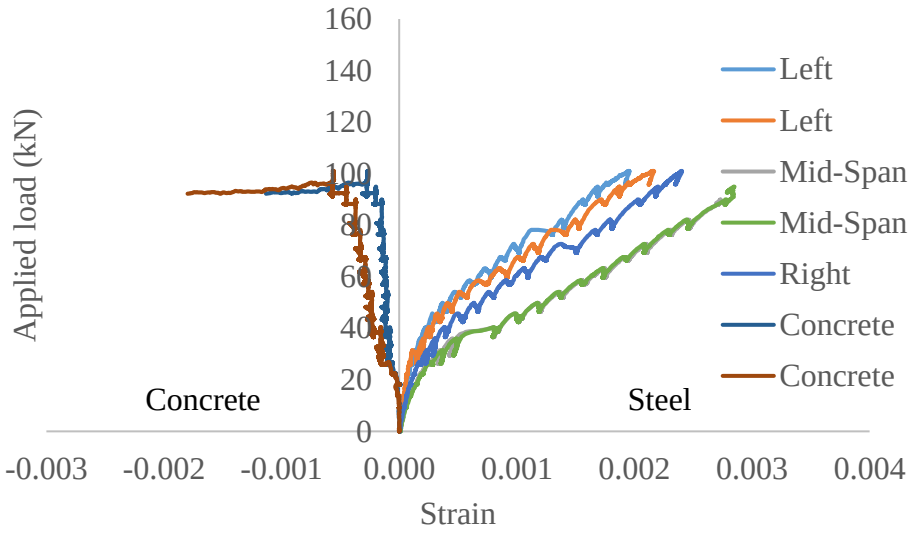

Figure 4.13: Typical load versus strain (THS-390-50).

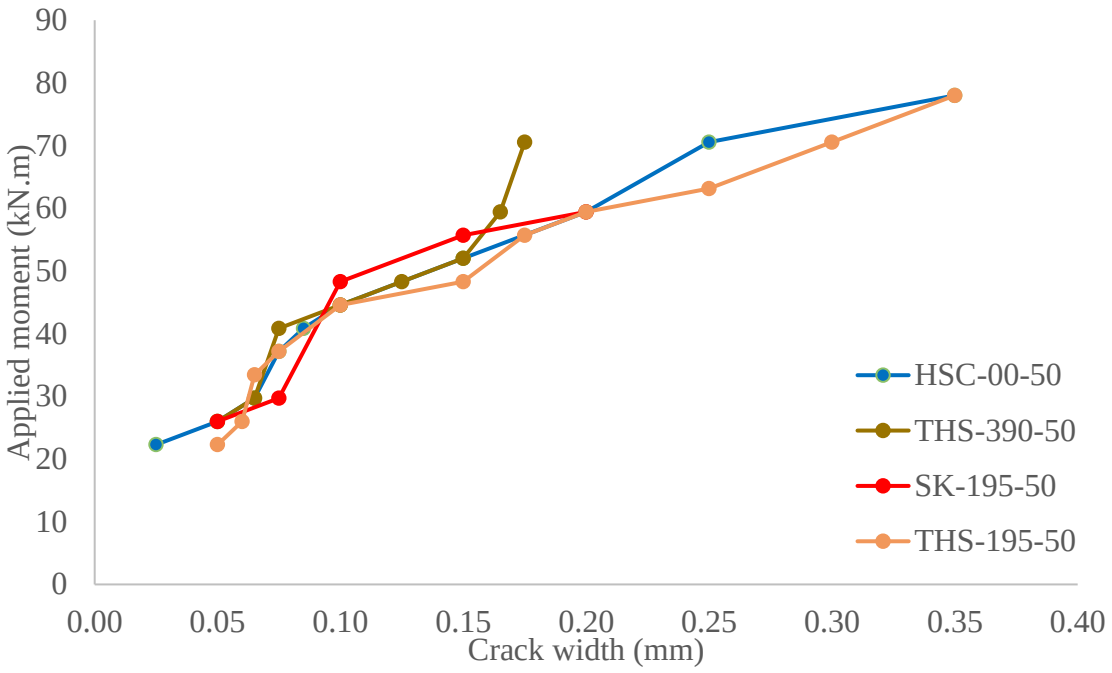

Figure 4.14: Moment versus crack width for specimens with 50 mm top layer.

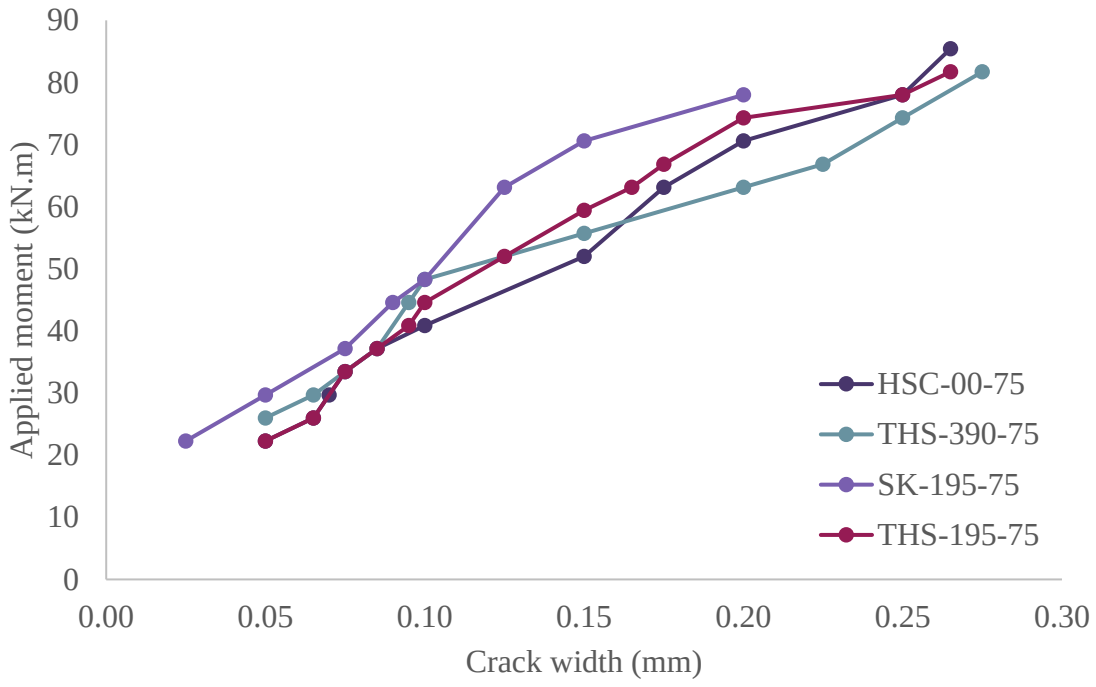

Figure 4.15: Moment versus crack width for specimens with 75 mm top layer.

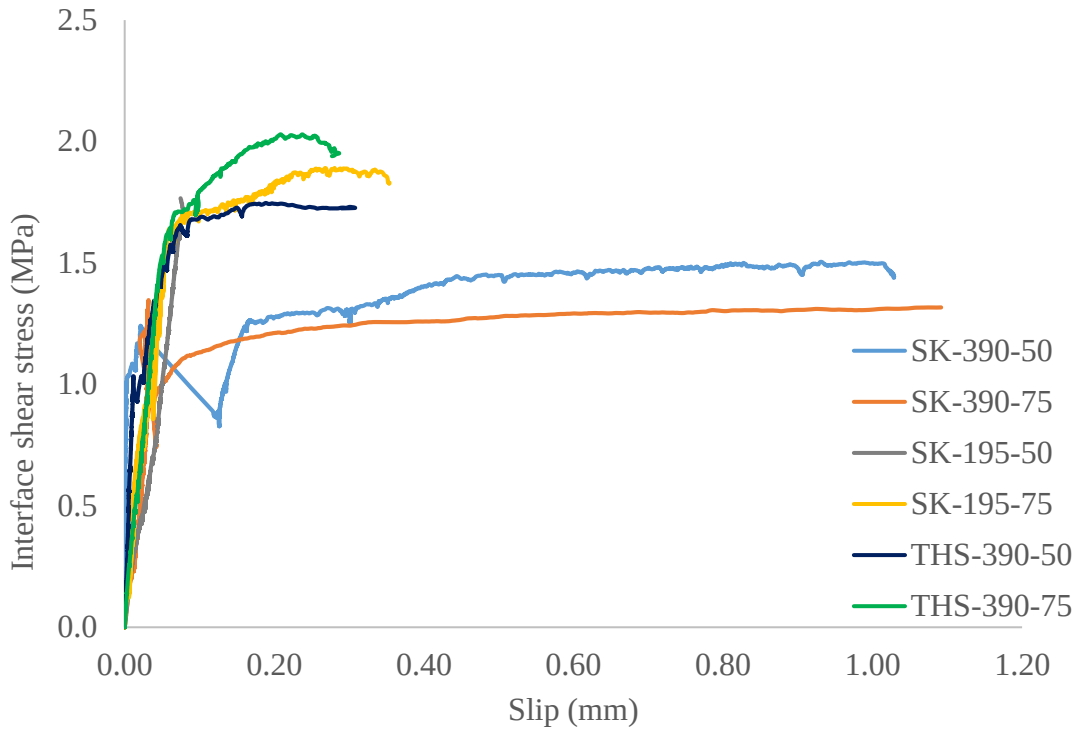

Figure 4.16: Stress verses slip for all specimens.

Table 4.1: Summary of test results.

Specimen	Yield load kN	Deflection at yield load mm	Peak load kN	Deflection at peak load mm	Failure load kN	Deflection at failure load mm
HSC-00-50	76	5.99	101	18.6	75	96.5
SK-390-50*	-	-	-	-	71	6.7
SK-195-50	77	5.6	110	30.1	102	46.4
THS-390-50	76	5.88	101	20.6	73	88.7
THS-195-50	86	6.72	122	23.7	97	76.8
HSC-00-75	77	4.77	129	26.5	106	87.4
SK-390-75*	-	-	-	-	92	7.2
SK-195-75	87	5.68	131	24.9	127	61.8
THS-390-75	79	4.65	140	23.2	111	85.6
THS-195-75	88	5.52	150	25.12	126	86.67

*Specimen failed pre-maturely due to interface failure

Table 4.2: Ductility and energy absorption.

Specimen	Ductility index		Energy absorption
	Δ_p/Δ_y	Δ_f/Δ_y	kN.m ($\times 10^3$)
HSC-00-50	3.1	15.5	8.73
SK-390-50	0.6	-	0.2
THS-390-50	3.5	12.5	8.45
SK-195-50	4.7	18.3	7.25
THS-195-50	3.5	14.4	10.95
HSC-00-75	5.6	22.4	8.91
SK-390-75	1.1	-	0.33
THS-390-75	5.0	27.3	11.05
SK-195-75	4.4	22.4	10.38
THS-195-75	4.5	24.6	11.31

Table 4.3: Cracked Stiffness.

Specimen	Compressive strength MPa	Stiffness
		Cracked
HSC-00-50	86.7	10.8
SK-390-50	86.1	17.8
THS-390-50	89.0	8.8
SK-195-50	82.5	11.4
THS-195-50	87.6	11.1
HSC-00-75	83.9	16.5
SK-390-75	83.2	12.5
THS-390-75	86.0	16.3
SK-195-75	87.5	13.3
THS-195-75	89.6	16.1

Table 4.4: Cracking moments.

Specimen	Shear connector		Experimental first crack		Code predictions			
	Type	Spacing mm	Load kN	Moment kN.m	ACI 318M-14 kN.m	CSA A.23.3-14 kN.m	EC 2 kN.m	CEB-FIB kN.m
HSC-00-50	-	0	26.7	22.3	14.77	15.27	15.5	22.92
SK-390-50	Shear key	390	31.1	26.0	14.73	15.21	18.5	22.77
THS-390-50	T-headed studs	390	31.1	26.0	14.97	15.47	18.97	23.54
SK-195-50	Shear key	195	22.2	18.5	14.42	14.91	18.12	21.82
THS-195-50	T-headed studs	195	26.7	22.3	14.86	15.35	18.85	23.17
HSC-00-75	-	0	26.7	22.3	17.87	18.47	23.61	27.27
SK-390-75	Shear key	390	22.2	18.6	17.79	18.39	28.28	27.05
THS-390-75	T-headed studs	390	31.1	26.0	18.09	18.69	28.62	27.96
SK-195-75	Shear key	195	26.7	22.3	18.24	18.85	28.87	28.44
THS-195-75	T-headed studs	195	26.7	22.3	18.47	19.08	29.1	29.13

Table 4.5: Deflections at the design service loads.

Specimen	Service Load kN	Deflection at experimental Service load mm	Theoretical deflection at service load mm	$\delta_{exp}/\delta_{theo}$
HSC-00-50	40.3	2.16	2.42	0.89
SK-390-50		4.23	-	-
THS-390-50		1.91	2.26	0.85
SK-195-50		2.15	2.32	0.93
THS-195-50		2.10	2.27	0.93
HSC-00-75	51.7	2.43	2.39	0.93
SK-390-75		4.41	-	-
THS-390-75		2.91	2.24	1.30
SK-195-75		2.53	2.23	1.16
THS-195-75		2.31	2.21	1.05
			Mean	1.18
			Standard Deviation	0.40

Table 4. 6: Deflections at 40% of experimental loads.

Specimen	Service load	Deflection at experimental Service load	Theoretical deflection at service load	$\delta_{exp}/\delta_{theo}$
	kN	mm	mm	
HSC-00-50	40.3	2.16	2.42	0.89
SK-390-50	28.6	3.66	-	-
THS-390-50	40.4	1.91	2.26	0.85
SK-195-50	43.6	2.41	2.61	0.92
THS-195-50	48.9	3.21	3.04	1.06
HSC-00-75	51.7	2.22	2.39	0.93
SK-390-75	36.8	3.36	-	-
THS-390-75	56.0	3.29	2.53	1.30
SK-195-75	52.5	2.55	2.28	1.12
THS-195-75	60.0	3.40	2.77	1.23
			Mean	1.40
			Standard Deviation	0.77

Table 4.7: Experimental and theoretical crack width at the design service load.

Specimen	Experimental Service load		Theoretical Crack width				W_{exp}/W_{theo}			
	Load kN	Crack width mm	BS 110 mm	CSA A.23.3-14 mm	EC 2-04 mm	Rilem TDf mm	BS 110	CSA A.23.3-14	EC 2-04	Rilem TDf
HSC-00-50	40.3	0.05	0.16	0.26	0.15	0.10	0.29	0.18	0.31	0.47
SK-390-50		-	-	-	-	-	-	-	-	-
THS-390-50		0.06	0.16	0.26	0.15	0.10	0.39	0.24	0.41	0.63
SK-195-50		0.10	0.16	0.26	0.15	0.10	0.63	0.38	0.65	1.01
THS-195-50		0.05	0.16	0.26	0.15	0.10	0.31	0.19	0.33	0.50
HSC-00-75	51.7	0.10	0.17	0.25	0.16	0.10	0.59	0.40	0.64	1.01
SK-390-75		-	-	-	-	-	-	-	-	-
THS-390-75		0.07	0.17	0.25	0.16	0.10	0.43	0.29	0.47	0.73
SK-195-75		0.08	0.17	0.25	0.16	0.10	0.44	0.30	0.48	0.75
THS-195-75		0.08	0.17	0.25	0.15	0.10	0.44	0.30	0.48	1.56
					Mean		0.48	0.31	0.52	0.89
					Standard Deviation		0.21	0.15	0.23	0.44

Table 4.8: Experimental and theoretical crack widths at service load coresponding to 40% of the ultimate loads.

Specimen	Experimental Service load		Theoretical Crack width				W_{exp}/W_{theo}			
	Load kN	Crack width mm	BS110-97 mm	CSA A.23.3-14 mm	EC 2-04 mm	Rilem TDf mm	BS110-97	CSA A.23.3-14	EC 2-04	Rilem TDf
HSC-00-50	40.4	0.05	0.16	0.26	0.15	0.10	0.31	0.19	0.33	0.50
SK-390-50	-	-	-	-	-	-	-	-	-	-
THS-390-50	40.4	0.06	0.14	0.26	0.15	0.10	0.44	0.23	0.40	0.61
SK-195-50	43.6	0.13	0.16	0.26	0.15	0.10	0.78	0.48	0.81	1.26
THS-195-50	48.9	0.10	0.17	0.26	0.15	0.10	0.59	0.38	0.65	1.01
HSC-00-75	51.7	0.10	0.17	0.25	0.16	0.10	0.59	0.40	0.64	1.01
SK-390-75	-	-	-	-	-	-	-	-	-	-
THS-390-75	56.0	0.09	0.18	0.25	0.16	0.10	0.48	0.35	0.56	0.88
SK-195-75	52.5	0.08	0.17	0.25	0.16	0.10	0.44	0.30	0.48	0.75
THS-195-75	60.0	0.11	0.20	0.25	0.15	0.10	0.55	0.44	0.71	1.56
					Mean		0.53	0.34	0.56	0.93
					Standard Deviation		0.13	0.09	0.16	0.33

Table 4.9: Comparison of nominal moments.

Specimen	Experimental kN.mm	CSA A.23.3-14 kN.mm	ACI 544 kN.mm	ACI 318M-14 kN.mm	Imam kN.mm
HSC-00-50	84.4	68.3	70.6	69.2	73.1
SK-390-50	72.6	76.6	78.9	77.1	81.9
THS-390-50	84.4	76.7	79.1	77.2	82.0
SK-195-50	91.0	76.5	78.8	77.0	81.7
THS-195-50	102.1	76.6	79.0	77.1	81.9
HSC-00-75	107.8	77.9	80.7	78.6	83.9
SK-390-75	78.0	87.5	90.3	88	93.9
THS-390-75	112.7	87.6	90.4	88	94.0
SK-195-75	116.9	87.6	90.5	88.1	94.1
THS-195-75	125.3	87.7	90.6	88.1	94.1

Chapter 5

Direct Shear Test

5.1 Introduction

The direct shear tests are presented in this chapter. A total of eight shear specimens were cast and tested. The parameters were: the thickness of the UHP-FRC top layer, the type of shear connectors, and the spacing between the shear connectors. The test details, test set-up, and test results are discussed in this chapter. The results are presented in terms of the interface shear stress versus slip. The experimental data is analyzed to investigate the effects of the parameters on the behaviour and the capacity of the specimens. Different code and proposed equations are used to calculate the shear capacity of both the flexural and shear specimens. A comparison between the flexural specimens from the previous chapter and the shear specimens in terms of their shear capacity is also presented.

5.2 Specimens details

To test the interface shear between the two layers of concrete, eight composite specimens were cast. The specimens can be divided into two groups. The bottom layer for all the specimens were the same and made with HP-FRC with a thickness of 180 mm. layer had a bottom reinforcement of four 15M bars and the other layer was 2-10M bars. The shear reinforcement consisted of two legged 10M stirrups every 200 mm. Figure 5.1 shows the detail of the test specimens. The first group consisted of four

composite specimens. The top layer was made with a 50 mm thick UHP-FRC concrete and was reinforced with a steel mesh of 10M in the middle. The two layers were connected through the shear connectors; two of the specimens had a spacing of 195 mm between the shear connectors and the other two had a spacing of 390 mm between the shear connectors. The shear connectors, which were in the top layer, had a width of 75 mm, a length of 75 mm, and a height of 25 mm. Both layers were 470 mm long and 300 mm wide. The second group consisted of four composite specimens (two layers of concrete on top of each other); the top layer was made of UHP-FRC concrete with a thickness of 75 mm and a steel mesh of 10M in the middle. The two layers were connected through the shear connectors; two of the specimens had a spacing of 195 mm between the shear connectors and the other two had a spacing of 390 mm between the shear connectors. The shear connectors, which were located in the top layer, had the following dimensions: a width of 75 mm, a length of 75 mm, and a height of 25 mm. Both layers were 470 mm long and 300 mm wide. For all groups, two of the specimens had T-headed studs filling the shear connectors and the other two had concrete filling its shear connectors, which are called shear keys, as shown in Table 5.1. Each specimen in this test had the same geometry as the flexural specimens. Table 5.1 shows the details of test specimen.

5.3 Casting and curing

The specimens were cast in two stages. The first stage was casting of the top layer, which was made of UHP-FRC at the structural lab of Ryerson University. The bottom layer was later cast from High Performance Fibre Reinforced Concrete (HP-

FRC) in the concrete lab of Memorial University. The casting of the bottom layer took several steps before casting. The shear voids for connectors were filled with white foam blocks in the top layer. This white foam blocks were removed and the specimens were cleaned before filling the shear connectors with either concrete or the T-headed studs. Then the formwork was placed around the top layer and the bottom layer was poured. To ensure that the concrete had been placed in the shear connectors, the concrete was manually poured with small quantities and compacted. The rest of the specimen was cast, as shown in Figure 5.2. Before casting the bottom layer, the specimens with T-headed studs were glued with epoxy which filled the whole void. The epoxy was left to cure for 48 hours before casting. Figure 5.2 shows details of casting the specimen.

All specimens were water cured for seven days after casting. The exposed surface was sprayed with water and a sheet of moist burlap was placed on top. Water curing helps to prevent premature cracking and shrinkage of the concrete. After 28 days of casting the UHP-FRC layer, the compressive was tested. Table 5.2 shows the compressive strength of HP-FRC, after 28 days of casting.

5.4 Test set-up

The specimens were tested when the bottom layer reached its targeted compressive strength in the structure labs of Memorial University. Direct shear test was used. The composite specimens were placed vertically in the loading machine as shown in Figure 5.3. Two different sets of steel plates were used to apply the load on the specimens. All steel plates used were 25 mm thick and they extended the full width of the specimen. The first set had a 50 mm plate and a bar that acted as a roller at the bottom and a 130 mm top plate. The second set had 70 mm bottom plate and a 105 mm top

plate. Figure 5.3 shows a schematic diagram of the specimen and the loading plates. A wooden box was placed for safety and to avoid any damage that could happen to the test machine. A disadvantage of the test is that the layers separate and could fail in a brittle manner. The specimen used simulated a portion of the composite specimen used in the large-scale flexural tests to evaluate the shear transfer strength of similar specimen.

To measure the slip between the two layers of the concrete, two LVDTs were used. An L-shaped steel plate was glued with epoxy to the top layer and the LVDT was attached to the bottom layer, as shown in Figure 5.3. One LVDT was placed in the front and the other was placed in the back of the specimen. Straps were also used to prevent the machine from being damaged when the two layers separate. A high-speed data acquisition system was used to record the data from the LVDTs and the load cell. The system recoded the data every three seconds. After the specimens were placed in the machine, they were loaded until failure in displacement control.

5.5 Test results

5.5.1 Stress versus slip

The slip at the interface was measured using the two LVDTs. Failure of the interface was defined by a sudden drop in the load. For a sample to have failed by relative slippage, the specimen should have a relative slippage more than 0.25 mm.

The stress versus slip plots differ based on the shear connector type and the amount of reinforcement. The idealization plots could be divided into two categories. The first category is the specimens with shear key, as shown in Figure 5.4 (a). Stage One: as the load continues to increase, the slope starts to change which means that the cohesive bond between the two layers have been lost. But the shear friction and the shear

keys are still transferring the horizontal shear stress across the interface. Stage Two: then the load continues to increase until the peak load was reached and the specimen could not carry any more load. A sudden drop in the load occurs and at that point shear friction were lost. While the shear keys are still intact and transferring the horizontal shear stress across the interface. Stage Three: after the load drop, the load increases to almost half of the peak load and a constant load is maintained, while gradually decreasing. This is attributed to the fact that the specimens continue to slip until the two layers are completely separated. This stage ends with the complete separation of the two layers.

The second category is the specimens with T-headed studs, as shown in Figure 5.4 (b). Stage One: as the load continues to increase, A slight drop in the load is observed means that the cohesive bond between the two layers have been lost. But the shear friction and the shear keys are still transferring the horizontal shear stress across the interface. Stage Two: the load continues to increase gradually increased until the specimen reached its peak load. Stage three: the load then starts to decrease gradually, which means the shear friction is lost and the dowel action from the T-headed studs still transferring the horizontal shear stress across the interface. This stage ends with the HP-FRC crushes.

5.5.1.1 Specimens with shear keys

Four composite specimens were cast and tested. These specimens had no shear reinforcement across the interface, only concrete was used to fill the shear connectors. Figure 5.5 shows some of the load versus slip for the specimens with shear keys. Figure 5.6 shows both the pre-cracking and the complete failure of the specimens (when the two layers separate completely).

The experimental interface shear stress could be evaluated by the equilibrium of the internal forces in the specimen as mentioned in Section 2.1. None the less, the experimental interface shear stress was calculated using ACI 318M-14 interface stress equation as follows:

$$v_n = \frac{V_u}{b_v d} \tag{5.1}$$

Specimens SSK-390-50 and SSK-390-75 showed a similar failure criteria was observed. At the beginning loading, the specimens reached a stress of 1.5 MPa. At this stage, the slope of stress versus slip has changed, which means that the specimens lost the cohesive bond and the interface started to crack, as shown in Figure 5.6. This point marked the end of stage one and the start of stage two. The stress continued to increase until it reached a peak stress of 2.2 MPa and 3.8 MPa, respectively After the specimen reached its peak stress, a sudden drop in stress had occurred. This could be attributed to the loss of the shear friction between the two layers of concrete, while the shear keys are still intact and transferring the horizontal shear stresses. At that point, the specimens ended stage two, and also marked the start of stage three. The stress then increased to almost half the peak stress and the specimen maintained an almost constant stress, as the shear keys were still intact and transferring the horizontal shear stresses along the interface, as shown in Figure 5.6. The second and last drop was due to the loss of the shear keys. This could be attributed to the fact that the HP-FRC had fibers, which was still transferring horizontal shear stress along the interface between the two layers of concrete. This happens until the fibers separate and the two layers had de-bonded completely.

Similar failure criteria occurred for specimens SSK-195-50 and SSK-195-75. The stress started to increase gradually until it reached a stress of 3.4 MPa and 3 MPa, respectively. When the specimens reached this stage, the slope of the stress versus slip has changed, which meant that the specimens had lost the adhesive bond between the layers and the interface started to crack. The change in slope marked the end of stage one and the beginning of stage two. Stage two started by a gradual increase in the stress until it reached a peak stress of 6.2 MPa and 7.7 MPa for SSK-195-50 and SSK-195-75, respectively. At stage two, the shear friction and the shear keys were transferring the horizontal shear stress along the interface. A constant stress was maintained before the sudden drop in the stress, as shown in Figure 5.6. This could be attributed to the fact that the distance between the shear keys was 195 mm, which enabled the specimen to sustain a better transferring ability of the horizontal shear stresses before de-bonding. The sudden drop in the stress was due to the loss of the shear friction between the two layers of concrete. The stress drop marked the end of stage two and the start of stage three. Stage three began with the gradual increase in the stress and then the specimens maintained an almost constant stress after the specimens reached their peak stresses. At this point the shear keys were transferring the horizontal shear stresses alone across the interface. At the end of stage three, the specimens experienced a sudden drop in the stress, which signified the end of the test and the two layers have finally completely separated. This could be the result of the fibers in the concrete that were filling the shear connectors and the shear keys were transferring the horizontal shear stresses along the interface. These specimens experienced an increase in the stress greater than the specimens with 390 mm spacing between the shear connectors. This was due to the decrease in the spacing between the shear keys, which increased the shear capacity of

the specimens and a better transferring ability of the horizontal shear stresses along the interface between the two layers of concrete.

5.5.1.2 Specimens with T-headed studs

STHS-390-50 and STHS-390-75 had similar failures. The stress gradually increased until the stress reached 3.9 MPa and 4.2 MPa, respectively. A slight drop in the stress resulted from the loss of the cohesive bond, as shown in Figure 5.7. At this stage, the de-bonding of the two layers started to occur. This indicated the end of stage one and the start of stage two. The stress gradually increased to reach a peak stress of 5 MPa and 5.6 MPa, respectively. This could be attributed to the fact that the shear friction and T-headed studs were transferring the horizontal shear stresses along the interface between the two layers of concrete. After the specimens reached their peak stress, the stress started to gradually decrease. This could be the end of stage two and the start of stage three. Stage three started when the dowel action of the T-headed studs started to transfer the horizontal shear stresses along the interface between the two layers of concrete and the shear friction was lost. At this point, the HP-FRC layer started to crush. These specimens experienced a smoother and more ductile failure mode with a gradual decrease in the stress, unlike the specimens with shear keys as these specimens experienced a sudden drop in the stress. This resulted from the fact that the T-headed studs affected the specimens with a smoother and more ductile failure mode of the shear specimens. This could also mean that the reinforcement in the interface yields for a more ductile failure, while the shear keys yield a more brittle failure.

Specimens STHS-195-50 and STHS-195-75 had the similar failure modes. The stress started to increase gradually until it reached 9.8 MPa and 8 MPa, respectively, as

shown in Figure 5.7. A small sudden drop in the stress occurred at this stage. This could be attributed to a loss in the cohesion bond between the two layers of concrete. At that point, stage one had ended and stage two had started. The stress then continued to increase gradually and the interface started to crack. The specimens reached a peak stress of 10.32 MPa and 11.8 MPa respectively. After the specimens reached their peak stress, the interface cracks started to grow, the HP-FRC layer started to crush, and the stress started to decrease gradually until it reached an almost constant stress. At that point, the shear friction had been lost between the two layers of concrete and only the T-headed studs were transferring the horizontal shear stresses across the interface. That marked the end of stage two and stage three began. At stage three, the dowel action started to transfer the horizontal shear stress along the interface between the two layers of concrete. Then stage three ended with the complete failure of the shear specimens. At the end of the test, the two layers were still intact. These specimens endured a higher stress than the specimens with shear connector spacing of 390 mm. That could be due to the decrease of the spacing between the shear connectors, which could have resulted in a better transferring ability of the horizontal shear stress across the interface between the two layers of concrete. STHS-195-50 and STHS-195-75 also yielded a higher stress than SSK-195-50 and SSK-195-75. That could be attributed to the presence of interface reinforcement along the interface, which yielded a more ductile failure for the specimens with T-headed studs.

5.6 Shear capacity

The horizontal transfer of the interface shear stress between the two layers of concrete is a vital point to consider, while designing the composite elements. There are a lot of equations have been developed along the years to predict the horizontal shear stress along the interface.

The different equations and code expressions used to estimate the horizontal shear capacity during are presented in this section. The calculations are carried out for both the flexural and shear specimens.

Table 5.5 shows the experimental values for the horizontal shear stresses for the flexural. The experimental horizontal shear stress along the interface were calculated with Equation 5.1. Specimens SK-390-50 and SK-390-75 had the lowest capacity among all the flexural specimens, with values of 1.03 MPa and 1.35 MPa respectively. THS-195-50 and THS-195-75 were the highest horizontal shear stresses, with values of 2.11 MPa and 2.17 MPa respectively. These two specimens had the T-headed studs at the interface and 195 mm spacing between the shear connectors, as this combination yielded the best transfer of horizontal shear stresses along the interface between the two layers of concrete. It was interpreted that the capacity of the interface increased with the decrease of the spacing between the shear connectors. The horizontal shear stress capacity of the flexural specimens also increased with adding the T-headed studs to the shear connectors from the shear keys. This could be attributed to the better transfer of the horizontal shear stress along the interface between the two layers of concrete. The increase in thickness did not affect the capacity of the section greatly. This could have happened due to the fact that the difference in thickness was not significant.

Table 5.7 lists the experimental data for the direct shear specimens. As expected, the specimens with T-headed studs gave a higher experimental shear capacity than the specimens with shear keys as expected, as shown in Table 5.7. This could be attributed to the fact that the T-headed studs had a better transferring ability for the horizontal shear stresses across the interface between the two layers of concrete than the shear keys.

5.6.1 Equations for specimens with Shear keys

In this investigation, four equations were considered. AASHTO 1990 Code Equation 5.2 and three equations were proposed equations, as follows Turmo et al. 2006 Equation 5.3, Rombach, 2002 Equation 5.4, and Buyukozturk et al. 1990 Equation 5.5. AASHTO 1990 equation is adapted from Koseki & Breen, 1983. Turmo et al. adopted the AASHTO 1990 equation with some adjustments and rewrote the equation as a help to be added to Eurocode.

AASHTO (1990) $$V_u = A_k \sqrt{f_{cm}}(0.9961 + 0.2048\sigma_n) + 0.6A_{sm}\sigma_n \quad (5.2)$$

Turmo et al. $$V_u = A_k \sqrt{f_{cm}}(0.9064 + 0.1863\sigma_n) + \mu A_{sm}\sigma_n \quad (5.3)$$

Rombach $$V_u = \frac{1}{\gamma_f}(0.14 f_{ck} A_k + \mu A_{sm}\sigma_n) \quad (5.4)$$

Buyukozturk et al. $$V_u = A_k \sqrt{(6.792\times10^{-3}) f_{cm}}(12 + 2.466\sigma_n) + \mu A_{sm}\sigma_n \quad (5.5)$$

5.6.1.1 Flexural specimens

Table 5.3 shows the experimental and estimated shear capacity using the above four equations. The experimental results showed that the capacity of the shear keys

increased when the thickness of the top layer increased. The capacity also increased when the spacing between the shear keys was decreased. This could be attributed to the increase of the number of shear keys lead to a better transfer of the horizontal shear stress along the interface between the two layers of concrete. Rombach's equation was the most conservative in estimating the interface capacity. AASHTO and Buyukozturk's equations were the most consistent with the experimental results.

5.6.1.2 Direct shear specimens

Table 5.4 shows the experimental and estimated shear capacity using the above four equations. It was noted that all the equations were under estimating the strength of the shear keys. The ASSHTO (1990) equation gave the highest estimation, which was the most consistent with the experimental results. The Buyuozturk 1990 equation gave the second highest estimate of the shear capacity of the shear specimens. On the other hand, The Rombach equation gave the lowest estimate for both the specimens with a spacing of 195 mm and 390 mm between the shear keys. The Turmo et al. 2006 equation estimates the shear capacity lower than the Buyuozturk equation but higher than the Rombach equation.

5.6.2 General Equations for calculating interface shear

Three code equations were used in this investigation and as follows: AASHTO LRFD Bridge Design Specification horizontal shear equation 2012 Equation 5.6, ACI 318M-14 horizontal shear stress Equation 5.7, and CSA horizontal shear stress equation A.23.3-14 Equation 5.8. These equations only take into consideration the shear friction and ignoring the shear keys for the specimens with shear keys.

Two proposed equations, from the different researchers, were used in this investigation. The equations are Kahn and Mitchel Equation 5.9, and Loov and Patnaik Equation 5.10. These equations were chosen based on their most common use in the design of composite elements. Mas and Hus equation was similar to Loov's equation, with only difference that they took the K=0.66. The compressive strength of the weaker concrete should be used in the following equations. These equations only take into consideration the shear friction and ignoring the shear keys for the specimens with shear keys.

AASHTO (2012)
$$V_n = cA_{cv} + \mu\left[A_v f_y + P_c\right] \le \min\begin{Bmatrix} K_1 f_c' A_{cv} \\ K_2 A_{cv} \end{Bmatrix} \quad (5.6)$$

ACI 318M-14
$$V_n = \lambda\left[1.8 + 0.6\frac{A_v f_y}{b_v s}\right] b_v d \quad (5.7)$$

CSA A.23.3-14
$$v_n = \lambda\phi_c(c + \mu\sigma) + \phi_s\rho_v f_y \cos\alpha_f \quad (5.8)$$

Khan and Mitchell
$$v_n = 0.05 f_c' + 1.4\frac{A_v f_y}{b_v s} \le 0.2 f_c' \quad (5.9)$$

Loov and Patnaik
$$v_n = K\sqrt{\left(0.1 + \frac{A_v f_y}{b_v s}\right) f_c'} \le 0.25 f_c' \quad (5.10)$$

5.6.1.2 Flexural specimens

Table 5.5 contains the experimental interface shear stress along with the interface shear stress capacities calculated using the Equations 5.6 through 5.11. The interface

shear stress for all the specimens could be found in Table 5.5. This value is greater than the predicted values by the different equations for a specimen that does not contain shear key.

From Table 5.5, it is apparent that CSA Equation 5.8 was the most consistent with the experimental results to estimate to the interface shear stress for the composite specimens with a shear connector spacing of 195mm and the specimens with T-headed studs and a shear connector spacing of 195 mm. CSA had a mean of 1.7 and a standard deviation of 0.67, as shown in Table 5.6. while Loov and Patnaik Equation 5.10 was the best in estimation the horizontal shear stress along the interface for composite specimens with spacing between the shear connector of 390 mm and yielded a mean and standard deviation of 1.82 and 1.01 respectively. On the other hand, AASHTO gave a very low estimate of the interface shear stress, with a mean and standard deviation of 2.33 and 0.89 respectively, and ACI was slightly unconservative. Kahn and Mitchell equation gave a very high estimate for the interface shear stress. Mau and Hsu Equation 5.11 was slightly higher in its predictions than the ACI Equation 5.7.

The shear interface shear slip was recorded to fail, when the slippage along the interface between the two layers of concrete had a value of more than 025 mm. For the samples THS-195-50 and THS-195-75, the interface shear stress was recoded for both specimens, although the specimens didn't fail in the interface. The specimens didn't experience any relative slippage along the interface. These two specimens recorded the highest values of highest horizontal shear stress along the interface.

5.6.2.2 Direct shear specimens

The same set of equations that were used with the flexural specimens, were used to predict the shear capacity of the shear specimens. The equations were used to be able to compare the results of the shear specimens to the flexural specimens. The experimental results were calculated with the load divided by the cross-sectional area. Three code equations and two proposed equations were used in this experimental investigation. These equations only take into consideration the shear friction and ignoring the shear keys for the specimens with shear keys.

Table 5.7 shows the experimental results and all the predictions from the equations used. It was noted that the prediction for the specimens with shear keys was all conservative. For the specimens with a spacing of 390 mm between the shear keys, the ACI (318M-14) gave the most consistent. For the specimens with shear keys and a spacing of 195 mm, Kahn and Mitchell equation had the best estimating ability. The AASHTO (2012), CSA (A23-14), and Loov and Patnaik equations gave a very conservative estimate for predicting the horizontal shear stresses across the interface.

The Kahn and Mitchel equation gave the highest estimates and the AASHTO equation gave the most conservatives estimate of all the equations for the specimens with T-headed studs. Although the ACI, CSA, and Loov and Patnaik equations gave near estimates to each other, but the ACI equation gave the nearest estimates for the specimens with T-headed studs.

5.7 Comparison between the flexural specimens and shear specimens

An elaborative discussion of the flexural specimens that were made from UHP-FRC and HP-FRC was made in Chapter 4. After conducting the shear capacity testing, a comparison between the flexural specimen and the shear specimens was necessary. Figure 5.8 shows the comparison between the flexural specimens and the shear specimens. It was noted that the shear specimens had a higher shear capacity than flexural specimens. This phenomenon was apparent for both the specimens with shear keys and the specimens with T-headed studs. This could be attributed to the fact that the shear specimens are only subjected to shear loads, while the flexural specimens are subjected to both shear and bending loads. This phenomenon coincides with the conclusions that were encountered from the investigation of Crane (Crane, 2012).

Table 5.1: Test specimens details.

Specimen	UHP-FRC thickness mm	HSC thickness mm	Total thickness mm	Shear connections	Spacing mm
SSK-390-50	50	180	230	Shear Key	390
SSK-195-50	50	180	230	Shear Key	195
STHS-390-50	50	180	230	T-Headed Studs	390
STHS-195-50	50	180	230	T-Headed Studs	195
SSK-390-75	75	180	255	Shear Key	390
SSK-195-75	75	180	255	Shear Key	195
STHS-390-75	75	180	255	T-Headed Studs	390
STHS-195-75	75	180	255	T-Headed Studs	195

Table 5.2: HP-FRC compressive strength.

Specimen	Compressive strength MPa
SSK-390-50	89
SSK-195-50	90
STHS-390-50	91
STHS-195-50	86
SSK-390-75	87
SSK-195-75	92
STHS-390-75	85
STHS-195-75	88
Average	88.5

Table 5.3: Calculations of horizontal shear stress using different equations for flexural specimens with shear keys only.

Specimen	Experimental MPa	AASHTO (1990) MPa	Turmo MPa	Rombach MPa	Buyukozturk MPa	Type of failure *
SK-390-50	1.03	0.88	0.80	0.57	0.88	1
SK-195-50	1.90	3.53	3.21	2.29	3.51	2
SK-390-75	1.35	0.88	0.80	0.57	0.88	1
SK-195-75	1.89	3.53	3.21	2.29	3.51	1

Type of failure

1- Specimens failed at interface.
2- Specimen failed in flexure before the shear capacity was reached.

Table 5.4: Comparison between the experimental and the equations for the direct shear specimens with shear keys only.

Specimen	Experimental stress MPa	AASHTO (1990) MPa	Buyukozturk MPa	Rombach MPa	Turmo et al. MPa
SSK-390-50	2.2	0.88	0.88	0.57	0.80
SSK-195-50	6.2	1.77	1.75	1.14	1.61
SSK-390-75	3.8	0.88	0.88	0.57	0.80
SSK-195-75	7.8	1.77	1.75	1.14	1.61

Table 5.5: Calculations of horizontal shear stress using general equations for flexural specimens.

Specimen	Experimental MPa	AASHTO (2012) MPa	ACI 318M-14 MPa	CSA A.23.3-14 MPa	Loov & Patnaik MPa	Kahn & Mitchell MPa	Type of failure*
SK-390-50	1.03	0.52	1.8	0.70	0.58	4.25	1
SK-195-50	1.90	0.52	1.80	0.70	0.58	4.25	2
SK-390-75	1.35	0.52	1.80	0.70	0.58	4.25	1
SK-195-75	1.89	0.52	1.80	0.70	0.58	4.25	2
THS-390-50	1.75	0.98	2.26	1.36	1.72	5.33	2
THS-390-75	2.03	0.98	2.26	1.36	1.72	5.33	2
THS-195-50	2.11	1.44	2.72	2.01	2.36	6.40	2
THS-195-75	2.17	1.44	2.72	2.01	2.36	6.40	2

Type of failure

1- Specimens failed at interface.
2- Specimen failed in flexure before the shear capacity was reached.

Table 5.6: Horizontal shear stress comparison for flexural specimens.

Specimen	$v_{n,exp}/v_{n,theo}$				
	AASHTO	ACI	CSA	Loov & Patnaik	Kahn & Mitchell
SK-390-50	1.98	0.57	1.46	1.77	0.24
SK-195-50	3.65	1.06	2.70	3.26	0.45
SK-390-75	2.60	0.75	1.92	2.32	0.32
SK-195-75	3.63	1.05	2.68	3.24	0.44
THS-390-50	1.78	0.77	1.29	1.02	0.33
THS-390-75	2.00	0.87	1.44	1.14	0.37
THS-195-50	1.46	0.77	1.05	0.89	0.33
THS-195-75	1.50	0.80	1.08	0.92	0.34
Mean	2.33	0.83	1.70	1.82	0.35
Standard Deviation	0.89	0.16	0.67	1.01	0.07

Table 5.7: Comparison between the experimental results and the code and the proposed equations for all the direct shear specimens.

Specimen	Experimental MPa	AASHTO (2012) MPa	ACI 318M-14 MPa	CSA A.23.3-14 MPa	Loov & Patnaik MPa	Kahn & Mitchell MPa
SSK-390-50	2.2	0.52	1.8	0.70	0.58	4.25
SSK-195-50	6.2	0.52	1.8	0.70	0.58	4.25
SSK-390-75	4.8	0.52	1.8	0.70	0.58	4.25
SSK-195-75	7.8	0.52	1.8	0.70	0.58	4.25
STHS-390-50	5.0	1.44	2.7	2.01	2.36	6.40
STHS-195-50	5.6	2.37	3.6	3.32	3.29	8.56
STHS-390-75	10.3	1.44	2.72	2.01	2.36	6.40
STHS-195-75	11.3	2.37	3.65	3.32	3.29	8.56

Table 5.8: Horizontal shear stress comparison for direct shear specimens.

Specimen	$v_{n,exp}/v_{n,theo}$				
	AASHTO	ACI	CSA	Loov & Patnaik	Kahn & Mitchell
SSK-390-50	4.2	1.2	3.1	3.7	0.5
SSK-195-50	4.2	1.2	3.1	3.7	0.5
SSK-390-75	4.2	1.2	3.1	3.7	0.5
SSK-195-75	4.2	1.2	3.1	3.7	0.5
STHS-390-50	1.5	0.8	1.1	0.9	0.3
STHS-195-50	0.9	0.6	0.7	0.7	0.3
STHS-390-75	1.5	0.8	1.1	0.9	0.3
STHS-195-75	0.9	0.6	0.7	0.7	0.3

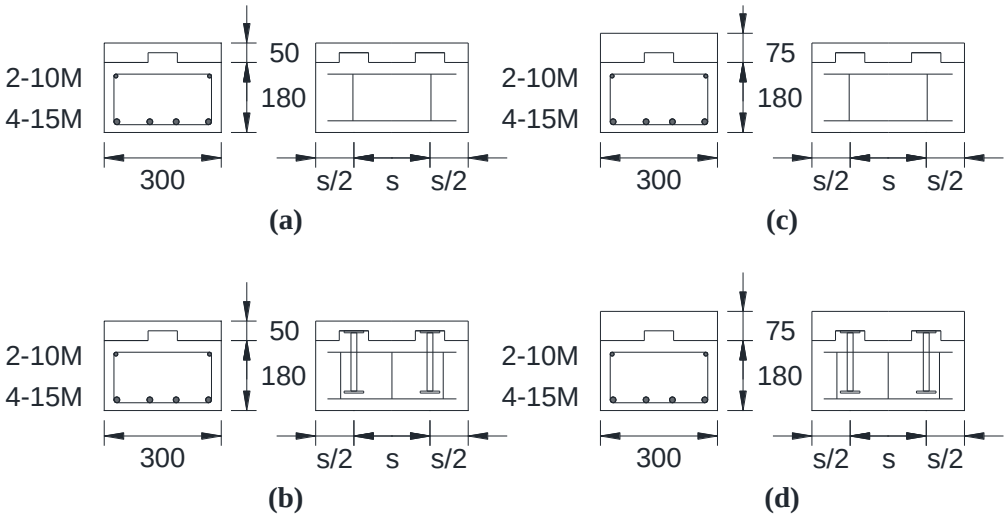

Figure 5.1: Shear specimens (a) 50 mm specimen with spacing of 195 mm and 390 mm between the shear keys (SSK-390-50 and SSK-195-50), (b) 50 mm specimen with spacing of 195 mm and 390 mm between the T-headed studs (STHS-390-50 and STHS-195-50), (c) 75 mm specimens with spacing of 195 mm and 390 mm between the shear keys (SSK-195-75 and STHS-195-75), (SSK-390-75 and STHS-390-75), (d) 75 mm specimens with spacing of 195 mm and 390 mm between the T-headed studs (SSK-195-75 and STHS-195-75), (SSK-390-75 and STHS-390-75).

Figure 5.2: Casting of the bottom layer (on the left specimen with shear keys and on the right specimen with T-headed studs filling the shear connectors).

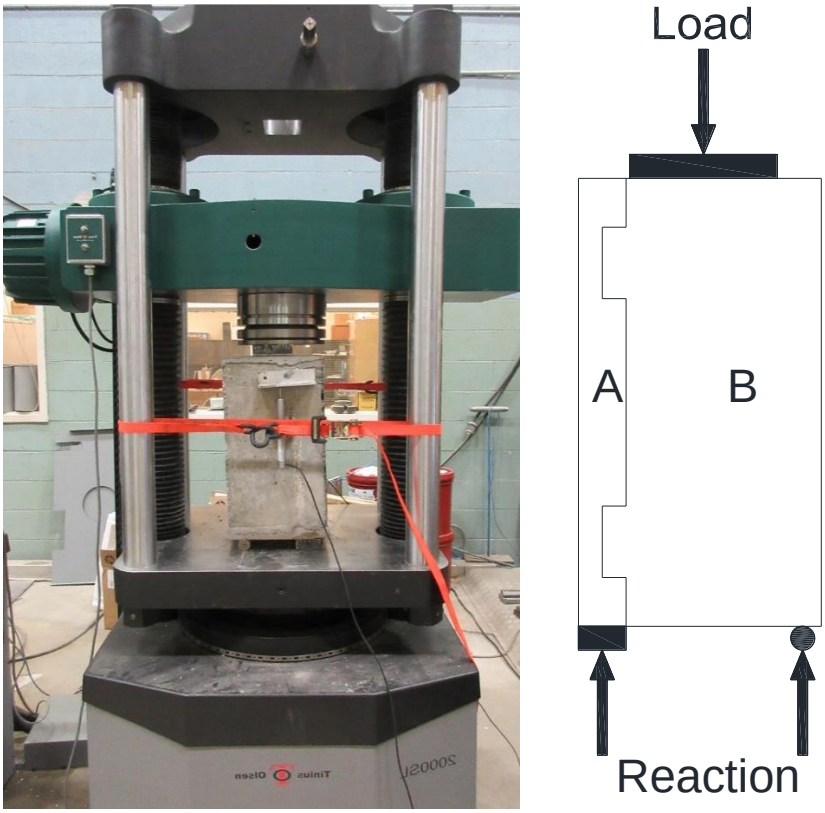

Figure 5.3: Direct Shear Test set-up.

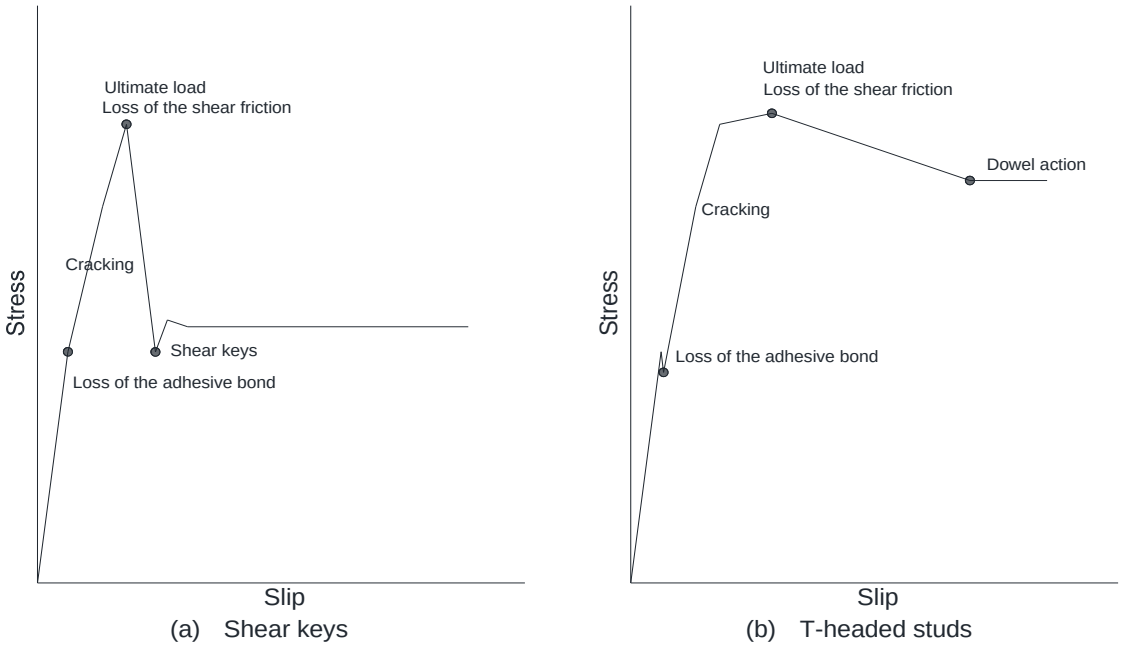

Figure 5.4: Typical Load versus Slip.

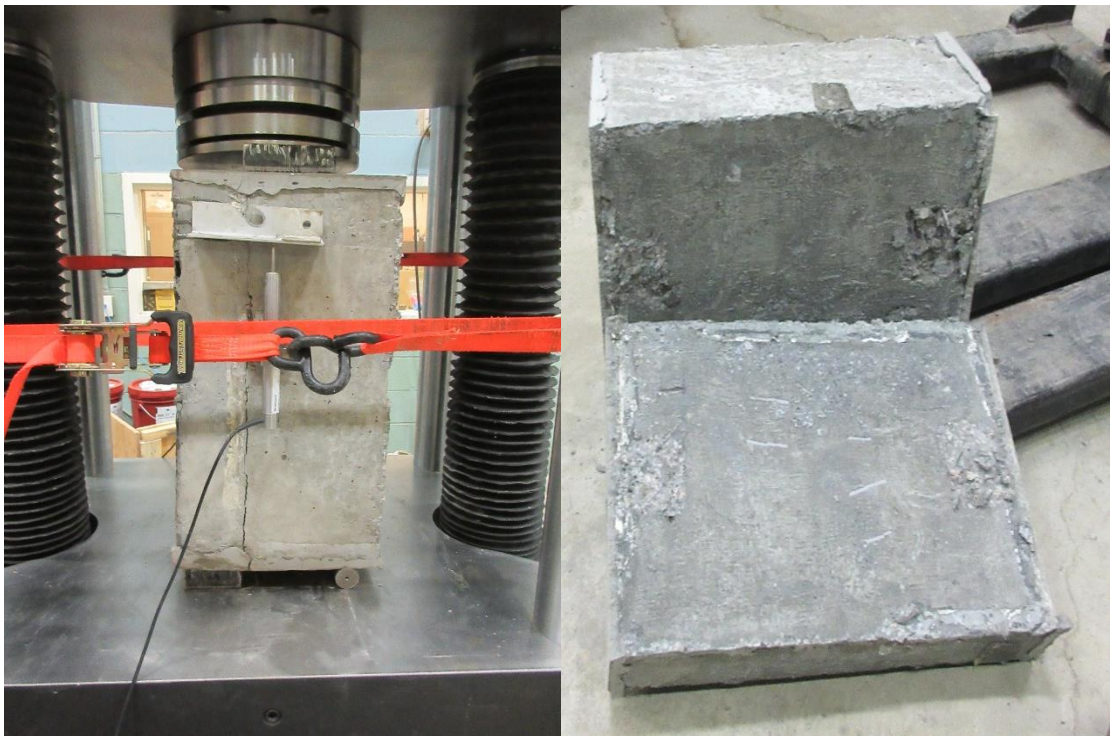

Figure 5.5: The pre-cracking and the complete failure of the shear specimens with shear keys.

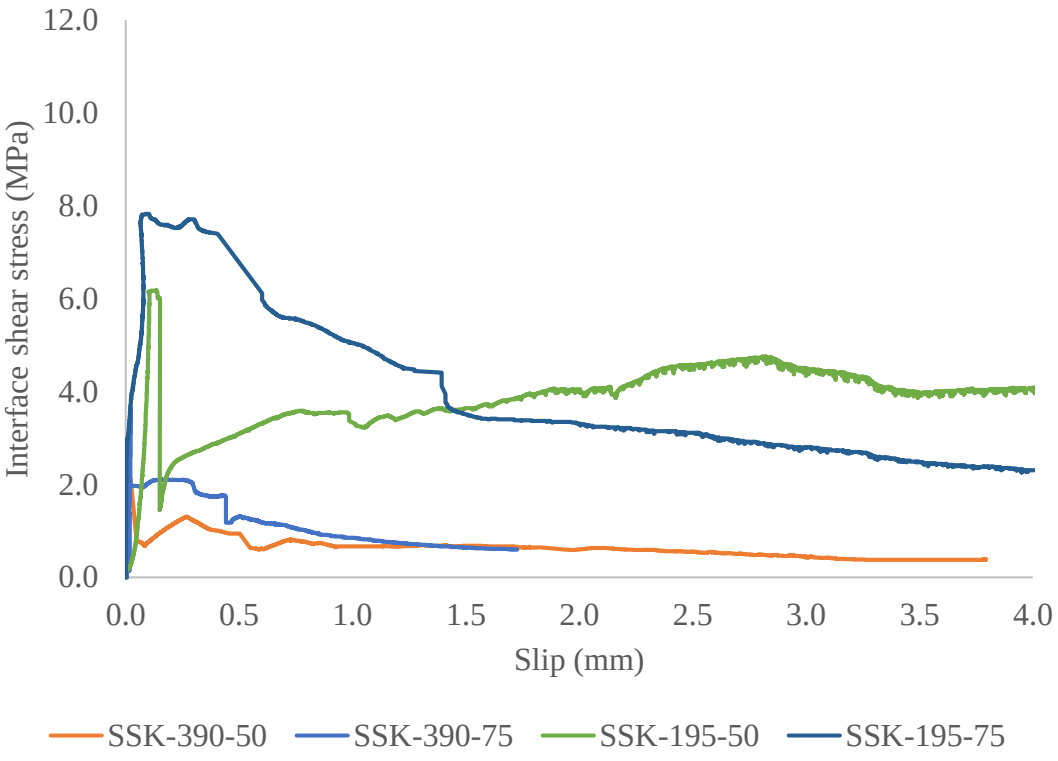

Figure 5.6: Stress versus slip for specimen with shear keys.

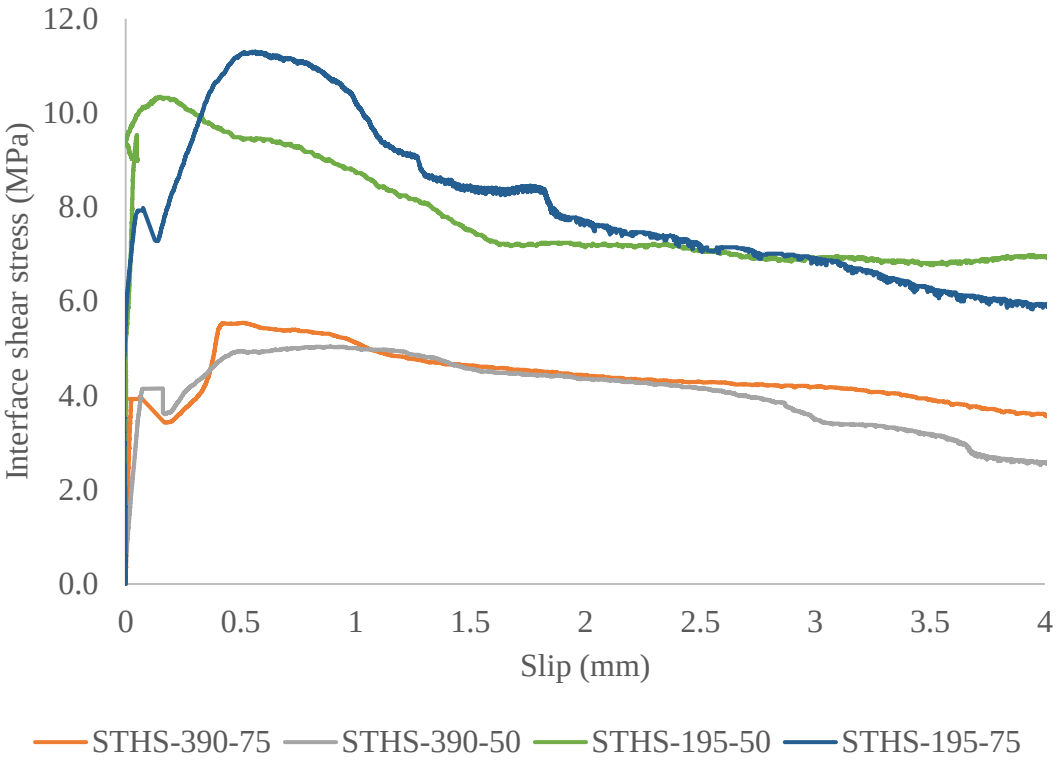

Figure 5.7: Stress versus slip for specimen with T-headed studs.

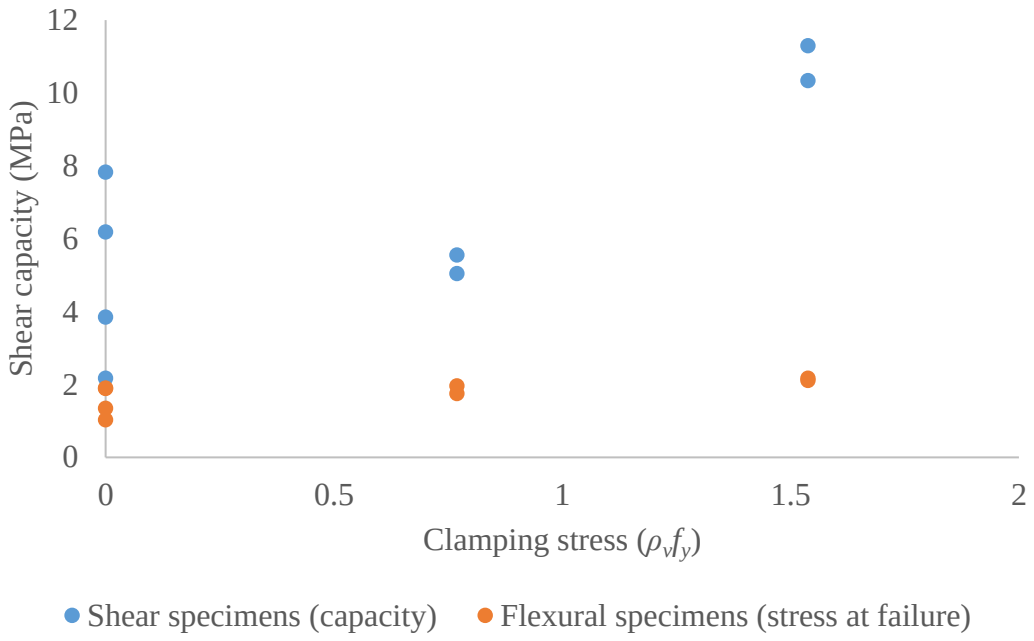

Figure 5.8: Comparison between flexural specimens and shear specimens.

Chapter 6

Summary and Conclusions

6.1 Introduction

In this thesis, an ice shield was proposed from UHP-FRC for offshore structures. Composite elements were designed and tested to simulate ice shield. The specimens consisted of UHP-FRC layer on top of a high performance fibre reinforced concrete (HP-FRC) one. A large amount of data was recorded and analyzed for the deflection, steel and concrete strain, crack propagation and profiles, and the slippage along the interface,

6.2 Experimental investigation

The experimental program was divided into flexural and direct shear testing. Three parameters were investigated. The flexural testing consisted of a total of 10 composite and reference specimens. Two specimens were non-composite reference specimens and eight were composite specimens. The test parameters used were the top layer thickness, the type of shear connectors, and the spacing between the shear connectors. The first group was the reference specimens. The second group consisted of four composite specimens with the same top layer thickness of 50 mm and different type and spacing of shear connectors. The spacing between the shear connectors was 390 mm and 195 mm. The two types of shear connectors were shear keys and T-headed studs.

The third group consisted of four similar composite flexural specimens. In this group, the specimens had 75 mm top layer.

To investigate the shear interface capacity of the specimens, direct shear tests were conducted. The direct shear tests were carried out on eight specimens. The specimens represented the interface of the flexural specimen. Each shear specimen would have top layer thickness, type of shear connector, and spacing between the shear connectors that is identical to the corresponding flexural specimen. A comparison between the shear capacity calculated from the direct shear and flexural testing was made. Different code and proposed equations by different researches were used to estimate the shear capacity for both the shear and flexural specimens.

From the experimental investigation, the following conclusions are made:

- The similar specimens with top layer thicknesses of 50 mm and 75 mm had approximately the same number and patterns of cracks at the serviceability and at failure. This indicates that the thickness of the top layer had no significant effect on the cracks that developed in the specimens.
- A crack at the interface between the two layers of concrete was noticed for some of the composite specimens and was the reason for the failure of some of the specimens. The flexural specimens with shear keys at 390 mm spacing experienced complete separation between the two layers along the interface. While, the specimens with T-headed studs did not develop any significant cracks along the interface. The specimens with shear keys and 390 mm spacing experienced an interface failure which was accompanied by a sudden drop in the load and loss of flexural capacity.

- The composite specimens had a higher ductility and energy absorption capacity than the non-composite ones.
- The specimens with shear keys and 195 mm spacing and T-headed studs with 390 mm spacing encountered a flexural failure after developing a fully composite action. However, the specimens developed inadequate ductility. The specimens with T-headed studs and 195 mm developed a fully composite action with sufficient ductility. The specimens with T-headed studs had better ductility than the specimens with shear keys.
- The increase in the thickness of the top layer led to an increase in the energy absorption capacity. The energy absorption increased when the spacing between the shear connectors decreased and the type of the shear connector changed.
- There was a small enhancement in the stiffness between the composite specimens with a top layer thickness of 75 mm and composite specimens with top layer thickness of 50 mm.
- All the steel and concrete strains experienced the same trends in similar specimens.
- When comparing the experimental cracking moment to the cracking moment predicted from the code equations, it showed that the experimental results were slightly higher than the code values.
- The deflection of the composite specimens did not have a significant difference from the non-composite specimens. The top layer did not contribute to the deflection at the serviceability limits. The modulus of elasticity of HP-FRC did

not differ greatly from the UHP-FRC, with values of 40 GPa and 50 GPa, respectively.

- The specimens with 75 mm top layer recorded a smaller crack width than the specimens with 50 mm top layer. The crack widths of all specimens at the service load were almost the same, which means that the top layer did not make any affect for the crack width at the service load. Most of the experimental crack width was below the allowed code limits.
- The ice shield increased the flexural capacity of the most composite flexural specimens when compared to the non-composite flexural specimens. The flexural capacity also increased when the shear keys were changed with T-headed studs.
- The flexural specimens with T-headed studs allowed for a better horizontal shear stress transfer along the interface between the two layers of concrete, that resultant in a higher flexural capacity and the development of a fully composite flexural specimen. THS-195-50 and THS-195-75 didn't record any relative slippage along the interface between the two layers of concrete.
- The decrease in the spacing and changing the shear connectors type (shear key to T-headed studs) recorded a higher shear capacity for the direct shear specimens.
- The T-headed studs affected the specimens with a smoother and more ductile failure mode of the direct shear specimens. The direct shear specimens with shear keys, the two layers separated completely at the end of the test. Unlike, the shear

specimens with T-headed studs, which made the two layers to stay, connected until the end of the test.

- Comparing the experimental shear capacity with the code and proposed expressions revealed that most code and proposed equations can adequately predict the interface capacity of the composite specimens.

References

AASHTO LRFD Bridge design Specifications. (2012). *AASHTO LRFD Bridge design specifications*. Washington, DC: American Association of State Highway and Transportation Officials.

Ali, M. A., & White, R. N. (2000). Enhanced Contact Model for Shear Friction of Normal and High-Strength Concrete. *ACI Structural Journal*, (96).

Anderson, A. R. (1960). Composite Deisgns in Precast and Cast-in-Place Concrete. *Progressive Architecture*, (41(9)), 172–179.

Bae, B., Choi, H., & Choi, C. (2016). Flexural Strength Evaluation of Reinforced Concrete Members with Ultra High Performance Concrete. *Advances inMaterials Science and Engineering*, *2016*.

Baran, E. (2015). Effects of cast-in-place concrete topping on flexural response of precast concrete hollow-core slabs. *Engineering Structures*, *98*, 109–117. http://doi.org/10.1016/j.engstruct.2015.04.017

Birkeland, P. W., & Birkeland, H. W. (1966). Connections in Precast Concrete Construction. *ACI Structural Journal*, *63*(3), 345–367.

British Standard Institution. (2002). *Structural Use of Concrete. Part 2: Code of Practice for Special Circumstances*. London.

Brühwiler, E. (2016). " Structural UHPFRC ": Welcome to the post- concrete era ! *First International Interactive Symposium on UHPC*, (January). http://doi.org/10.21838/uhpc.2016.key

Buyukozturk, B. O., Bakhoum, M. M., & Beattie, S. M. (1990). SHEAR BEHAVIOR OF JOINTS IN PRECAST CONCRETE SEGMENTAL BRIDGES. *Journal of Structural Engineering*, *116*(12), 3380–3401.

CEN (Comité Européen de Normalisation). (2004). *Eurocode 2 : Design of concrete structures —part 1: general rules and rules for buildings, BS EN 1992-1-1:2004*. Brussels: BS EN 1992-1-1:2004.

Convener, O. O., & OtherAuthors, and 19. (2009). *Concrete structures for oil and gas fields in hostile marine environments*. fib.

Crane, C. K. (2012). *SHEAR AND SHEAR FRICTION OF ULTRA-HIGH PERFORMANCE CONCRETE BRIDGE GIRDERS*. Gerorgia Institute of Technology.

Crane, C. K., & Kahn, L. F. (2012). Interface Shear Capacity of Small UHPC I HPC Composite T-Beams. In *Ultra-High Performance Concrete and Nanotechnology in Construction* (pp. 1–9).

Dutal. (2018). http://www.ductal.com.

Fathifazl, G., Razaqpur, A. G., Isgor, O. B., Abbas, A., Fournier, B., & Foo, S. (2009). Flexural Performance of Steel-Reinforced Recycled Concrete Beams. *ACI Structural Journal*, *106*(106), 858–867.

GU, C., YE, G., & SUN, W. (2015). Ultrahigh performance concrete-properties , applications and perspectives. *Science China Technological Sciences*, *58*(4), 587–599. http://doi.org/10.1007/s11431-015-5769-4

Hussein, L., & Amleh, L. (2015). Structural behavior of ultra-high performance fiber reinforced concrete-normal strength concrete or high strength concrete composite members. *CONSTRUCTION & BUILDING MATERIALS*. http://doi.org/10.1016/j.conbuildmat.2015.05.030

Imam, M., Vandewalle, L., & Mortelmans, F. (1995). Shear moment analysis of reinforced high strength concrete beams containing steel fibres. *Canadian Journal for Civil Engineering*, *470*, 462–470.

Kahn, L. F., & Mitchell, A. D. (2002). Shear friction tests with high-strength concrete. *ACI Structural Journal*, *99*(1), 98–103.

Kahn, L. F., & Slapkus, A. (2004). Interface Shear in High Strength Composite T-Beams. *PCI Journal*, (July-August), 102–110.

Koseki, K., & Breen, J. E. (1983). EXPLORATORY STUDY OF SHEAR STRENGTH OF JOINTS, (2).

Kovach, J. D., & Naito, C. (2008). *Horizontal Shear Capacity of Composite Concrete Beams without Interface Ties By*.

Loov, R. E. (1978). Design of precast connections, Paper presented at a seminar organized by Compa International Pte, Ltd. *Paper Presented at a Seminar Organized by Compa International Pte, Ltd*, 8.

Loov, R. E., & Patnaik, A. K. (1994). Horizontal Shear Strength of Composite Concrete Beams with a Rough Interface. *PCI Journal*, *39*, 48–67.

Makita, T. (2014). *Fatigue behaviour of UHPFRC and R-UHPFRC - RC composite members*. ÉCOLE POLYTECHNIQUE FÉDÉRALE DE LAUSANNE.

Masse, M. B. (2015). *Structural Behavior of R-UHPFRC – RC Composite Slabs*. ÉCOLE POLYTECHNIQUE FÉDÉRALE DE LAUSANNE.

Mast, R. F. (1968). Auxiliary Reinforcement in Concrete Connections. *American Society ofCivil Engineers, Journal of Structural Division*, *94*(6), 1485–1505. http://doi.org/10.1260/1369-4332.18.8.1173

Mattock, A. H., & Hawkins, N. M. (1972). Shear Transfer in Reinforced Concrete-Recent Research. *PCI Journal*, *11*(44), 55–75. http://doi.org/10.2777/37605

Mattock, A. H., & Kaar, P. H. (1961). Precast-Prestressed Concrete Bridges, 4. Shear Tests of Continous Girders. *PCI Journal*, *3*(1), 19–46.

Mattock, A. H., Li, W. K., & Wang, T. C. (1976). Shear transfer in lightweight reinforced concrete. *PCI Journal*, *21*(1), 20–39.

Mau, S., & Hsu, T. (1988). Reader Comments on "Influence of Concrete Strength and Load History on the Shear Friction Capacity of Concrete Members by Walraven et al. *PCI Journal*, *33*(1), 166–168. http://doi.org/10.1193/1.2757714

Momayez, A., Ehsani, M. R., Ramezanianpour, A. A., & Rajaie, H. (2005). Comparison of methods for evaluating bond strength between concrete substrate and repair materials. *Cement and Concrete Research*, *35*, 748–757. http://doi.org/10.1016/j.cemconres.2004.05.027

Nematollahi, B., R, R. S. M., Jaafar, M. S., & Voo, Y. L. (2012). A review on ultra high performance “ductile” concrete (UHPdC) technology. *International Journal of Civil and Structural Engineering*, *2*(3), 1003–1018. http://doi.org/10.6088/ijcser.00202030026

Nes, L. G., & Øverli, J. A. (2015). Structural behaviour of layered beams with fibre-reinforced LWAC and normal density concrete. *Materials and Structures*, *49*(1–2), 689–703. http://doi.org/10.1617/s11527-015-0530-9

Noshiravani, T., & Brühwiler, E. (2013). Experimental Investigation on Reinforced Ultra-High- Performance Fiber-Reinforced Concrete Composite Beams Subjected to Combined Bending and Shear. *ACI Structural Journal*, (110), 251–262.

Othman, H., & Marzouk, H. (2016). Impact response of ultra-high-performance reinforced concrete plates. *ACI Structural Journal*, *113*(6), 1325–1334. http://doi.org/10.14359/51689157

Raths, C. H. (1977). Reader Comments: Design Proposals for Reinforced Concrete Corbels. *PCI Journal*, *22*(2), 93–39.

RILEM TC 162-TDF members. (2003). *RILEM TC 162-TDF : Test and design methods for steel fibre reinforced concrete* (Vol. 33).

Rombach, G. (2002). Precast segmental box girder bridges with external prestressing - design and construction. *INSA Rennes: Segmental Bridges*, 1–15.

Saiidi, M., Vrontinos, S., & Douglas, B. (1990). Model for the Response of Reinforced Concrete Beams Strengthened by Concrete Overlays. *ACI Structural Journal*, (87), 687–695.

Santos, P. M. D., & Júlio, E. N. B. S. (2014). Interface Shear Transfer on Composite Concrete Members. *ACI Structural Journal*, (111), 113–122. http://doi.org/10.14359/51686543

Standards, C. (2014). *CSA A23.3-14: Design of concrete structures*.

Tsioulou, O. T., & Dritsos, S. E. (2010). A theoretical model to predict interface slip due to bending. *Materials and Structures*, *44*(4), 825–843. http://doi.org/10.1617/s11527-010-9669-6

Turmo, J., Ramos, G., & Aparicio, A. C. (2006). Shear strength of dry joints of concrete panels with and without steel fibres Application to precast segmental bridges. *Engineering Structures*, *28*, 23–33. http://doi.org/10.1016/j.engstruct.2005.07.001

Walraven, J., Frenay, J., & Pruijssers, A. (1987). Influence of concrete strength and load history on the shear friction capacity of concrete members. *PCI Journal*, *32*(1), 66–84. Retrieved from http://avkbmmz.pci.org/pdf/publications/journal/1987/January-February/JL-87-JANUARY-FEBRUARY-5.pdf%5Cnhttp://pci.orgwww.pci.org/pdf/publications/journal/1988/January-February/JL-88-JANUARY-FEBRUARY-11.pdf

Wille, K., Naaman, A. E., El-Tawil, S., & Parra-Montesinos, G. J. (2011). Ultra-high performance concrete and fiber reinforced concrete: achieving strength and ductility without heat curing. *Materials and Structures*, *45*(3), 309–324. http://doi.org/10.1617/s11527-011-9767-0

Appendices

Appendix A

Photographs for crack patterns

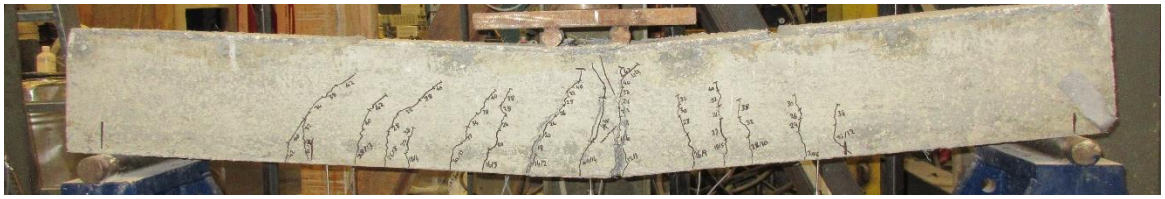

Figure A.1: Crack pattern for HSC-00-50.

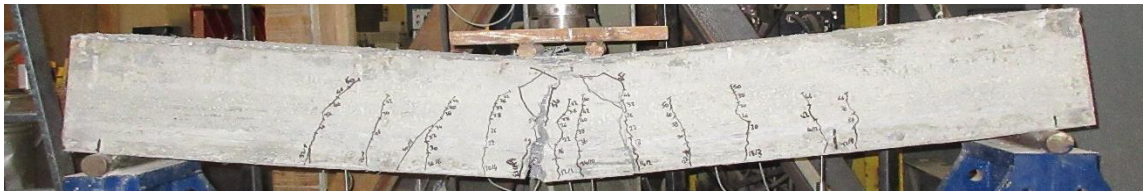

Figure A.2: Crack pattern for HSC-00-75.

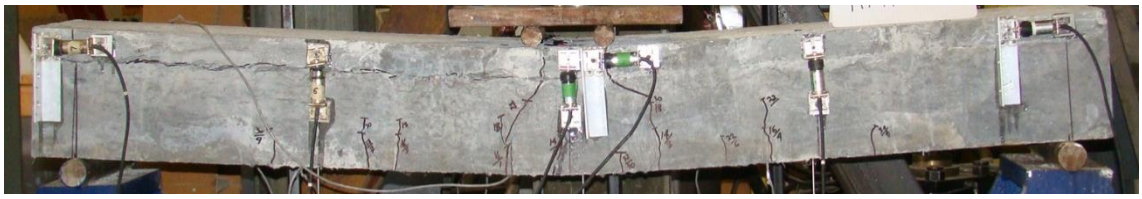

Figure A.3: Crack pattern for SK-390-50.

Figure A.4: Crack pattern for SK-390-75.

Figure A.5: Crack pattern for SK-195-50.

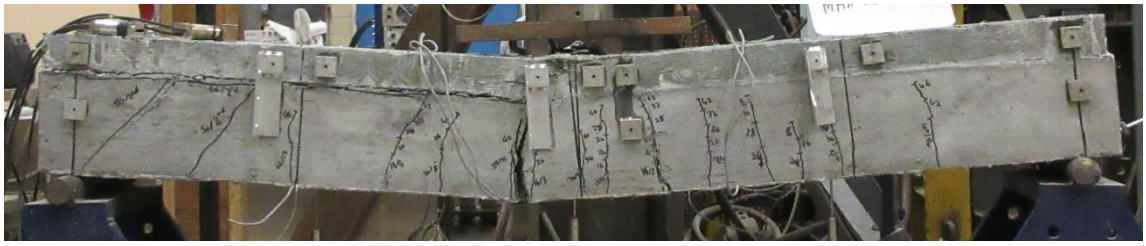

Figure A.6: Crack pattern for SK-195-75.

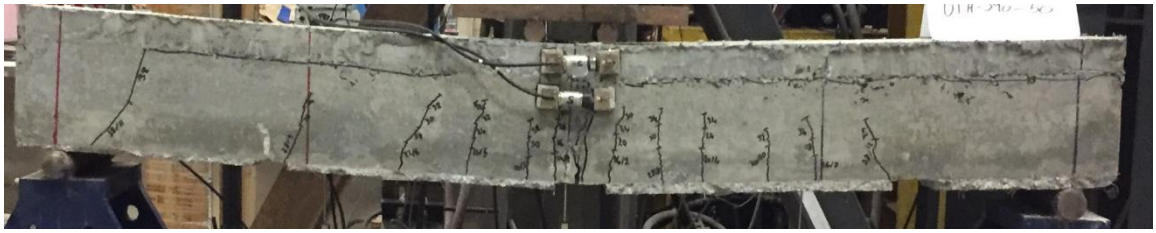

Figure A.7: Crack pattern for THS-390-50.

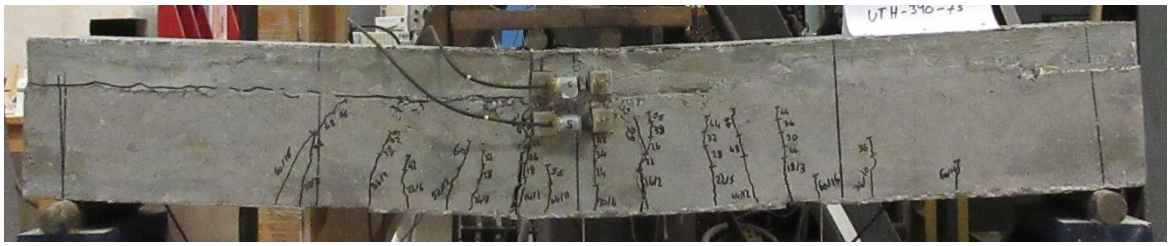

Figure A.8: Crack pattern for THS-390-75.

Figure A.9: Crack pattern for THS-195-50.

Figure A.10: Crack pattern for THS-195-75.

Appendix B

Load versus deflection graphs from all LVDTs

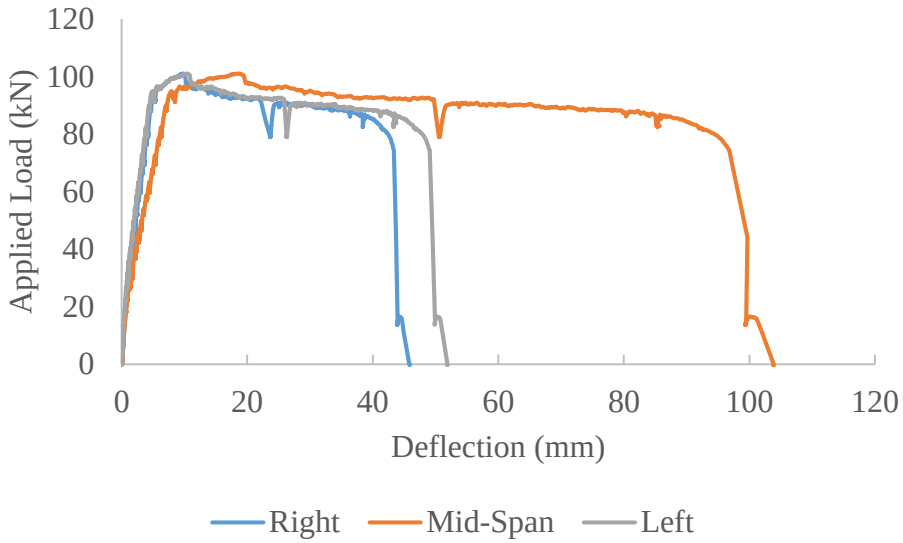

Figure B.1: Load versus deflection for HSC-00-50.

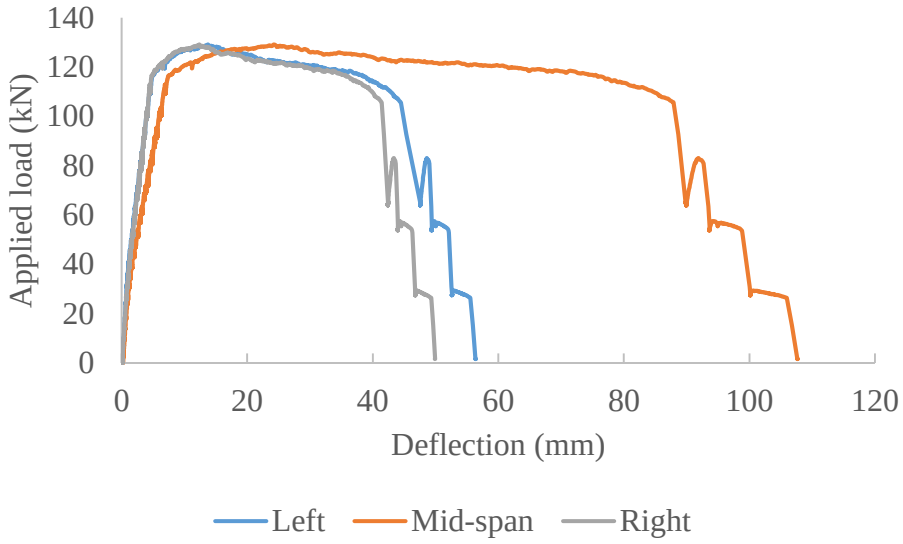

Figure B.2: Load versus deflection for HSC-00-75.

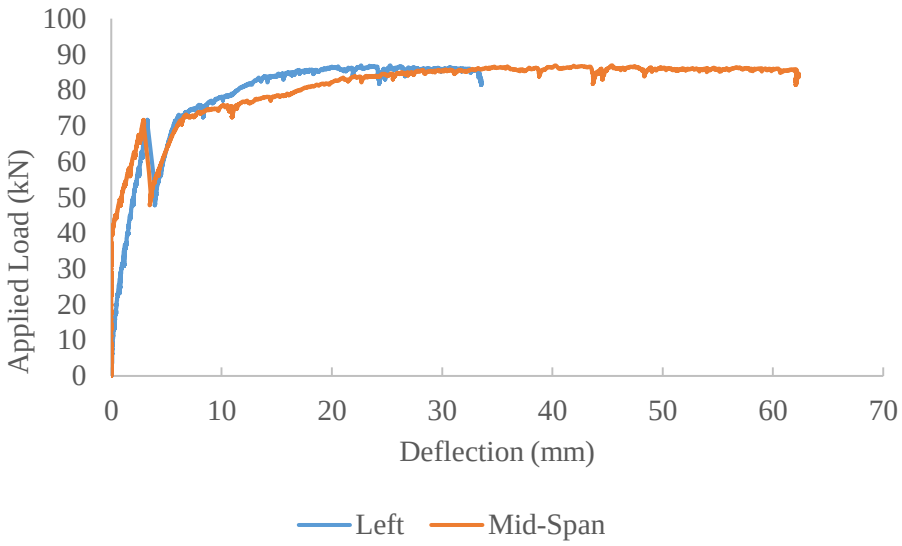

Figure B.3: Load versus Deflection for SK-390-50.

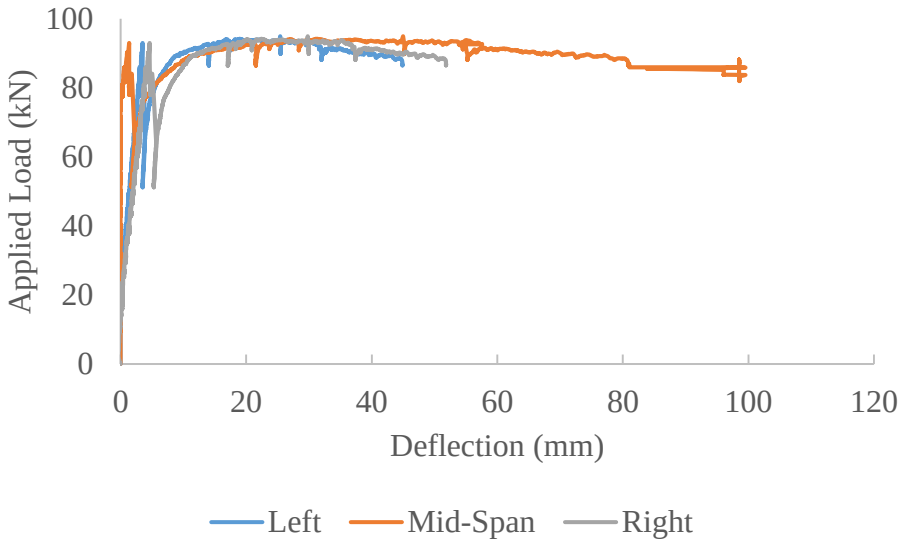

Figure B.4: Load versus deflection for SK-390-75.

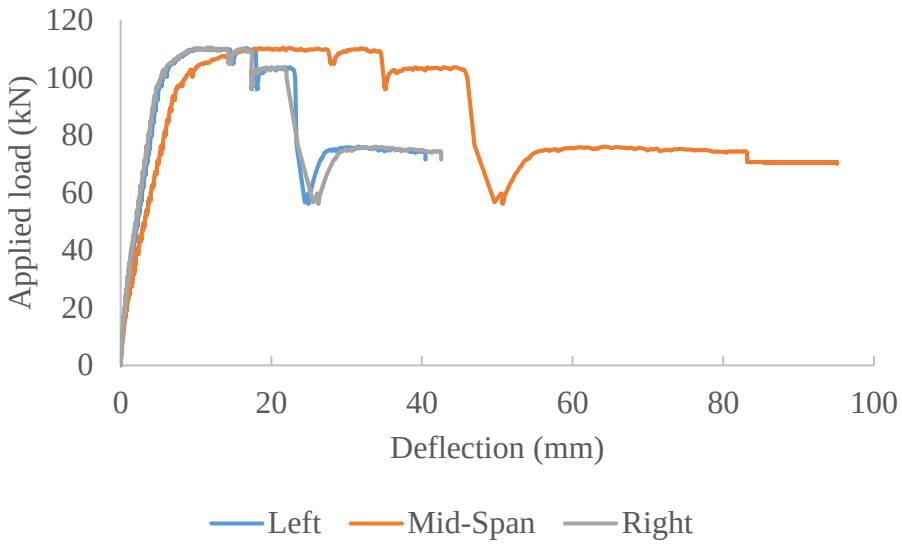

Figure B.5: Load versus deflection for SK-195-50.

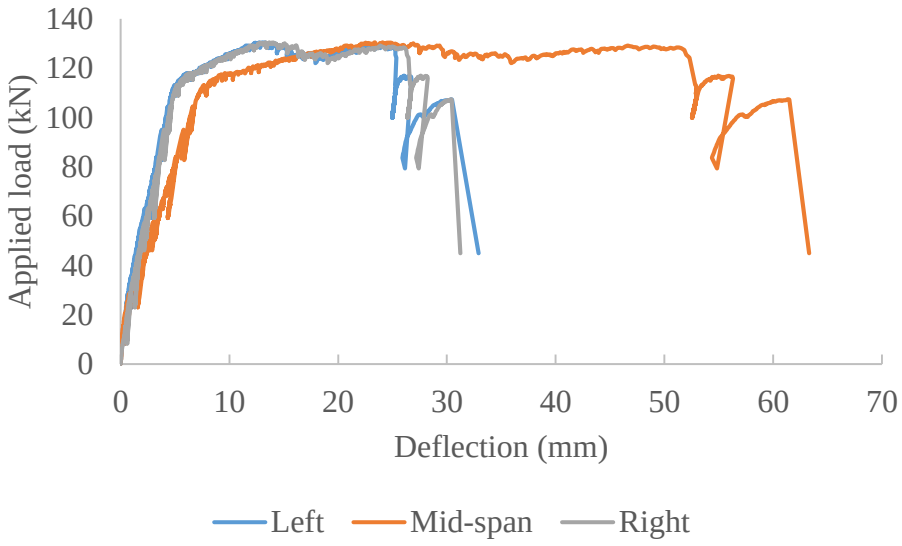

Figure B.6: Load versus deflection for SK-195-75.

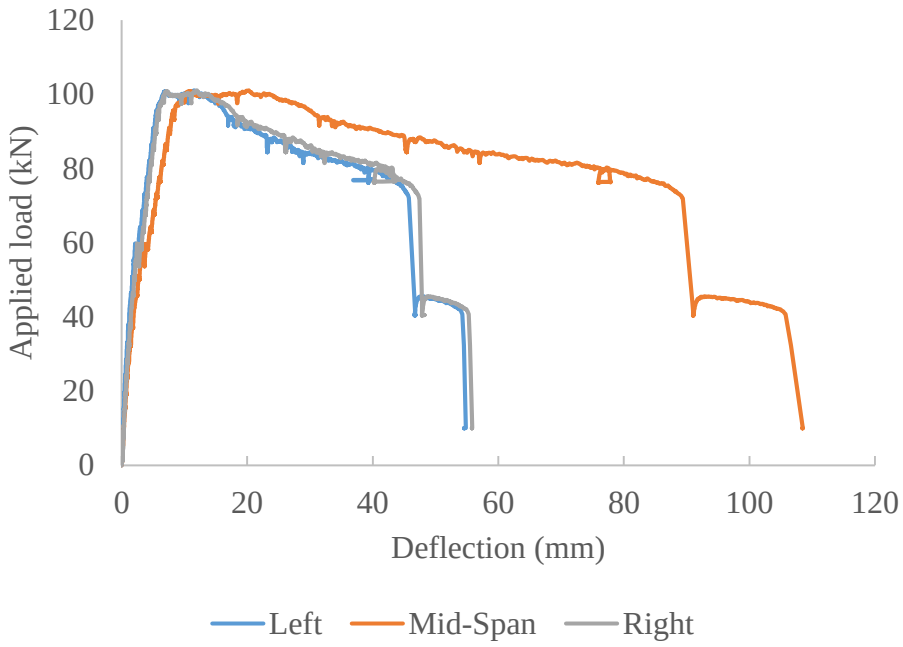

Figure B.7: Load versus deflection for THS-390-50.

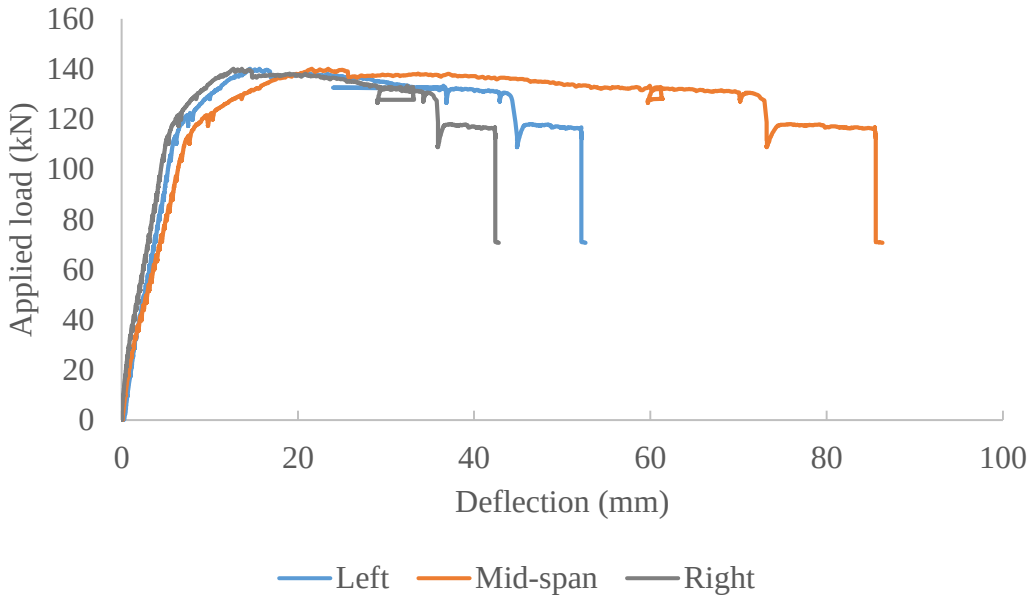

Figure B.8: Load versus deflection for THS-390-75.

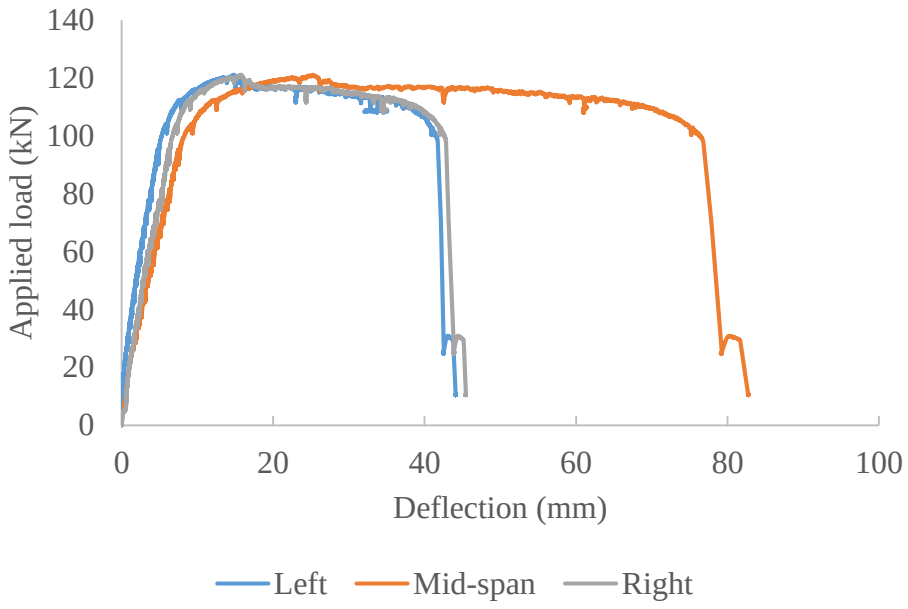

Figure B.9: Load versus deflection for THS-195-50.

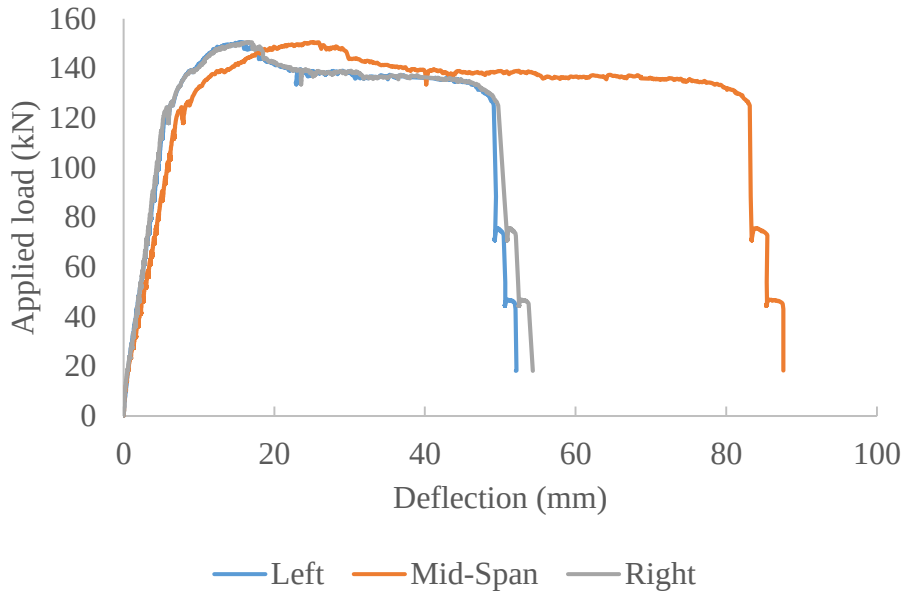

Figure B.10: Load versus deflection for THS-195-75.

Appendix C

Load versus Steel Strain plots for all the data collected from all the strain gauges

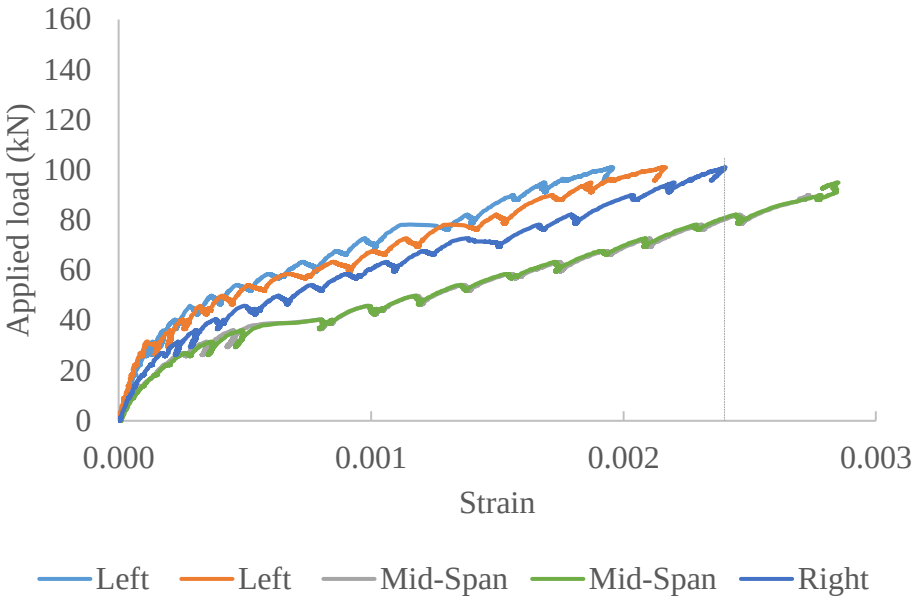

Figure C.1: Steel strain for HSC-00-50.

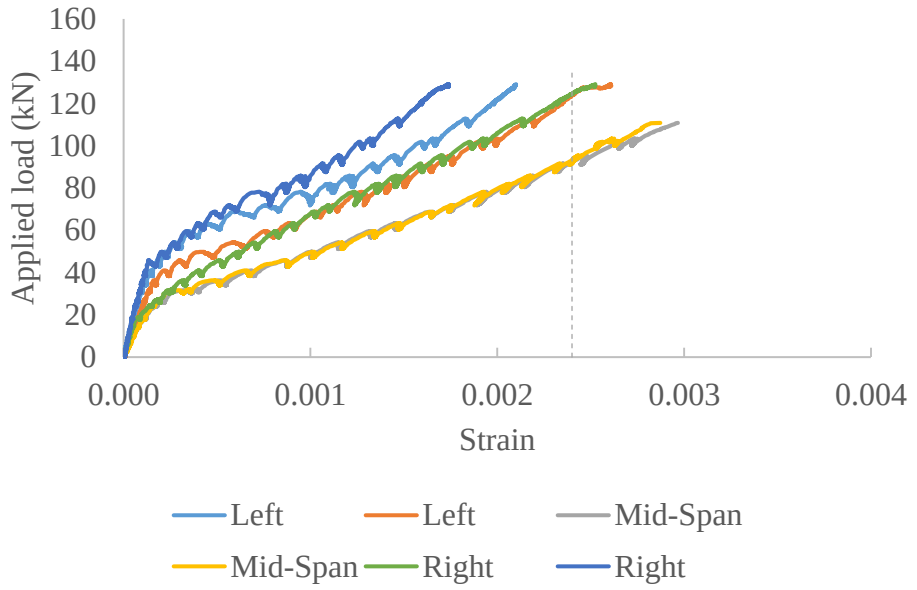

Figure C.2: Steel strain for HSC-00-75.

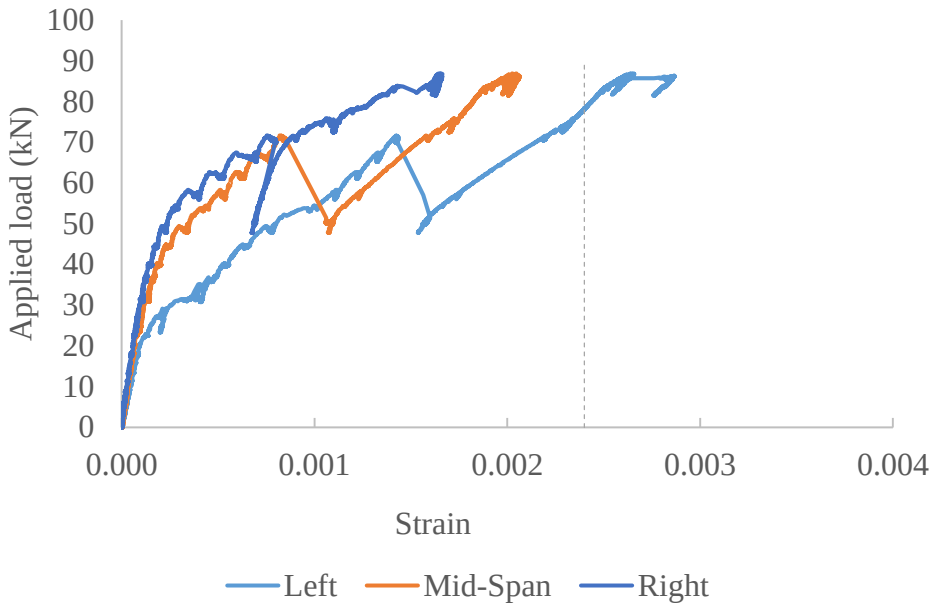

Figure C.3: Steel strain for SK-390-50.

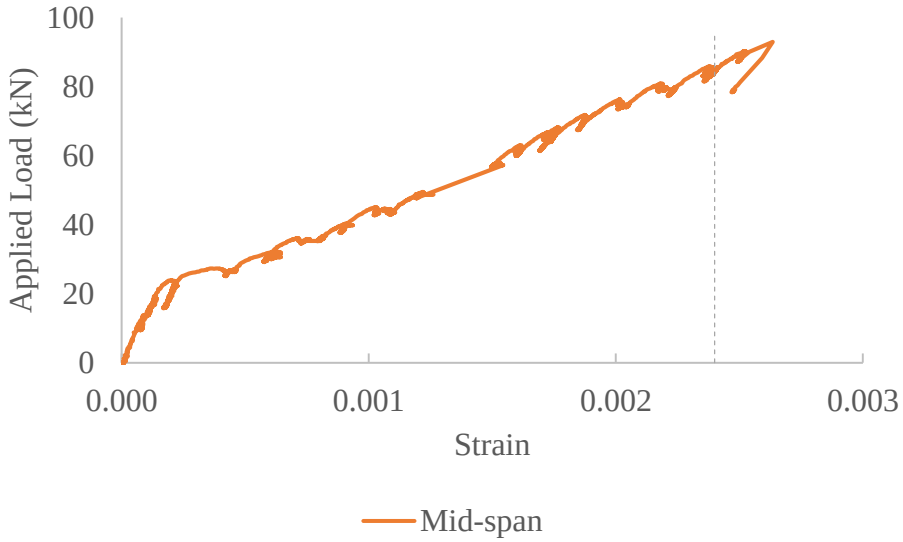

Figure C.4: Steel strain for SK-390-75.

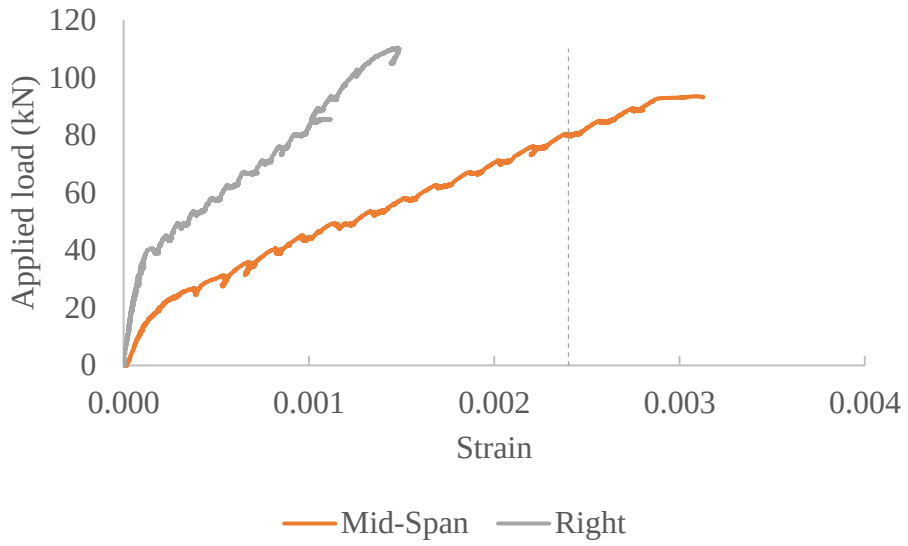

Figure C.5: Steel strain for SK-195-50.

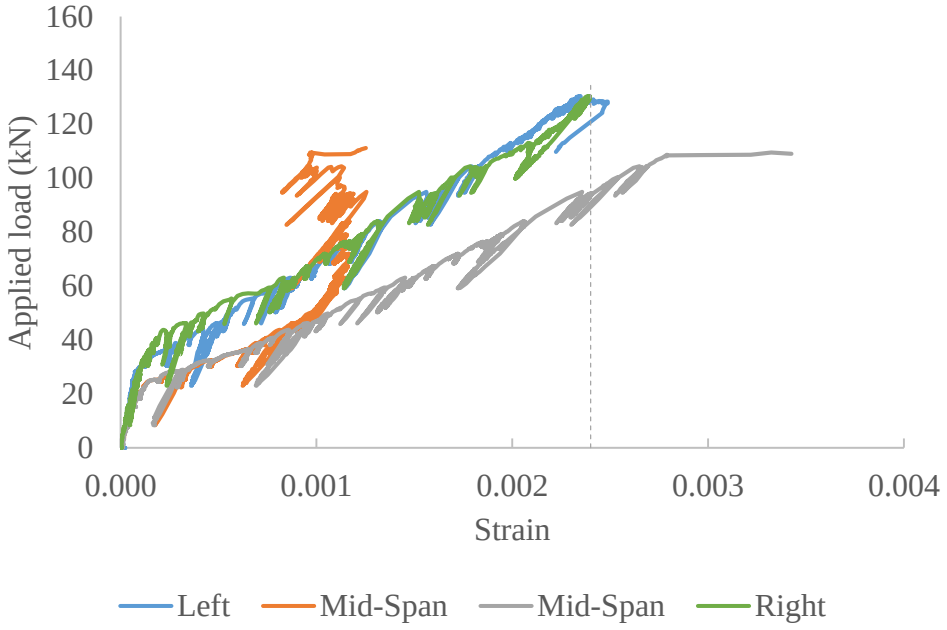

Figure C.6: Steel strain for SK-195-75.

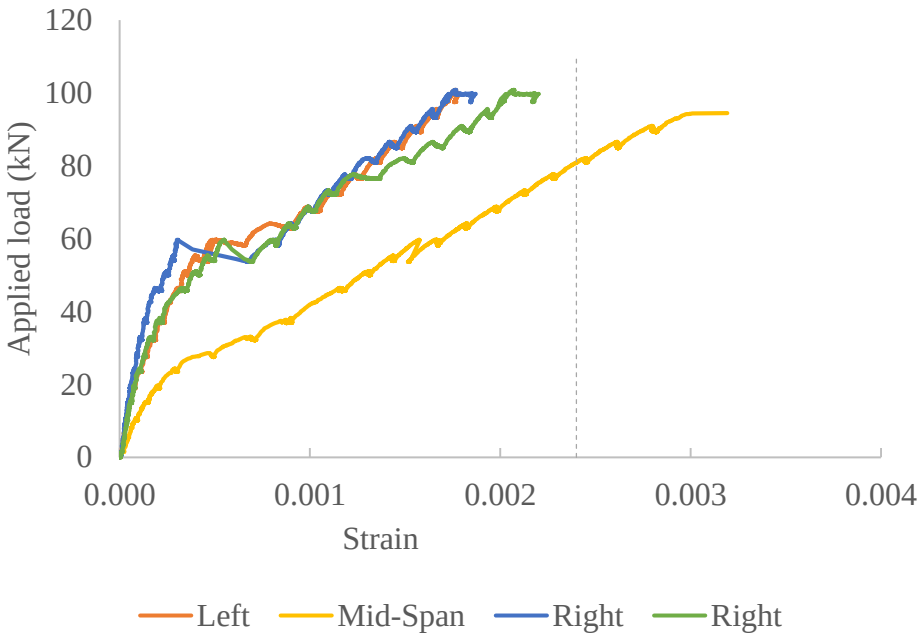

Figure C.7: Steel strain for THS-390-50.

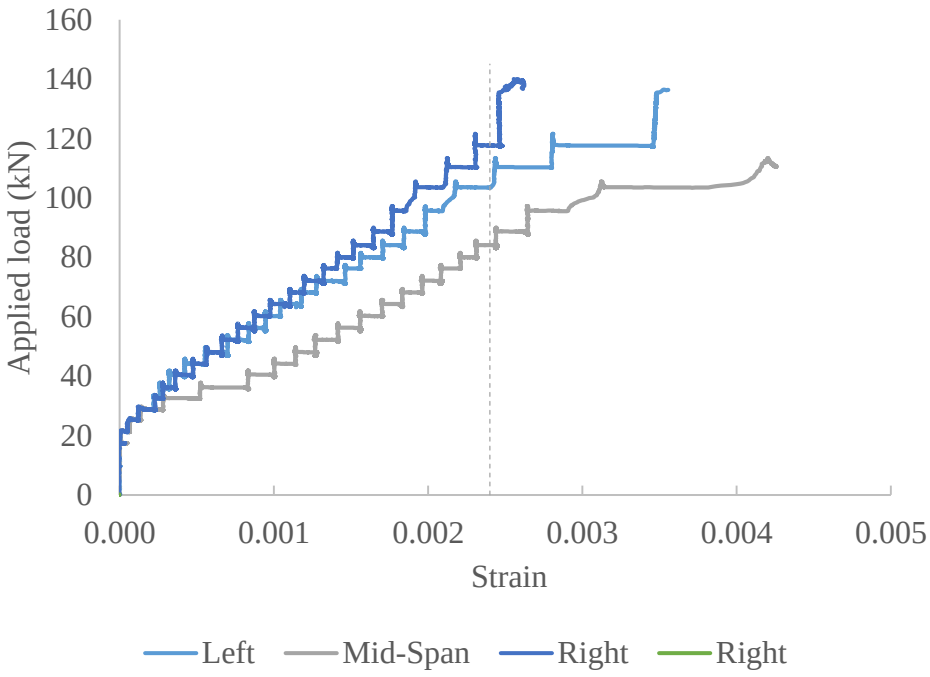

Figure C.8: Steel strain for THS-390-75.

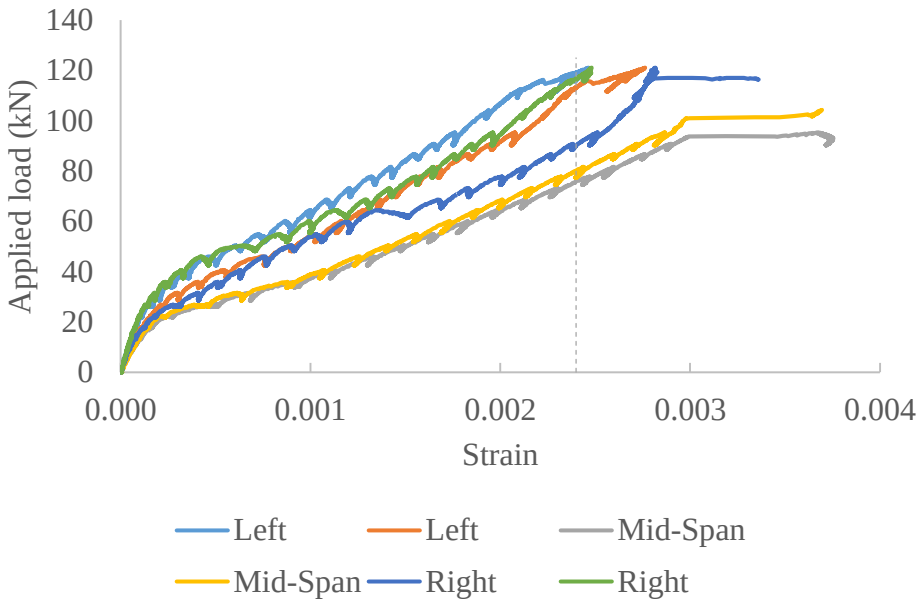

Figure C.9: Steel strain for THS-195-50.

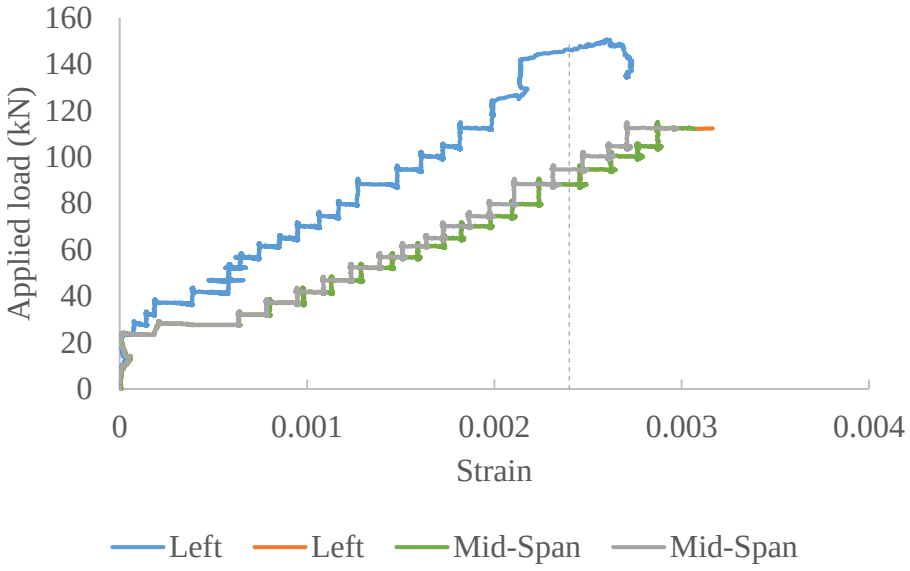

Figure C.10: Steel strain for THS-195-75.

Appendix D

Load versus Concrete strain plots for all the data collected from all the strain gauges

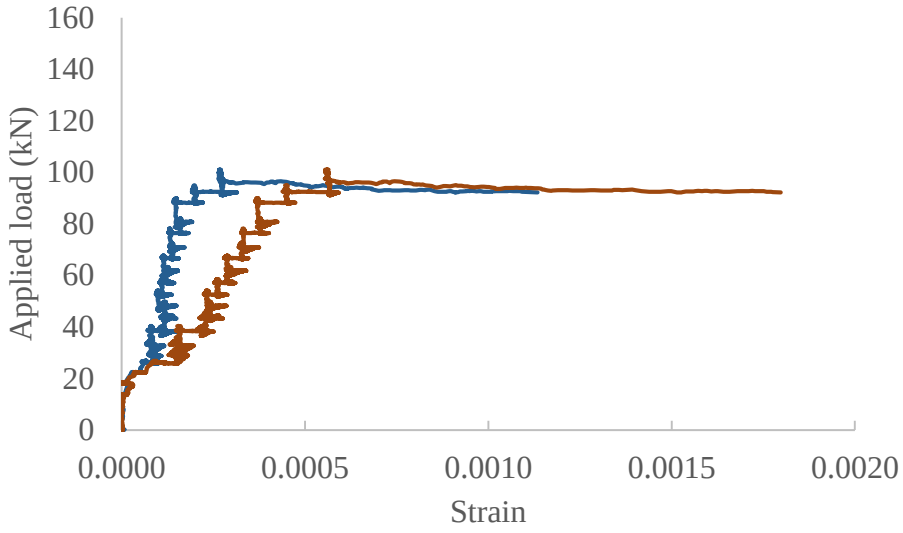

Figure D.1: Concrete strain for HSC-00-50.

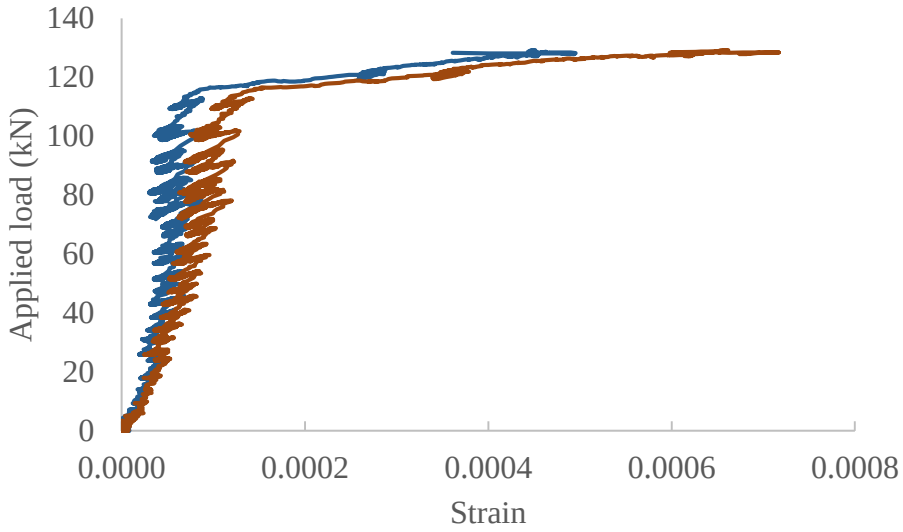

Figure D.2: Concrete strain for HSC-00-75.

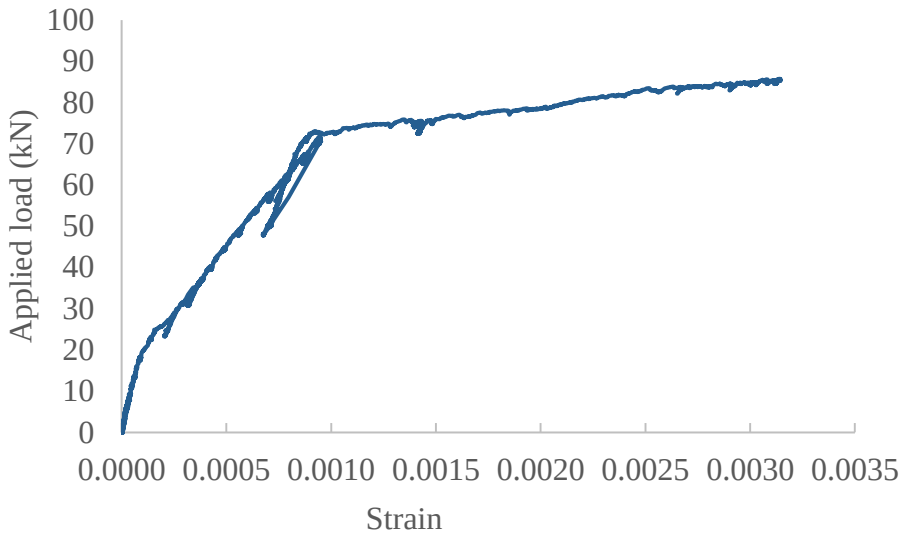

Figure D.3: Concrete strain for SK-390-50.

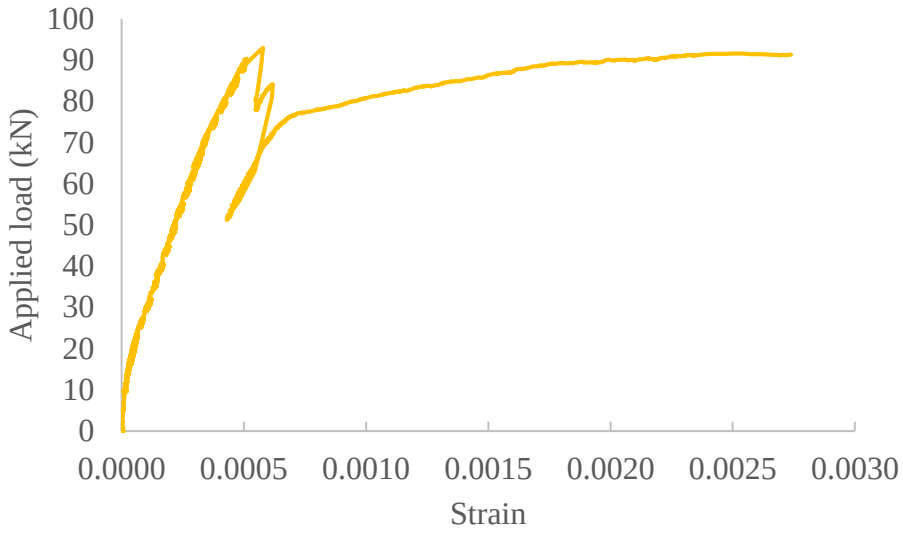

Figure D.4: Concrete strain for SK-390-75.

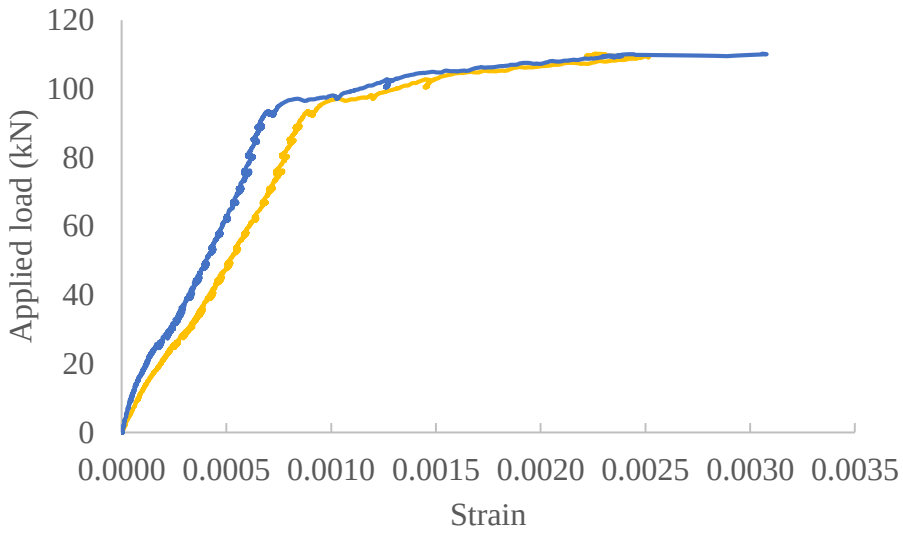

Figure D.5: Concrete strain for SK-195-50.

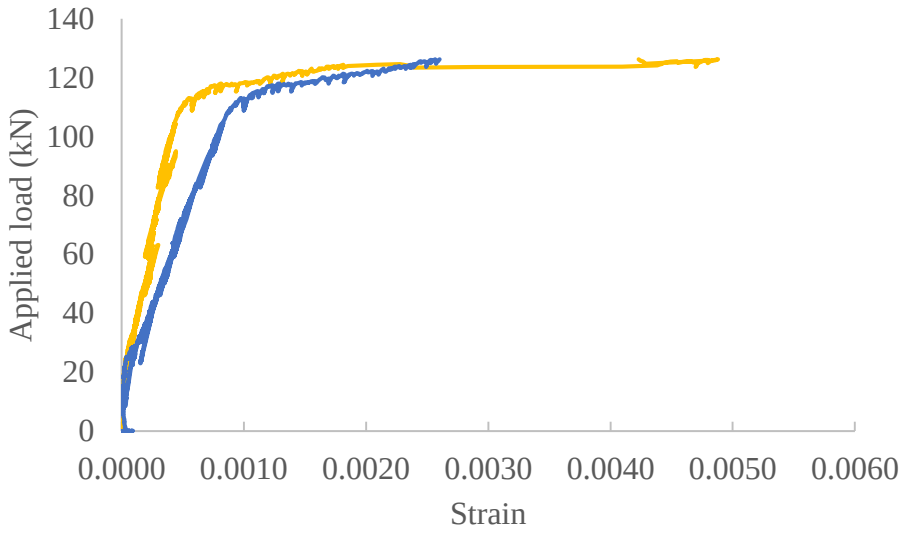

Figure D.6: Concrete strain for SK-195-75.

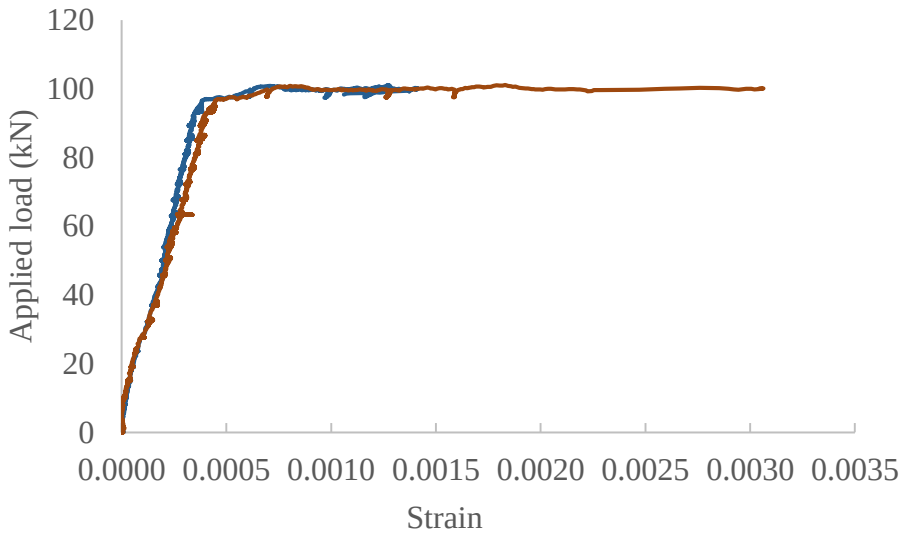

Figure D.7: Concrete strain for THS-390-50.

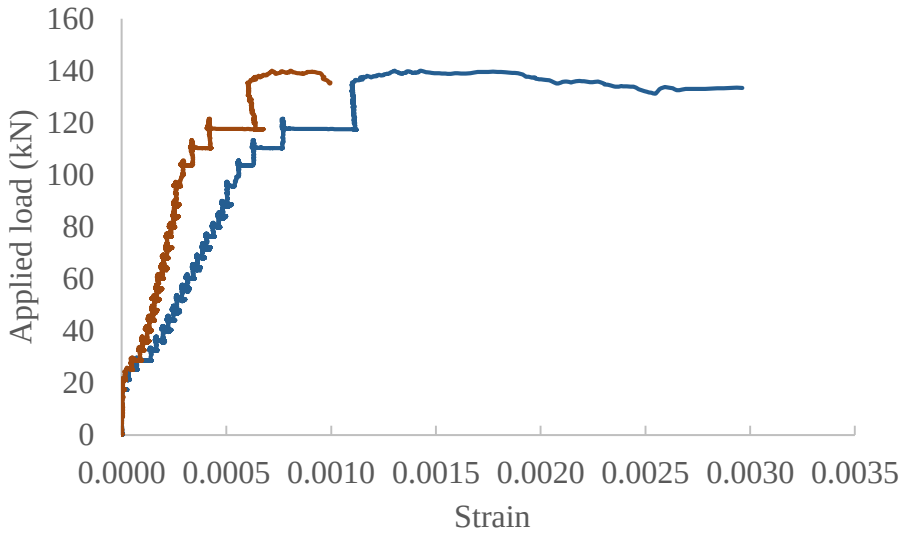

Figure D.8: Concrete strain for THS-390-75.

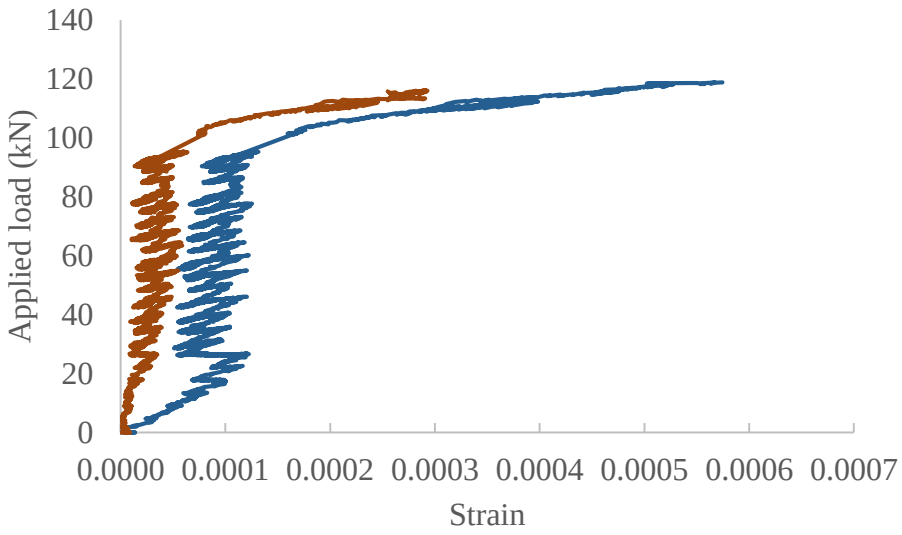

Figure D.9: Concrete strain for THS-195-50.

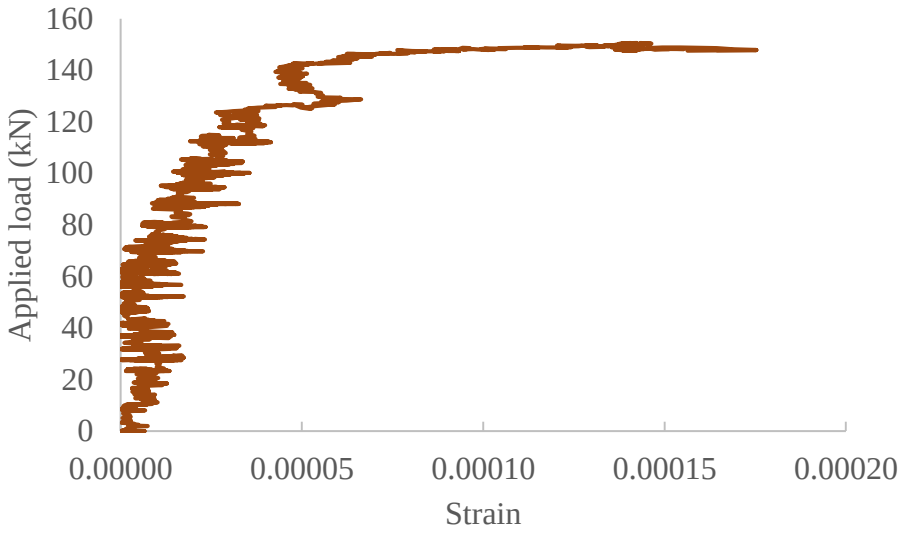

Figure D.10: Concrete strain for THS-195-75.